Leveraging Host Energy Metabolism to Modulate Influenza A Virus Defective Genome Production

By

ILECHUKWU O. AGU

DISSERTATION

Submitted in partial satisfaction of the requirements for the degree of

DOCTOR OF PHILOSOPHY

in

Biochemistry, Molecular, Cell and Developmental Biology

in the

OFFICE OF GRADUATE STUDIES

of the

UNIVERSITY OF CALIFORNIA

DAVIS

Approved:

_____

Samuel L. Diaz-Muñoz, Chair

_____

John G. Albeck

_____

Enoch P. Baldwin

Committee in Charge

2024

Preface

This dissertation marks the latest milestone in my decades-long transition (2014-2024) from active service in US Air Force logistics back to the biosciences. Departing from the traditional single-narrative style, the three chapters of this dissertation are formatted as standalone, albeit related, pre-print manuscripts. My success is thanks to the support of many individuals.

To the Craft Consultants, I am never alone because you are with me, always. Your collective presence brings healing and fills me with excitement for the future. In moments of doubt, you remind me of the incredible power within me, and when I stray, you guide me back on track. Elizabeth “Bob The Builder” Agu, your unwavering support, boundless generosity, and exceptional leadership have not only shaped my success but also the success of others. Thousands have been inspired by your dedication to empowerment and mentorship, reaching new heights in their careers and beyond. Ejike “Ozzy” Agu, with your talent and deep understanding of human nature, you continue to rise in the corporate and entertainment spheres. Ekene “AllSpark” Agu, your collaborative nature and strategic prowess shine brightly as you continue to navigate the launch of Peppermint Inc. Emeka “Ozo Guy” Agu, your lionhearted resilience and advocacy for Enugu-Ngwo commands respect and admiration. And to Donald “Donny Brasco” Ali, my comrade in our shared journey to California for career transitions, your partnership and determination are invaluable.

To my BMCDB cohort, our deep camaraderie in the early days of graduate school transformed what could easily have been a grueling ordeal into an exciting adventure. From potlucks and picnics to classes, final exams, lab rotations, and the dreaded 10-minute talks, we had each other, and I'll cherish those memories. Ram, your support during my qualifying exam and your contributions to the computational arm of the cluster-forming assay were invaluable.

Dr. Engebrecht, I couldn't have asked for a more diligent and experienced Academic Advisor. Your mentorship on graduate student work-life balance, lab selection, and elective courses has been crucial to my success, and I'm grateful.

To the Diaz-Munoz Lab, Sam, your nurturing disposition and diligent training empowered me to innovate and develop the cluster-forming assay. Ivy, you're the backbone of our lab operations. Sari, Alex, and Kishana, I've finally reached this milestone, and Courtney, hang in there—I'll see you on the postdoc side.

To my committee, Sam, John, and Enoch, your guidance throughout the study's life cycle was invaluable, and with your expertise, we uncovered a significant association between Influenza A pathogenesis and host cell metabolism.

To my *Outer Haven*, Dipta & Annie, Vince & Holly, Keith & Joanna, Monu & Lycia, Uncle Dennis & Aunty Kany, your support and sanctuary provided respite during challenging times, and I'm grateful for the memories and experiences we shared.

To the Huskies—Vincent "Vince" Horn, Troy “Fisticuffs” Breland, and Jonathan “Jonny Boy” Burks—our regular Zoom calls that began during the COVID lockdown rekindled our camaraderie in ways that provided me with immense strength and support throughout my PhD journey. I deeply appreciate your unwavering friendship and look forward to nurturing our bond. Huskies 4 Lyfe!

Abstract

Influenza A virus remains a critical public health threat due to the emergence of novel strains, low vaccination rates, and antiviral resistance, necessitating the development of novel broad-spectrum therapeutics. One promising approach involves manipulating defective viral genomes (DVGs) produced during influenza replication. These DVGs, through defective interference (DI), reduce the abundance of standard viral genomes (SVGs), thereby decreasing viral yield in a strain-independent manner and leading to milder clinical outcomes. While research has traditionally focused on viral factors influencing DVG production, recent studies have shifted attention to host cell factors. Our research demonstrates that host cell metabolism significantly influences DVG production. By manipulating host anabolic signaling with alpelisib—an inhibitor of host PI3Kα—we observed significantly altered responses in the production of DVGs and non-infectious virions in a strain-specific manner (H1N1/H3N2). This finding was partially facilitated by our development of a novel cluster-forming assay to simultaneously titrate infectious and non-infectious viral particles with high throughput and improved precision. Furthermore, a screen of various metabolites and signaling molecules identified adenosine and insulin as potent inducers of DVG production, while TCA cycle inhibitors and the purine analog favipiravir increased total viral genome production. Cyanobacterial extracts also elicited significant alterations in DVG production, particularly in A/H3N2 infections. These findings underscore the extensive scope of host-virus metabolic signaling crosstalk and the potential to target host metabolic pathways to influence influenza infection severity in a DVG-dependent manner. Our study advances the understanding of DVG production mechanisms and highlights novel antiviral intervention strategies, including targeting PI3K-AKT and Ras-MAPK signaling

pathways, TCA cycle metabolism, purine-pyrimidine metabolism, and cyanotherapeutic approaches. This research not only reveals the host's role in viral genome interactions but also opens new avenues for the development of broad-spectrum influenza therapeutics.

Table of Contents

Host cell state impacts the production of Influenza A defective viral genomes and non-infectious particles

Running head: host metabolism influenza defective interference

Ilechukwu Agu[1] & Samuel L. Díaz-Muñoz[1,2*]

[1] Department of Microbiology and Molecular Genetics
University of California, Davis
One Shields Ave
Davis CA 95616

[2] Genome Center
University of California, Davis
One Shields Ave
Davis CA 95616

*Address correspondence to: Samuel L. Díaz Muñoz, samdiazmunoz@ucdavis.edu

Abstract

Influenza A virus remains a global threat to public health due to the emergence of novel strains, low vaccination rates, and antiviral resistance, prompting the need for novel, broad-spectrum therapeutics. Defective viral genomes (DVGs) produced during influenza replication have shown broad-spectrum therapeutic potential via *defective interference* (DI), wherein DVG accumulation depletes the relative abundance of standard viral genomes (SVG) needed to sustain pathogenesis —which ultimately diminishes viral yield in a strain-indiscriminate manner. Decades of research have focused on the viral factors affecting the production and maintenance of DVGs in influenza infections, and the host factors affecting DVGs have been neglected. Uncovering host factors that affect DVG production could help predict infection outcomes based on host state and facilitate the manipulation of host state to increase DVG production, potentially leading to milder clinical outcomes. The therapeutic potential in increasing *in situ* production of DVGs is evident, but barriers to progress have persisted for decades, chief among them being a lack of tailored methodologies and workflows to reliably quantify DI metrics, as well as early research findings

that dismissed host cell involvement in the production of DVGs and the defective interfering particles (DIP) that carry them. As a result, no collectively sustained effort to uncover contributing factors of DI emergence has been undertaken, and the molecular mechanism of DVG *de novo* production remains unknown in spite of evidence implicating host involvement. This review summarizes (i) newly discovered associations between host cell state and Influenza A virus DVG production, (ii) the extensive host-virus metabolic signaling crosstalk that refocused the host as a potential contributor to DVG/DIP production, and (iii) the methodological innovations that facilitated these recent discoveries.

Host metabolism can modulate *in situ* hallmarks of DI

Within the infected host, Influenza A virus has a bipartite existence as intracellular viral genomic segments undergoing replication and assembly into progeny particles, and extracellular progeny particles in search of new cells to infect. Owing to the error-tolerant nature of the viral polymerase, there is a striking diversity of mutants among the genomic segments that in turn carries over to the particle level as mutant genomes are packaged into combinatorially variant particles. This within-host pool of closely related yet distinct “individuals” at the genome- and particle-level possess variable fitness upon which natural selection—in the form of host immune responses, antiviral treatments, and interactions among the viral segments and particles—acts, favoring the variants better adapted to prevailing conditions. Fortunately for the sieged host, there is periodic emergence of deletion-containing viral genomes that fail to express functional proteins, while simultaneously outcompeting standard genomes for packaging into progeny viral particles (Henle, 1943; Von Magnus, 1954; Davis, 1980; Nayak, 1982; Saira, 2013). Accumulation of these deletion-containing, defective viral genomes (DVGs)—and the defective interfering particles (DIP) they are assembled into—undermines the capacity of standard viral genomes (SVGs) (Ranum, 2024) and fully infectious particles (FIP) to sustain propagation. Moreover, DVGs and DIPs also accelerate the host innate immune response (Zhang, 2020); leading to the self-limiting pathogenesis and mild disease severity that characterizes defective interference (DI) (Dimmock, 2014; Vasilijevic, 2017). The therapeutic potential of *on-demand DI induction* remains unrealized because the mechanism(s) of *de novo* DVG production during Influenza A infection remains unsolved (Dimmock, 2014; Manzoni, 2018; Vignuzi, 2019; Wu, 2022). This mechanism could be elucidated by identifying more factors that influence DVG

production, as groups of these factors likely share common processes involved in DVG formation. Host cell metabolism exemplifies one such shared process, as evidenced by the recently discovered impact of metabolic drugs on DVG production (Chapter 2, Chapter 3).

The host cell's metabolic signaling state is the most recent of the few known *in situ* modulators of DVG and DIP production, joining the likes of infection multiplicity (Von Magnus, 1954; Bangham, 1990), virus polymerase gene mutations (Vasilijevic, 2017), and virus matrix gene mutations (Perez-Cidoncha, 2014). Pharmacological disruption of virus-host metabolic crosstalk with an inhibitor of growth metabolic signaling in the host cell has been shown to modulate *in situ* hallmarks of DI early in infection, and to varying degrees depending on flu virus strain (Chapter 2). Pre-exposure of MDCK cells to a PI3Kα inhibitor—alpelisib—prior to A/Texas/50/2012(H3N2) infection significantly increased the relative abundance of non-infectious progeny viral particles. In particular, 2.5 uM alpelisib stood out for driving a co-incident decrease in total viral particles together with the spike in non-infectious particle relative abundance; a paired outcome that represents the generally accepted hallmark of DI (Dimmock, 2014; Manzoni, 2018; Vignuzi, 2019; Wu, 2022). Altogether, A/Texas/50/2012(H3N2) pathogenesis showed acute vulnerability to alpelisib-induced host metabolic signaling disruption very early in infection (18 hr post infection) and at a wide dosage range. The opposite was true for A/California/07/2009(H1N1), where all but the 20uM dose of alpelisib exacted a net-zero effect on the proportion of non-infectious particles (Chapter 2). At the genomic level, both strains showed an increasing trend of DVG production with higher concentrations of alpelisib (Chapter 2). This finding is intriguing given their different particle-level outcomes, suggesting a

viral genome sorting mechanism that favors the assembly of non-infectious progeny particles in A/Texas/50/2012 (H3N2) compared to A/California/07/2009 (H1N1). This could be an interesting topic for future investigation.

In the same vein as the Alpelisib study, a pharmacological screen also revealed novel metabolic signaling drugs that act through the host to modulate *in situ* hallmarks of DI early in infection (Chapter 3). Adenosine strongly amplified DVG production of polymerase complex segments across H1N1 and H3N2 subtypes of Influenza A virus, and differentially enhanced DVG production across other genomic segments between the subtypes (Chapter 3). Insulin showed strain-specific effects on polymerase complex DVGs, increasing DVG production in the H3N2 subtype (Chapter 3). TCA cycle inhibitors 4-OI and UK5099 significantly boosted total viral genome (TVG) production across multiple segments, mimicking the Warburg effect observed in tumor cells (Chapter 3). These metabolic signaling molecules collectively link host metabolism to DVG production through their shared impact on altering metabolic signaling pathways within the host cell. In addition to these drugs, a low dose of the mutagenic nucleoside analog precursor Favipiravir increased TVG production across H1N1 and H3N2 subtypes while slightly reducing DVG proportions in the H3N2 subtype, indicating that nucleotide misincorporation may not be essential for DVG production (Chapter 3). Lastly, cyanobacterial extracts selectively suppressed the production of antigenic segments in the H3N2 subtype, highlighting the potential of natural products in modulating segment-selective forces that act during replication and capsid assembly (Chapter 3; Silva, 2018).

Of the few known modulators of DVG and DIP production, host cell metabolic signaling state is unique for being the most therapeutically actionable i.e. it is easily druggable. This discovery was made possible in part by the extensively characterized crosstalk between host metabolism and influenza infection outcomes.

Host-Influenza interactions: a history of metabolic crosstalk

At the cellular level, Influenza A induces various metabolic changes within infected cells that favor productive pathogenesis. In a particularly striking example, A/Puerto Rico/8/34(H1N1) infection disrupted proteosomal degradation of hypoxia-inducible-factor-1α (HIF-1α) in the mitochondria of human lung cells (A549) and mouse lung tissue, allowing for accumulation and translocation of this transcription factor (HIF-1α) to the nucleus where it facilitates expression of pro-glycolytic enzymes (Ren, 2019). This aberrant reprogramming of host cell glucose catabolism disrupts the normoxic oxidation of pyruvate by upregulating hexokinase (HK2), pyruvate kinase M2 (PKM2), and pyruvate dehydrogenase kinase (PDK3) (Ren, 2021). This state, similar to that of tumor cells, is characterized by enhanced glycolysis and the redirection of pyruvate from complete breakdown into CO_2 gas, preserving the reduced-carbon biomass needed to feed anabolic pathways that drive the proliferation of tumor cells (Lunt, 2011; Liu, 2019) or viruses.

Influenza A virus also upregulates host biosynthetic pathways that support viral proliferation via direct binding of the viral NS1 effector protein to the regulatory subunit (p85β) of host Class 1a phosphoinositide-3-kinase (PI3Kα). This interaction releases the catalytic p110α subunit to

initiate the PI3Kα signaling cascade (Hale, 2006; Li, 2008; Ayllon, 2012; Kuss-Duerkop 2017; Lopes 2017; Cho, 2020) with strain-dependent intensity (Ayllon, 2012; Chapter 2), even in the absence of typical growth factors like insulin. Consequently, NS1's actions shift host metabolism towards a state marked by increased pools of precursor metabolites (Luo, 2018; Saha, 2014; Al-Saffar, 2010) vital for uninterrupted replication of virion components.

Conversely, host metabolism can equally influence the course of influenza infection. In a straightforward example, growth media supplementation with the Tricarboxylic Acid Cycle inhibitor malonate drove dose-dependent decreases in the total particle yield of viral progeny (Ackermann, 1951). Other metabolic factors such as obesity, diabetes, and nutritional status have been shown to impact susceptibility to influenza infection and follow-on disease severity. For instance, extreme nutritional states of either diet-induced obesity or caloric restriction impaired immune function and increased the risk of complications from influenza infection in mice (Gardner, 2011). Additionally, obese patient groups shed higher viral loads which also contained more virulent mutants relative to the non-obese cohorts in human infections (Honce, 2019; Honce, 2020).

From the molecular mechanisms underlying host cell detection of the Z-conformation RNA of DVGs (Zhang, 2020) to the interferon-independent protection of co-infected influenza DI virus on Type I and Type III interferon-deficient mice (Wang, 2023), there is a steadily expanding body of work on how DVGs affect the host. Strangely, the reverse is not the case, as evidenced by a striking absence of research into the effects of host cells on DVG production. In truth, host

cell involvement in DI virus production was wrongly dismissed well over half a century ago, and the extensive host-influenza metabolic crosstalk characterized in the intervening decades served to refocus the host as a key contributing factor.

The “Not” Star: Early inquiries wrongly dismissed host cell involvement in Influenza A DI virus production

Shortly after the discovery of non-infectious Influenza A particles and their antiviral potential (Henle, 1943; Von Magnus, 1954), scientists speculated about the role of host cells in their production; no doubt in response to mounting evidence of viral sensitivity to perturbation of host cell functions like the tricarboxylic acid cycle (Ackermann, 1951), glycolysis (Kilbourne, 1959), Vitamin A metabolic signaling (Blough, 1963) etc. However, initial attempts to establish a connection between host parameters and DIP production
found only a meandering correlation with virally induced cell damage (Ginsberg, 1954). These early probes also had some limitations, like overlooking the effect of MOI (Choppin, 1969; De, 1980) and the misattribution of control variables (Choppin, 1969; Choppin, 1970). As such, these studies were unsuccessful in disentangling host effects from MOI and consistently found MOI to be the primary determinant of DIP production while the host had no effect. These findings and subsequent support for MOI as the main determinant of DIP production (Von Magnus, 1954; Bangham, 1990) appear to have diverted the collective pursuit for inducers of DIP production away from the host cell. This diversion is evidenced by the abrupt drop-off in research, which failed to resurge despite the emergence of supporting evidence over the subsequent decades.

The intervening decades following the dismissal of host cell involvement in DIP production saw several missed opportunities to refocus the host cell as a potential controlling factor. A recent review (Wu, 2022) observed that the per-segment DVG profile of flu strains may differ with the cell type infected, citing the disparate DVG outcomes of A/Puerto Rico/8/34 infection in two independent studies that used different cell types; embryonated eggs (Jennings, 1983) and MDCK cells (Frensing, 2014). In another case, researchers discovered that the fatty acid and phospholipid profile of the A/Puerto Rico/8/34 envelope differed significantly between infectious and non-infectious particles (Blough, 1969; Blough, 1970). This discrepancy suggests that lipid-driven changes in host cell membrane rigidity might differentially affect the efficiency with which nascent DVG and standard genomes are packed into progeny particles. Lastly, Influenza A polymerase replication fidelity suffers under low concentration of its ribonucleotide triphoshpate (rNTP) substrate *in vitro* (Aggarwal, 2010). Given that internal deletions of DVGs have the appearance of a replication error product, their *de novo* production may also be driven by low rNTP concentration or other environmental determinants of polymerase physiochemistry and fidelity, such as pH, temperature, rNTP pool balance, choice of metal ion cofactor (Mg^{2+} or Mn^{2+}), crowding etc. (Aggarwal, 2010; Ganai, 2016) that are regulated by host signaling networks. Moreover, altering the physiochemistry of influenza polymerase through sequence mutations directly affected DVG accumulation (Vasilijevic, 2017), indicating the potential for physiochemical changes induced by various factors, including those originating from the host, to yield similar effects.

The above-mentioned examples are just a glimpse into a broader pool of uncurated findings implicating host involvement in DIP production, which has been slow to rekindle interest in this once-dismissed area (Ginsberg, 1954; Choppin, 1969; Choppin, 1970; De 1980). A persistent barrier to discovering more factors shaping DIP production is the absence of methodologies capable of not only quantifying DI phenomena at sufficient resolution but also doing so with precision and high throughput. In fact, assays enabling precise quantification of DVGs (Jaworski, 2017; Te, 2018; Chapter 2) and non-infectious viral particles (Chapter 2; Amarilla, 2021) have only recently been developed. This review now turns to past and current methods of quantifying DVGs and DIPs, with an emphasis on methodological shortfalls and recent innovations that promise to revitalize research in this field.

Methodological approaches to quantifying DI phenomena, past and present

Standalone titration of fully infectious (FIP) or non-infectious particles provides an incomplete representation of disease state, due to their entangled antagonism which shapes to Influenza A pathogenesis. The same rings true at genome-level, where standalone counts of SVGs or DVGs overlook the entangled effects of both segment types on disease progression and outcomes. This is why *interference* is best quantified in terms of ratios or proportions of the different viral sub-groups relative to each other; both at the particle and genome level. Options to quantify interference at the particle-level include DIP:FIP ratio, or DIP relative abundance. In the same vein, genome-level interference can be represented via the DVG:SVG ratio, or DVG relative abundance.

Particle-level DI: Quantifying non-infectious particles

Particle-level interference during Influenza A virus infection was first quantified as the ratio of FIPs to total particles (Ginsberg, 1954). FIPs were titrated via plaque assay (Cooper, 1961) and reported as the number of plaque-forming units (PFU), while total particles were titrated via hemagglutination assay (Hirst, 1942) and reported as the number of hemagglutination units (HAU). However, the PFU:HAU ratio had low precision because HAU is only an approximation of total particles, not an actual count. Additionally, the PFU:HAU ratio did not directly report on interference but rather productive infectivity, meaning that observed changes in the metric may or may not be due to interference.

The infectious center reduction assay (Nayak, 1978) was the breakthrough assay that first quantified an interference metric from Influenza A virus infection, albeit indirectly and with imprecision. Co-infecting a viral sample (Sample A) of known PFU with a viral sample (Sample B) of unknown titer, and then measuring the reduction in titer of Sample A allowed researchers to quantify Sample B's interference as defective interfering units (DIU/mL) (Nayak, 1978; Janda, 1979; De, 1980). The DIU:PFU ratio could now be derived to report on interference in an Influenza A infection. However, the DIU metric is imprecise because it does not directly measure interfering particles but derives interference from another metric.

The cluster-forming assay is the most recent innovation in Influenza A viral particle titration. It reproducibly titrates non-infectious Influenza A particles directly, in a physiologically relevant adherent cell monolayer model (Chapter 2). The methodological innovation of the cluster-

forming assay lies in the replacement of the plaque assay's solid agar overlay with a semi-solid overlay that is aspirated post assay, allowing for immunofluorescence (IF) staining and imaging of the monolayer. In the resulting IF image, infectious and non-infectious particles are clearly resolvable based on whether an infection event has propagated to adjacent cells (fully infectious) or remains confined to a single cell (non-infectious) (Chapter 2). Fully infectious and non-infectious particles are then summed to yield the total particles, which is used to divide the number of non-infectious particles to derive the relative abundance of non-infectious particles; a precise metric of defective interference based on the actual count of infective and non-infective particles (Chapter 2).

Genome-level DI: Quantifying defective viral genomes

Progress in particle-level DI quantitation initially outpaced DVG quantitation, with the infectivity-hemagglutination ratio (PFU:HAU) (Ginsberg, 1954) entering use a full 20+ years ahead of the discovery of Influenza A DVGs. Initially termed "subgenomic RNAs", DVGs were discovered via polyacrylamide gel electrophoresis (PAGE) of phenol-extracted viral RNA (Crumpton, 1978; Nayak, 1978). They were quantified either qualitatively by the presence or absence of a gel band (Crumpton, 1978), or quantitatively by determining the molar ratios of standard and DVG segments relative to a reference segment (Nayak, 1978). This quantitative method involved creating an autoradiograph from a PAGE gel of radioactively labeled RNA segments, wherein band intensities on the autoradiograph correlated with the amount of RNA and was analyzed using densitometry to measure the counts per minute (CPM) for each band. These CPM values were then compared to the CPM of a reference segment to determine the

relative abundance of each RNA segment (Nayak, 1978). Although pioneering, the molar ratio method was imprecise because CPM is only an approximation of total genomes per segment, not an actual count.

Quantitative PCR (qPCR) allows for Influenza A virus DVG detection via the use of internally binding primer sets that targeted regions flanking the known deletion sites in the viral genome (Fonville, 2015). This allows the amplification of both full-length and defective genomes, but detection in this manner is limited to DVGs of known deletion sites. As such, a forward approach to detect all possible deletion junctions in any given viral sample will require a vast amount of custom primer sets, which will significantly reduce throughput and prove technical difficult. What's more, the specific DVGs that qPCR manages to detect are subject to imprecise quantitation due to (i) PCR amplification bias, and (ii) the inference of genomic cDNA production from the probe fluorescence instead of being directly counted.

The most recent—and highest precision—workflow to detect internal deletions in Influenza A genomic segments is the pairing of next- (NGS) or third-generation sequencing (TGS) with downstream bioinformatics. TGS in particular allows investigators to classify sequenced reads on the basis of internal deletions or other recombination events they harbor, but these recombination events must first be flagged via the alignment of sequenced reads to the matching reference Influenza A genome. DVG-tailored sequence alignment tools like ViReMa (Routh, 2013; Yeung, 2022; Sotcheff, 2023), DI-tector (Beauclair, 2018) and VODKA (Sun, 2019), as well as other capable aligners like TopHat2 (Kim, 2013), STAR Aligner (Dobin, 2013) and

HMMER (Eddy, 2011) have been successfully used to detect deletion-containing reads in NGS and TGS datasets (Jaworski, 2017; Alnaj, 2021; Ranum, 2024; Chapter1; Chapter 3; Vasilijevic, 2017; Te, 2018; Saira, 2013). However, both generations of sequencing platforms—NGS and TGS—currently boast different efficiencies and capabilities with regard to detecting and quantifying Influenza A DVGs.

The highest throughput and accuracy (100.0%) for Influenza A virus sequencing are achieved with the NGS short-read sequencing Illumina platform (Sanderson, 2024; Cheng, 2023). However, the need for sequencing library fragmentation in NGS makes it difficult to distinguish fragmented DVG and full-length segments. Consequently, DVG deletion junction mapping and abundance are the primary capabilities of the Roche/454 (Saira, 2013) and Illumina (Alnaj, 2019) NGS platforms. Experimental and computational artifacts from physical DNA fragmentation can be mitigated by various methods, such as using simulated control datasets to validate deletion breakpoints (Alnaj, 2019), or employing ClickSeq to avoid physical fragmentation and enzyme-mediated ligation of sequencing adapters. In ClickSeq, sequencing library preparation starts with a reverse transcriptase reaction using semi-random DNA primers, deoxyribonucleotides (dNTPs), and a 3′-modified nucleotide analog that randomly terminates DNA synthesis, producing variably sized 3′-blocked cDNA fragments similar to dideoxy-Sanger sequencing (Routh, 2015). These fragments are then purified and reacted with sequencing adapters bearing a 5'-modified chemical group, which binds both molecules at their 3' and 5' ends into ssDNA substrate for PCR amplification to generate a viral cDNA library (Routh, 2015). Despite ClickSeq's advantages, the dependence on library fragmentation—whether physical or

non-physical—limits NGS platforms to reporting the location and abundance of deletion breakpoints per segment (Jaworski, 2017). Fortunately, advancements in TGS platforms have allowed researchers to overcome the limitations of NGS-derived data.

End to end sequencing of the Influenza A virus genomic segments on the Oxford Nanopore Technologies long-read sequencing platform has made it possible to detect deletions of all possible lengths in any given viral segment, and therefore classify and count the number of standard and deletion-containing genomes in a given sample (Chapter 2; Chapter 3); a feat as yet not achieved with NGS-derived genomic data of Influenza A. Additionally, the 99.1% modal read accuracy of current generation Oxford Nanopore hardware and software (Sanderson, 2024) is a 1.5 percentage point improvement from the previous generation (Ni, 2023). This trend of improvement puts Oxford Nanopore is on track to rival Illumina in modal accuracy in the coming years, or outperform Illumina if the short-read platform is unable to expand its capabilities to include long-read sequencing.

End-to-end sequencing of Influenza A virus genomic segments using the Oxford Nanopore Technologies long-read sequencing platform allows for the detection of deletions of all possible lengths in any viral segment. This enables the classification and counting of standard and deletion-containing genomes in a sample (Chapter 2; Chapter 3)—a feat not yet achieved with NGS-derived genomic data for Influenza A. Furthermore, the current generation of Oxford Nanopore hardware and software boasts a 99.1% modal read accuracy, a 1.5 percentage point improvement over the previous generation (Ni, 2023). This trend places Oxford Nanopore on

track to rival Illumina's modal accuracy in the coming years, or even surpass Illumina, should the NGS platform fail to expand its capabilities to include long-read sequencing (Sanderson, 2024).

In recent Influenza A DVG investigations, cDNA sequencing has become the preferred method of sequencing library preparation (Saira, 2013; Vasilijevic, 2017; Te, 2018; Alnaj, 2021; Ranum, 2024; Chapter 2; Chapter 3). However, PCR amplification introduces a risk of bias, affecting the accuracy of segment and deletion junction counts. To enhance precision, researchers now use DNA primers with unique molecular identifiers (UMIs) during the reverse transcriptase reaction, incorporating UMIs into viral cDNA before amplification. In the bioinformatics process, amplicons with identical UMIs are collapsed into a single representative read, accurately reflecting the true count of viral cDNA (Karst, 2021). Advancements in direct RNA sequencing on third-generation sequencing platforms (Keller, 2018) promise further innovation by eliminating the need for PCR and UMI-deduplication (Ranum, 2024). In lieu of the mainstream adoption of direct RNA sequencing in the Influenza A DVG research, UMI-deduplicated amplicons are classified as DVGs and SVGs and summed to yield the total viral genomes (TVG). Dividing DVG by TVG provides a precise relative abundance of DVGs and an accurate count of mapped deletion junctions based on the actual count of genomic segments (Chapter 2; Chapter 3).

Conclusion

The mechanism(s) of *de novo* DVG production during Influenza A infection remains unsolved. The discovery of related factors that impact the production of DVGs and non-infectious viral particles holds the promise of informing the chain of events that lead to the *de novo* emergence of DVGs. The potential for the host cell to modulate Influenza A DVG production is a logical target of inquiry because of the utter dependence viral pathogenesis has on host cell machinery. *Host effects* were pursued for a time (Ginsberg, 1964; Choppin, 1969; Choppin, 1970; De, 1980), but abandoned in the wake of findings that increasingly pointed to the multiplicity of DIPs in the inoculum as the main contributor of DVG production (Choppin, 1970; De, 1980; Bangham, 1990). There has also been an absence of a concerted effort to uncover the causes and mechanisms behind DVG *de novo* emergence in the subfield of Influenza A DI research, which was most likely due to the absence of methodologies to quantity DVGs and non-infectious with the requisite precision, at meaningful resolutions, and with sufficient throughput. Fortunately, methodological innovations such as cluster-forming assay to titer non-infectious particles (Chapter 2; Amarilla, 2021), and the combination of long-read genome sequencing with unique molecular identifier deduplication to titer DVGs directly (Jaworski, 2017; Chapter 2; Chapter 3) have led to discovery of associations between the host cell state—particularly metabolism and metabolic signaling—and DVG production. Hopefully, these new methodologies and discoveries will facilitate more discoveries, and the eventual mapping of mechanisms that underlie *de novo* DVG production.

Acknowledgements

This project was funded by NIH grant 4R00AI119401-02 to SDM. IA was supported by NIH grant 4R00AI119401-02 to SDM and Craft Consult Biotechnology Dissertation Fellowship. John Albeck and Enoch Baldwin provided helpful feedback on this manuscript.

References

1. ACKERMANN WW, KLERNSCHMIDT E. Concerning the relation of the Krebs cycle to virus propagation. J Biol Chem. 1951 Mar;189(1):421-8. PMID: 14832255.

2. Aggarwal S, Bradel-Tretheway B, Takimoto T, Dewhurst S, Kim B. Biochemical characterization of enzyme fidelity of influenza A virus RNA polymerase complex. PLoS One. 2010 Apr 29;5(4):e10372. doi: 10.1371/journal.pone.0010372. PMID: 20454455; PMCID: PMC2861597.

3. Al-Saffar NM, Jackson LE, Raynaud FI, Clarke PA, Ramírez de Molina A, Lacal JC, Workman P, Leach MO. The phosphoinositide 3-kinase inhibitor PI-103 downregulates choline kinase alpha leading to phosphocholine and total choline decrease detected by magnetic resonance spectroscopy. Cancer Res. 2010 Jul 1;70(13):5507-17. doi: 10.1158/0008-5472.CAN-09-4476. Epub 2010 Jun 15. PMID: 20551061; PMCID: PMC2896552.

4. Amarilla AA, Modhiran N, Setoh YX, Peng NYG, Sng JDJ, Liang B, McMillan CLD, Freney ME, Cheung STM, Chappell KJ, Khromykh AA, Young PR, Watterson D. An Optimized High-Throughput Immuno-Plaque Assay for SARS-CoV-2. Front Microbiol. 2021 Feb 12;12:625136. doi: 10.3389/fmicb.2021.625136. PMID: 33643253; PMCID: PMC7906992.

5. Bangham CR, Kirkwood TB. Defective interfering particles: effects in modulating virus growth and persistence. Virology. 1990 Dec;179(2):821-6. doi: 10.1016/0042-6822(90)90150-p. PMID: 2238471.

6. Beauclair G, Mura M, Combredet C, Tangy F, Jouvenet N, Komarova AV. *DI-tector*: defective interfering viral genomes' detector for next-generation sequencing data. RNA. 2018 Oct;24(10):1285-1296. doi: 10.1261/rna.066910.118. Epub 2018 Jul 16. PMID: 30012569; PMCID: PMC6140465.

7. BLOUGH HA. The effect of vitamin A alcohol on the morphology of myxoviruses. I. The production and comparison of artificially produced filamentous virus. Virology. 1963 Mar;19:349-58. doi: 10.1016/0042-6822(63)90074-6. PMID: 13971826.

8. Blough HA, Merlie JP, Tiffany JM. The fatty acid composition of incomplete influenza virus. Biochem Biophys Res Commun. 1969 Mar 31;34(6):831-4. doi: 10.1016/0006-291x(69)90255-1. PMID: 5779767.

9. Blough HA, Merlie JP. The lipids of incomplete influenza virus. Virology. 1970 Mar;40(3):685-92. doi: 10.1016/0042-6822(70)90213-8. PMID: 5461847.

10. Cheng C, Fei Z, Xiao P. Methods to improve the accuracy of next-generation sequencing. Front Bioeng Biotechnol. 2023 Jan 20;11:982111. doi: 10.3389/fbioe.2023.982111. PMID: 36741756; PMCID: PMC9895957.

11. Cho JH, Zhao B, Shi J, Savage N, Shen Q, Byrnes J, Yang L, Hwang W, Li P. Molecular recognition of a host protein by NS1 of pandemic and seasonal influenza A viruses. Proc Natl Acad Sci U S A. 2020 Mar 24;117(12):6550-6558. doi: 10.1073/pnas.1920582117. Epub 2020 Mar 9. PMID: 32152123; PMCID: PMC7104383.

12. Choppin PW. Replication of influenza virus in a continuous cell line: high yield of infective virus from cells inoculated at high multiplicity. Virology. 1969 Sep;39(1):130-4. doi: 10.1016/0042-6822(69)90354-7. PMID: 4980034.

13. Choppin PW, Pons MW. The RNAs of infective and incomplete influenza virions grown in MDBK and HeLa cells. Virology. 1970 Nov;42(3):603-10. doi: 10.1016/0042-6822(70)90306-5. PMID: 5529979.

14. COOPER PD. The plaque assay of animal viruses. Adv Virus Res. 1961;8:319-78. doi: 10.1016/s0065-3527(08)60689-2. PMID: 13881155.

15. Crumpton WM, Dimmock NJ, Minor PD, Avery RJ. The RNAs of defective-interfering influenza virus. Virology. 1978 Oct 15;90(2):370-3. doi: 10.1016/0042-6822(78)90322-7. PMID: 726256.

16. Davis AR, Hiti AL, Nayak DP. Influenza defective interfering viral RNA is formed by internal deletion of genomic RNA. Proc Natl Acad Sci U S A. 1980 Jan;77(1):215-9. doi: 10.1073/pnas.77.1.215. PMID: 6928614; PMCID: PMC348239.

17. De BK, Nayak DP. Defective interfering influenza viruses and host cells: establishment and maintenance of persistent influenza virus infection in MDBK and HeLa cells. J Virol. 1980 Dec;36(3):847-59. doi: 10.1128/JVI.36.3.847-859.1980. PMID: 7463559; PMCID: PMC353712.

18. Dimmock NJ, Easton AJ. Defective interfering influenza virus RNAs: time to reevaluate their clinical potential as broad-spectrum antivirals? J Virol. 2014 May;88(10):5217-27. doi: 10.1128/JVI.03193-13. Epub 2014 Feb 26. PMID: 24574404; PMCID: PMC4019098.

19. Dobin A, Davis CA, Schlesinger F, Drenkow J, Zaleski C, Jha S, Batut P, Chaisson M, Gingeras TR. STAR: ultrafast universal RNA-seq aligner. Bioinformatics. 2013 Jan 1;29(1):15-21. doi: 10.1093/bioinformatics/bts635. Epub 2012 Oct 25. PMID: 23104886; PMCID: PMC3530905.

20. Dong G, Peng C, Luo J, Wang C, Han L, Wu B, Ji G, He H. Adamantane-resistant influenza a viruses in the world (1902-2013): frequency and distribution of M2 gene mutations. PLoS One. 2015 Mar 13;10(3):e0119115. doi: 10.1371/journal.pone.0119115. PMID: 25768797; PMCID: PMC4358984.

21. Eddy SR. Accelerated Profile HMM Searches. PLoS Comput Biol. 2011 Oct;7(10):e1002195. doi: 10.1371/journal.pcbi.1002195. Epub 2011 Oct 20. PMID: 22039361; PMCID: PMC3197634.

22. Fonville JM, Marshall N, Tao H, Steel J, Lowen AC. Influenza Virus Reassortment Is Enhanced by Semi-infectious Particles but Can Be Suppressed by Defective Interfering Particles. PLoS Pathog. 2015 Oct 6;11(10):e1005204. doi: 10.1371/journal.ppat.1005204. PMID: 26440404; PMCID: PMC4595279.

23. Frensing T, Pflugmacher A, Bachmann M, Peschel B, Reichl U. Impact of defective interfering particles on virus replication and antiviral host response in cell culture-based influenza vaccine production. Appl Microbiol Biotechnol. 2014 Nov;98(21):8999-9008. doi: 10.1007/s00253-014-5933-y. Epub 2014 Aug 19. PMID: 25132064.

24. Ganai RA, Johansson E. DNA Replication-A Matter of Fidelity. Mol Cell. 2016 Jun 2;62(5):745-55. doi: 10.1016/j.molcel.2016.05.003. PMID: 27259205.

25. Gardner EM, Beli E, Clinthorne JF, Duriancik DM. Energy intake and response to infection with influenza. Annu Rev Nutr. 2011 Aug 21;31:353-67. doi: 10.1146/annurev-nutr-081810-160812. PMID: 21548773.

26. GINSBERG HS. Formation of non-infectious influenza virus in mouse lungs: its dependence upon extensive pulmonary consolidation initiated by the viral inoculum. J Exp Med. 1954 Dec 1;100(6):581-603. doi: 10.1084/jem.100.6.581. PMID: 13211916; PMCID: PMC2136397.

27. Hale BG, Jackson D, Chen YH, Lamb RA, Randall RE. Influenza A virus NS1 protein binds p85beta and activates phosphatidylinositol-3-kinase signaling. Proc Natl Acad Sci U S A. 2006 Sep 19;103(38):14194-9. doi: 10.1073/pnas.0606109103. Epub 2006 Sep 8. PMID: 16963558; PMCID: PMC1599933.

28. Henle W, Henle G. INTERFERENCE OF INACTIVE VIRUS WITH THE PROPAGATION OF VIRUS OF INFLUENZA. Science. 1943 Jul 23;98(2534):87-9. doi: 10.1126/science.98.2534.87. PMID: 17749157.

29. Hirst GK. THE QUANTITATIVE DETERMINATION OF INFLUENZA VIRUS AND ANTIBODIES BY MEANS OF RED CELL AGGLUTINATION. J Exp Med. 1942 Jan 1;75(1):49-64. doi: 10.1084/jem.75.1.49. PMID: 19871167; PMCID: PMC2135212.

30. Honce R, Schultz-Cherry S. Impact of Obesity on Influenza A Virus Pathogenesis, Immune Response, and Evolution. Front Immunol. 2019 May 10;10:1071. doi: 10.3389/fimmu.2019.01071. PMID: 31134099; PMCID: PMC6523028.

31. Honce R, Karlsson EA, Wohlgemuth N, Estrada LD, Meliopoulos VA, Yao J, Schultz-Cherry S. Obesity-Related Microenvironment Promotes Emergence of Virulent Influenza Virus Strains. mBio. 2020 Mar 3;11(2):e03341-19. doi: 10.1128/mBio.03341-19. PMID: 32127459; PMCID: PMC7064783.

32. Janda JM, Davis AR, Nayak DP, De BK. Diversity and generation of defective interfering influenza virus particles. Virology. 1979 May;95(1):48-58. doi: 10.1016/0042-6822(79)90400-8. PMID: 442544.

33. Jaworski E, Routh A. Parallel ClickSeq and Nanopore sequencing elucidates the rapid evolution of defective-interfering RNAs in Flock House virus. PLoS Pathog. 2017 May 5;13(5):e1006365. doi: 10.1371/journal.ppat.1006365. PMID: 28475646; PMCID: PMC5435362.

34. Jennings PA, Finch JT, Winter G, Robertson JS. Does the higher order structure of the influenza virus ribonucleoprotein guide sequence rearrangements in influenza viral RNA? Cell. 1983 Sep;34(2):619-27. doi: 10.1016/0092-8674(83)90394-x. PMID: 6616623.

35. Karst SM, Ziels RM, Kirkegaard RH, Sørensen EA, McDonald D, Zhu Q, Knight R, Albertsen M. High-accuracy long-read amplicon sequences using unique molecular identifiers with Nanopore or PacBio sequencing. Nat Methods. 2021 Feb;18(2):165-169. doi: 10.1038/s41592-020-01041-y. Epub 2021 Jan 11. PMID: 33432244.

36. Keller MW, Rambo-Martin BL, Wilson MM, Ridenour CA, Shepard SS, Stark TJ, Neuhaus EB, Dugan VG, Wentworth DE, Barnes JR. Direct RNA Sequencing of the Coding Complete Influenza A Virus Genome. Sci Rep. 2018 Sep 26;8(1):14408. doi: 10.1038/s41598-018-32615-8. Erratum in: Sci Rep. 2018 Oct 19;8(1):15746. PMID: 30258076; PMCID: PMC6158192.

37. KILBOURNE ED. Inhibition of influenza virus multiplication with a glucose antimetabolite (2-deoxy-D-glucose). Nature. 1959 Jan 24;183(4656):271-2. doi: 10.1038/183271b0. PMID: 13622777.

38. Kim D, Pertea G, Trapnell C, Pimentel H, Kelley R, Salzberg SL. TopHat2: accurate alignment of transcriptomes in the presence of insertions, deletions and gene fusions. Genome Biol. 2013 Apr 25;14(4):R36. doi: 10.1186/gb-2013-14-4-r36. PMID: 23618408; PMCID: PMC4053844.

39. Kuss-Duerkop SK, Wang J, Mena I, White K, Metreveli G, Sakthivel R, Mata MA, Muñoz-Moreno R, Chen X, Krammer F, Diamond MS, Chen ZJ, García-Sastre A, Fontoura BMA. Influenza virus differentially activates mTORC1 and mTORC2 signaling to maximize late stage replication. PLoS Pathog. 2017 Sep 27;13(9):e1006635. doi: 10.1371/journal.ppat.1006635. PMID: 28953980; PMCID: PMC5617226.

40. Li Y, Anderson DH, Liu Q, Zhou Y. Mechanism of influenza A virus NS1 protein interaction with the p85beta, but not the p85alpha, subunit of phosphatidylinositol 3-kinase (PI3K) and up-regulation of PI3K activity. J Biol Chem. 2008 Aug 22;283(34):23397-409. doi: 10.1074/jbc.M802737200. Epub 2008 Jun 5. PMID: 18534979.

41. Liu G, Summer R. Cellular Metabolism in Lung Health and Disease. Annu Rev Physiol. 2019 Feb 10;81:403-428. doi: 10.1146/annurev-physiol-020518-114640. Epub 2018 Nov 28. PMID: 30485759; PMCID: PMC6853603.

42. Lopes AM, Domingues P, Zell R, Hale BG. Structure-Guided Functional Annotation of the Influenza A Virus NS1 Protein Reveals Dynamic Evolution of the p85β-Binding Site during Circulation in Humans. J Virol. 2017 Oct 13;91(21):e01081-17. doi: 10.1128/JVI.01081-17. PMID: 28814525; PMCID: PMC5640874.

43. Lunt SY, Vander Heiden MG. Aerobic glycolysis: meeting the metabolic requirements of cell proliferation. Annu Rev Cell Dev Biol. 2011;27:441-64. doi: 10.1146/annurev-cellbio-092910-154237. PMID: 21985671.

44. Luo Y, Xu W, Li G, Cui W. Weighing In on mTOR Complex 2 Signaling: The Expanding Role in Cell Metabolism. Oxid Med Cell Longev. 2018 Oct 30;2018:7838647. doi: 10.1155/2018/7838647. PMID: 30510625; PMCID: PMC6232796.

45. Manzoni TB, López CB. Defective (interfering) viral genomes re-explored: impact on antiviral immunity and virus persistence. Future Virol. 2018 Jul;13(7):493-503. doi: 10.2217/fvl-2018-0021. Epub 2018 Jun 12. PMID: 30245734; PMCID: PMC6136085.

46. Ni Y, Liu X, Simeneh ZM, Yang M, Li R. Benchmarking of Nanopore R10.4 and R9.4.1 flow cells in single-cell whole-genome amplification and whole-genome shotgun sequencing. Comput Struct Biotechnol J. 2023 Mar 24;21:2352-2364. doi: 10.1016/j.csbj.2023.03.038. PMID: 37025654; PMCID: PMC10070092.

47. Nayak DP, Tobita K, Janda JM, Davis AR, De BK. Homologous interference mediated by defective interfering influenza virus derived from a temperature-sensitive mutant of influenza virus. J Virol. 1978 Oct;28(1):375-86. doi: 10.1128/JVI.28.1.375-386.1978. PMID: 702654; PMCID: PMC354277.

48. Ren L, Zhang W, Han P, Zhang J, Zhu Y, Meng X, Zhang J, Hu Y, Yi Z, Wang R. Influenza A virus (H1N1) triggers a hypoxic response by stabilizing hypoxia-inducible factor-1α via inhibition of proteasome. Virology. 2019 Apr;530:51-58. doi: 10.1016/j.virol.2019.02.010. Epub 2019 Feb 11. PMID: 30780125.

49. Ren L, Zhang W, Zhang J, Zhang J, Zhang H, Zhu Y, Meng X, Yi Z, Wang R. Influenza A Virus (H1N1) Infection Induces Glycolysis to Facilitate Viral Replication. Virol Sin. 2021 Dec;36(6):1532-1542. doi: 10.1007/s12250-021-00433-4. Epub 2021 Sep 14. PMID: 34519916; PMCID: PMC8692537.

50. Routh A, Johnson JE. Discovery of functional genomic motifs in viruses with ViReMa-a Virus Recombination Mapper-for analysis of next-generation sequencing data. Nucleic Acids Res. 2014 Jan;42(2):e11. doi: 10.1093/nar/gkt916. Epub 2013 Oct 16. PMID: 24137010; PMCID: PMC3902915.

51. Routh A, Head SR, Ordoukhanian P, Johnson JE. ClickSeq: Fragmentation-Free Next-Generation Sequencing via Click Ligation of Adaptors to Stochastically Terminated 3'-Azido cDNAs. J Mol Biol. 2015 Aug 14;427(16):2610-6. doi: 10.1016/j.jmb.2015.06.011. Epub 2015 Jun 24. PMID: 26116762; PMCID: PMC4523409.

52. Saha A, Connelly S, Jiang J, Zhuang S, Amador DT, Phan T, Pilz RB, Boss GR. Akt phosphorylation and regulation of transketolase is a nodal point for amino acid control of purine synthesis. Mol Cell. 2014 Jul 17;55(2):264-76. doi: 10.1016/j.molcel.2014.05.028. Epub 2014 Jun 26. PMID: 24981175; PMCID: PMC4104231.

53. Saira K, Lin X, DePasse JV, Halpin R, Twaddle A, Stockwell T, Angus B, Cozzi-Lepri A, Delfino M, Dugan V, Dwyer DE, Freiberg M, Horban A, Losso M, Lynfield R, Wentworth DN, Holmes EC, Davey R, Wentworth DE, Ghedin E; INSIGHT FLU002 Study Group; INSIGHT FLU003 Study Group. Sequence analysis of in vivo defective interfering-like RNA of influenza A H1N1 pandemic virus. J Virol. 2013 Jul;87(14):8064-74. doi: 10.1128/JVI.00240-13. Epub 2013 May 15. PMID: 23678180; PMCID: PMC3700204.

54. Sanderson ND, Hopkins KMV, Colpus M, Parker M, Lipworth S, Crook D, Stoesser N. Evaluation of the accuracy of bacterial genome reconstruction with Oxford Nanopore R10.4.1 long-read-only sequencing. Microb Genom. 2024 May;10(5). doi: 10.1099/mgen.0.001246. PMID: 38713194.

55. Silva T, S Salomon P, Hamerski L, Walter J, B Menezes R, Siqueira JE, Santos A, Santos JAM, Ferme N, Guimarães T, O Fistarol G, I Hargreaves P, Thompson C, Thompson F, Souza TM, Siqueira M, Miranda M. Inhibitory effect of microalgae and cyanobacteria extracts on influenza virus replication and neuraminidase activity. PeerJ. 2018 Oct 26;6:e5716. doi: 10.7717/peerj.5716. PMID: 30386690; PMCID: PMC6204821.

56. Sotcheff S, Zhou Y, Yeung J, Sun Y, Johnson JE, Torbett BE, Routh AL. ViReMa: a virus recombination mapper of next-generation sequencing data characterizes diverse recombinant viral nucleic acids. Gigascience. 2023 Mar 20;12:giad009. doi: 10.1093/gigascience/giad009. PMID: 36939008; PMCID: PMC10025937.

57. Sun Y, Kim EJ, Felt SA, Taylor LJ, Agarwal D, Grant GR, López CB. A specific sequence in the genome of respiratory syncytial virus regulates the generation of copy-back defective viral genomes. PLoS Pathog. 2019 Apr 17;15(4):e1007707. doi: 10.1371/journal.ppat.1007707. Erratum in: PLoS Pathog. 2019 Oct 3;15(10):e1008099. PMID: 30995283; PMCID: PMC6504078.

58. Te Velthuis AJW, Long JC, Bauer DLV, Fan RLY, Yen HL, Sharps J, Siegers JY, Killip MJ, French H, Oliva-Martín MJ, Randall RE, de Wit E, van Riel D, Poon LLM, Fodor E. Mini viral RNAs act as innate immune agonists during influenza virus infection. Nat Microbiol. 2018 Nov;3(11):1234-1242. doi: 10.1038/s41564-018-0240-5. Epub 2018 Sep 17. PMID: 30224800; PMCID: PMC6203953.

59. Vasilijevic J, Zamarreño N, Oliveros JC, Rodriguez-Frandsen A, Gómez G, Rodriguez G, Pérez-Ruiz M, Rey S, Barba I, Pozo F, Casas I, Nieto A, Falcón A. Reduced accumulation of defective viral genomes contributes to severe outcome in influenza virus infected patients. PLoS Pathog. 2017 Oct 12;13(10):e1006650. doi: 10.1371/journal.ppat.1006650. PMID: 29023600; PMCID: PMC5638565.

60. VON MAGNUS P. Incomplete forms of influenza virus. Adv Virus Res. 1954;2:59-79. doi: 10.1016/s0065-3527(08)60529-1. PMID: 13228257.

61. Vignuzzi M, López CB. Defective viral genomes are key drivers of the virus-host interaction. Nat Microbiol. 2019 Jul;4(7):1075-1087. doi: 10.1038/s41564-019-0465-y. Epub 2019 Jun 3. PMID: 31160826; PMCID: PMC7097797.

62. Wang C, Honce R, Salvatore M, Chow D, Randazzo D, Yang J, Twells NM, Mahal LK, Schultz-Cherry S, Ghedin E. Influenza Defective Interfering Virus Promotes Multiciliated Cell Differentiation and Reduces the Inflammatory Response in Mice. J Virol. 2023 Jun 29;97(6):e0049323. doi: 10.1128/jvi.00493-23. Epub 2023 May 31. PMID: 37255439; PMCID: PMC10308934.

63. Wu M, Zhou E, Sheng R, Fu X, Li J, Jiang C, Su W. Defective Interfering Particles of Influenza Virus and Their Characteristics, Impacts, and Use in Vaccines and Antiviral Strategies: A Systematic Review. Viruses. 2022 Dec 12;14(12):2773. doi: 10.3390/v14122773. PMID: 36560777; PMCID: PMC9781619.

64. Yeung J, Routh AL. ViReMaShiny: an interactive application for analysis of viral recombination data. Bioinformatics. 2022 Sep 15;38(18):4420-4422. doi: 10.1093/bioinformatics/btac522. PMID: 35904541; PMCID: PMC9477530.

65. Zhang T, Yin C, Boyd DF, Quarato G, Ingram JP, Shubina M, Ragan KB, Ishizuka T, Crawford JC, Tummers B, Rodriguez DA, Xue J, Peri S, Kaiser WJ, López CB, Xu Y, Upton JW, Thomas PG, Green DR, Balachandran S. Influenza Virus Z-RNAs Induce ZBP1-Mediated Necroptosis. Cell. 2020 Mar 19;180(6):1115-1129.e13. doi: 10.1016/j.cell.2020.02.050. PMID: 32200799; PMCID: PMC7153753.

Influenza A defective viral genomes and non-infectious particles are increased by host PI3K inhibition via anti-cancer drug alpelisib

Running head: Host cell metabolism affects influenza A defective virus production

Ilechukwu Agu[1], Ivy José[1], Abhineet Ram[2], Daniel Oberbauer[2], John Albeck[2], Samuel L. Díaz Muñoz[1, 3*]

[1] Department of Microbiology and Molecular Genetics
University of California, Davis
One Shields Ave
Davis CA 95616

[2] Department of Molecular and Cellular Biology,
University of California, Davis
One Shields Ave
Davis CA 95616

[3] Genome Center
University of California, Davis
One Shields Ave
Davis CA 95616

*Address correspondence to: Samuel L. Díaz Muñoz, samdiazmunoz@ucdavis.edu

Abstract

RNA viruses produce abundant defective viral genomes during replication, setting the stage for interactions between viral genomes that alter the course of pathogenesis. Harnessing these interactions to develop antivirals has become a recent goal of intense research focus. Despite decades of research, the mechanisms that regulate the production and interactions of Influenza A defective viral genomes are still unclear. The role of the host is essentially unexplored; specifically, it remains unknown whether host metabolism can influence the formation of defective viral genomes and the particles that house them. To address this question, we manipulated host cell anabolic signaling activity and monitored the production of defective viral genomes and particles by A/H1N1 and A/H3N2 strains, using a combination of single-cell immunofluorescence quan-

tification, third-generation long-read sequencing, and the cluster-forming assay, a novel method we developed to titer defective and fully-infectious particles simultaneously. Here we show that alpelisib (Piqray), a highly selective inhibitor of mammalian Class 1a phosphoinositide-3 kinase (PI3K) receptors, significantly changed the proportion of defective particles and viral genomes (specifically deletion-containing viral genomes) in a strain-specific manner, under conditions that minimize multiple cycles of replication. alpelisib pre-treatment of cells led to an increase in defective particles in the A/H3N2 strain, while the A/H1N1 strain showed a decrease in total viral particles. In the same infections, we found that defective viral genomes of polymerase segments increased in both the A/H3N2 and A/H1N1 strains. The A/H1N1 strain, additionally showed a dose-dependent increase in total number of defective viral genomes. In sum, we provide evidence that host cell metabolism can increase the production of defective viral genomes and particles at an early stage of infection, shifting the makeup of the infection and potential interactions among virions. Given that Influenza A defective viral genomes can inhibit pathogenesis, our study presents a new line of investigation into metabolic states associated with less severe flu infection and the potential induction of these states with metabolic drugs.

Introduction

RNA virus infections frequently produce defective viral genomes, which can influence the course of infection through interactions such as complementation and interference (Dimmock, 2014). Non-clinical studies have extensively associated defective viral genome accumulation with reduced disease severity, while fewer but notable clinical studies have demonstrated this trend in Influenza A (Vasilijevic, 2017) and Respiratory Syncytial Virus (Felt, 2021) infections (Brennan, 2024). Consequently, defective viral genomes have become a recent focus of intense pre-clinical research (Smith, 2016; Meng, 2017; Wasik, 2018; Zhao, 2018; Bdier, 2019; Yamagata, 2019; Tapia, 2019; Harding, 2019), with their antiviral potential holding substantial implications for clinical applications and pandemic preparedness.

The study of the mechanisms that influence the production of defective viral genomes and the outcome of these virus-virus interactions during an infection have become a top priority in order to realize their public health potential. Influenza A virus infections are primarily composed of virions that cannot mount a complete infectious cycle. Only 1 – 30% of virions can propagate fully from cell to cell (Brooke, 2013; Brooke, 2017; Diefenbacher, 2018). While there are a variety of reasons why virions are not fully infectious—for example SNPs, faulty protein expression etc—virions harboring genome segments with internal sequence deletions (Davis, 1980; Nayak, 1982; Saira, 2013) are termed defective interfering particles (DIP) because their accumulation by *de novo* or exogenous means diminishes the productivity of Influenza A infections and leads to mild disease outcomes; a phenomenon termed *defective interference* (DI) (Dimmock, 2014; Manzoni, 2018; Vignuzi, 2019; Wu, 2022). These deletion-containing viral genomes (hereafter

DelVGs, after Alnaji et al. 2019) do not produce the proteins necessary for a single DIP to complete an infection, leading to a non-propagative infection that relies on virus coinfection to disseminate (Yamagata, 2019). However, upon complementation, DelVGs and their encoded defective proteins (Ranum, 2024) actively interfere with the production of full-length viruses. This rising relative abundance of DelVGs at the expense of full-length viral genomes (Dimmock, 2014; Ranum, 2024) has been associated with mild disease outcomes (Vasilijevic, 2017). This flood of complementation-dependent virions sets the stage for interactions that can alter the course of Influenza A pathogenesis, inspiring research into the factors that influence the generation of DelVGs.

DelVGs have been associated with high infection multiplicity (Von Magnus, 1954) and specific mutations of the viral polymerase (Rodriguez, 2013; Vasilijevic, 2017) or matrix genes (Perez-Cidoncha, 2014). At a molecular level, the best evidence on how DelVGs are generated (Alnaji, 2020) supports a model whereby the polymerase pauses synthesis while still processing template and resumes synthesis downstream, leading to an internal deletion (Nayak, 1982; Winter, 1981). The molecular determinants of this pause and why it occurs more frequently in some viral genome segments remains unknown (Alnaji, 2020). While it was dogma that a packaging advantage (Brooke, 2014; Alnaji, 2021; Meng, 2017; Odagiri, 1997) was the mechanism behind DelVG suppression of full-length virus (Brooke, 2014; Von Magnus, 1954; Pelz, 2021; Huang, 1970; Frensing, 2013; Alnaji, 2020), a recent study examining *de novo* intracellular DelVG generation in strain PR8 suggests that there is no packaging advantage (Alnaji, 2021). Studies have shown that both the DelVG RNA and its encoded proteins contribute to the suppression of full-

length virus (Meng, 2017; Dadonaite, 2019; Hara, 2013; Octaviani 2011, Ranum, 2024). Notably, a recent study suggests that protein production from DelVGs was considerable and that some of these proteins competed for binding with their full-length cognates, impairing polymerase function (Ranum, 2024). Thus, considerable effort has gone into investigating the viral factors that influence DelVG production and the effects of DelVGs on the host (Wang, 2023). However, an almost completely unexplored potential modulator of DelVG production is the host cell.

Host cell variables, particularly metabolism and metabolic signaling, can affect progeny virus yield and the severity of infection. A comprehensive review of the impact of extreme nutritional states—such as caloric restriction and diet-induced obesity—on flu infection found eroded immune response and survivability in mice (Gardner, 2011). In humans, non-obese patient groups routinely shed lower progeny viral loads relative to obese patient groups (Honce, 2019; Honce, 2020). At a cellular level, reprogramming host tricarboxylic acid cycle with excess malonate diminishes total viral progeny yield in a dose-dependent manner (Ackermann, 1951). Influenza A itself has adaptations to steer host metabolism in a manner that facilitates productive infection, further proof of the outsized role of host metabolism in influenza pathogenesis. Specifically, some flu strains have specific mutations that affect PI3K, a crucial upstream gatekeeper of pro-growth signal transduction networks (Wee, 2017 ; Hopkins, 2020). A highly-conserved Y89 residue on the influenza NS1 effector protein has a selective and inhibitory interaction with the SH2 domain of host p85β—the regulatory subunit of Class 1a phosphoinositide-3-kinase (PI3K)—which unleashes the catalytic p110α subunit to aberrantly activate PI3K signaling in the ab-

sence of a bona fide signaling growth factor like insulin (Hale, 2006; Li, 2008). Thus, the action of NS1 contorts host metabolism into a state characterized by increased pools of the very precursor metabolites (Luo, 2018 ; Saha, 2014 ; Al-Saffer, 2010) necessary for uninterrupted biosynthesis of virion components, facilitating pathogenesis (Hale, 2006; Li, 2008). Inhibiting NS1::p85β with ΔNS1(Y89F) expectedly diminishes viral-induced PI3K activation and progeny yield (Hale, 2006). Because diminished viral yield can result from DelVG accumulation and the inducers of DelVG production remain unknown, it is a reasonable secondary hypothesis that NS1::p85β inhibition—or other form of PI3K inactivation—diminishes viral yield wholly or in part via the induction of DelVG production. However, to our knowledge, the impact of host metabolic signaling on the production of Influenza A defective particles and DelVGs has not been studied.

Given the well-established crosstalk between host metabolism and Influenza A pathogenesis, it is surprising more research has not focused on the role of hosts in shaping DelVG production. A key barrier to the pursuit of this missed opportunity is the lack of tools that can quantitatively measure the virion and genome composition of infections. To fill this gap, we implemented two tools. First, we developed the cluster-forming assay to simultaneously titer defective and fully infectious Influenza A virions by modifying the well-known immunofocus assay (Baker, 2013) and implementing a computational pipeline that automated analysis of fluorescent microscopy images. Second, to quantify DelVGs and full-length genomic segments simultaneously, we used long-read sequencing of whole genome amplicons with unique molecular identifiers (UMI) to enable read de-duplication (Routh, 2013; Jaworski, 2017; Sotcheff, 2023; Karst, 2021). Armed

with these tools, knowledge of flu-induced PI3K-AKT pathway activation, and single-cell phospho-AKT (pAKT) measurement as a readout for PI3K network activity, we explored if alpelisib —a highly selective small molecule inhibitor of PI3K (Furet, 2013; Fritsch, 2014; Yang, 2019)— affected defective virion and DelVG production. We hypothesized that disrupting flu-mediated activation of PI3K signaling with alpelisib would increase defective virion and DelVG production.

We found that alpelisib pre-treatment increases DelVG production in both circulating human Influenza A virus subtypes, and changes the viron composition of infections. We first confirmed that alpelisib suppresses PI3K network signaling activity in MDCK-London cells and that this treatment overrides virus-induced PI3K network signaling upregulation during infections. Under these conditions, alpelisib increased DelVGs production in both strains, with further evidence for a dose-dependent effect in the A/H1N1 strain. At the virion level, the proportion of defective particles in the A/H3N2 strain was significantly altered, while the total number of viral particles in the A/H1N1 strain was significantly. Collectively, these results suggest that host Class 1a PI3K metabolic signaling receptors inactivation affects the outcome of Influenza A virus infections, steering the population towards more defective particles and DelVGs. Our results highlight the importance of host cell factors in determining the outcome of influenza virus infections, potentially informing host metabolic states that predict infection outcomes (Engels, 2017), as well as therapeutics that can induce host-mediated changes towards mild infection outcomes.

Methods

Cells and Viruses

We obtained MDCK-London cells from the Unites States Centers for Disease Control and Prevention (CDC) Influenza Reagent Resource (IRR). We maintained cells in minimum essential media (MEM) plus 5% fetal bovine serum (FBS). Egg-passaged wildtype A/California/07/2009(H1N1) and A/Texas/50/2012(H3N2) influenza strains were a gift from the lab of Dr. Ted Ross. These initial stocks were double plaque purified in MDCK cells (ATCC/BEI) and propagated thereafter at low multiplicity of infection (MOI = 0.001) in MDCK cells (ATCC/BEI).

Alpelisib Dosing Assay

To confirm that alpelisib inhibits PI3K network signaling in MDCK-London cells, we seeded MDCK-London cells overnight at low density in MEM plus 5% FBS media for 24 hr into collagen-treated, glass-bottom 96-well tissue culture plates. We then serum-weaned the partially confluent monolayers for 24 hr in MEM plus 5% bovine serum albumin (BSA). Three hours prior to conclusion of serum weaning, we spiked a 10 uL pre-treatment of DMSO vehicle control or 21X alpelisib directly into 200 uL of the serum weaning supernatant to reach a 1X concentration. At the end of serum weaning, we mock-infected monolayers with MEM plus 2% BSA and 1% Anti-Anti (Virus Infection Media; VIM) or virus-infected at a multiplicity (MOI) of 1 in VIM; no trypsin was used. As part of the inoculation regimen, we spiked 1.9 uL of DMSO or 21X alpelisib into 40 uL of the inoculum supernatant for a 1X concentration, in order to sustain drug effects throughout the virus-monolayer adsorption period. After the 1 hr adsorption incubation,

we aspirated inocula, washed monolayers and topped with VIM, and we spiked 10 uL of DMSO or 21X alpelisib directly into 200 uL of VIM supernatant for a 1X concentration. After 17 hr p.i., we harvested and titrated supernatants to determine fully infectious (i.e., propagation-capable) and defective (i.e. propagation-incapable) progeny virus yield via the novel cluster-forming assay (see Methods and Supplementary Materials). We fixed monolayers, conducted immunofluorescence (IF) staining, and imaged to derive cellular-level phospho-AKT signal intensity (see Methods) as a readout for PI3K network signaling activity. We ran three biological replicates of the experiment on different days.

Single-cell Dose Response pAKT Immunofluorescence Quantification

At the end of the alpelisib-treated flu infections, we fixed monolayers with 4% paraformaldehyde (PFA). Primary staining was carried out with rabbit monoclonal antibodies targeting pAKT(S473) (Cell Signaling mAb#4060) and mouse monoclonal antibodies targeting Influenza A nucleoprotein (Millipore Sigma MAB8257). Secondary staining was respectively carried out with fluorophore-conjugated goat-anti-rabbit (Thermo Fisher Scientific A-21245) and goat-anti-mouse (Jackson ImmunoResearch 115-645-062) antibodies. We imaged IF-stained monolayers on a Andor Zyla 5.5 scMOS camera and a 20x/0.75 NA objective microscope. Images were then processed to derive cellular-level pAKT, and nucleoprotein signal intensities. The image data were stored as .nd2 files and retrieved using the Bio-Formats toolbox for MATLAB, which can be obtained from www.openmicroscopy.org/bio-formats. Subsequently, a specialized MATLAB cell segmentation pipeline (Pargett, 2017) was employed to process the images. Briefly, this pipeline utilized Hoechst 33342 as nuclear markers to identify the nuclei of individual cells. Af-

ter cell identification and segmentation, single-cell pAKT signal was quantified by calculating the average pixel intensities within each individual cell. These intensity values were then background subtracted. To measure the background signal intensity, a well without any cells was imaged. The MATLAB pipeline output florescence for each cells in AU units. To control for any biases in image selection, we randomly subsampled a third of the data set prior to analyses reported; results were comparable with the full data set (see code for details https://github.com/pomoxis/Alpelisib-SIP).

Cluster-forming Assay: Titration of Fully Infectious and Defective Virions

To determine the titer of fully infectious (i.e., propagation-capable) and defective (i.e. propagation-incapable) virions simultaneously, we developed the cluster-forming assay. This assay combines aspects of the conventional plaque assay with the immunocytochemical staining and microscopy. Specifically, the cluster-forming assay employs a low-viscosity overlay medium that remains in a semi-solid state, restricting diffusion of progeny virus to directly adjacent cells, much like a plaque assay. This low viscosity overlay is removable, so that monolayers can be fixed, stained with IF antibodies, and imaged like an immunofocus assay. The basic principle is that virions that were fully infectious would spread from cell to cell, forming clusters of florescence, while virions that were unable to spread would appear as individual foci.

We briefly describe this assay below and provide detailed methods in Supplement: We seeded MDCK-London cells overnight (24 hr) at high density in MEM plus 5% FBS media into colla-

gen-treated, glass-bottom 96-well tissue culture plates. We inoculated the confluent monolayers with serial dilutions of virus-borne supernatant and incubated for 1 hr to facilitate virus-monolayer adsorption, after which we aspirated the inoculum, washed monolayers with VIM, and overlaid monolayers with medium-viscosity culture medium (VIM plus 4% carboxymethyl cellulose and 1 ug/mL TPCK-Trypsin). At 11 hr p.i. we aspirated overlay medium and fixed monolayers with 4% PFA. We stained fixed monolayers with fluorophore-conjugated ICC/IF antibodies targeting Influenza A nucleoprotein (NP) and counter-stained with Hoechst. We imaged IF-stained monolayers on a fluorescence microscope to reveal the number of productive (i.e. infections that spread from cell-to cell) and non-productive units (i.e., infections that did not spread from cell-cell) infection events, respectively depicted by a cluster of infected cells (productive clustering unit/PCU), or solitary infected cells (non-clustering unit/NCU) (**Figure 2.4**, **Supplementary Figures 2.1-2.5**).

To quantify PCUs and NCUs, we utilized MATLAB's image processing toolbox. Immunofluorescence images were processed to create object masks for each unit, and nuclear segmentation was performed via the Hoechst signal. Masks were refined and filtered, and the number of cells within each unit was determined. The R Programming Language was employed to classify clusters as PCUs or NCUs based on size, followed by calculation of NCU titer and proportion.

Viral Genome Sequencing by Nanopore Long-read Sequencing

To derive the genomic sequences of progeny Influenza A virus from our treatments, we began by isolating viral genomic RNA from 100 uL of treatment group supernatants (Zymo Research,

Quick-DNA/RNA Viral MagBead kit R2140). Next, we used a 2-cycle RT-PCR reaction (Invitrogen SuperScript™ III One-Step RT-PCR System with Platinum™ Taq DNA Polymerase kit 12574026) to reverse transcribe viral genomic RNA into the first cDNA strand (1st PCR cycle), and then synthesize the second cDNA strand (2nd PCR cycle). The RT reaction to produce the first cDNA strand was primed with a 45bp forward primer (Integrated DNA Technologies) that included a complementary sequence to the uni12 region shared by all flu genomic segments (12bp), flanked with a unique molecular identifier (UMI) sequence (12bp) and a landing pad sequence for downstream barcoding primers (21bp): fwd 5'-TTTCTGTTGGTGCTGATATTGNNNNNNNNNNNNAGCRAAAGCAGG-3'.

The PCR reaction to generate the second cDNA strand was primed with a 47bp reverse primer that included a complementary sequence to the uni13 region shared by all flu genomic segments (13bp), flanked by a UMI sequence (12bp) and the barcoding primer landing pad sequence (22bp): rev 5'-ACTTGCCTGTCGCTCTATCTTCNNNNNNNNNNNNAGTAGAAACAAGG-3'. We used AMPure XP beads (Beckman Coulter, AMPure XP A63881) with manufacturer's instructions to remove excess primers, followed by a 17-cycle amplification PCR (Invitrogen, Platinum SuperFi Master Mix 12358-050) of the umi-tagged reads with barcoding primers (Oxford Nanopore Technologies, PCR Barcoding Expansion 1-96 kit EXP-PBC096). The low number of cycles was designed to minimize PCR duplicates. We then pooled 60 ng of barcoded amplicons from each sample, cleaned and concentrated this pooled sample (Zymo Research, Select-A-Size DNA Clean & Concentrator D4080), and prepared a sequencing library in accordance with manufacturer instructions (Oxford Nanopore Technologies, Ligation-Sequencing-Kit-V14 SQK-LSK114). We loaded the pooled libraries into an R10 flow cell connected to a MinION MkIB

device and ran a 72 hr sequencing protocol from the MinKNOW control software. Upon sequencing run termination, we used the Guppy basecaller software to barcode-demultiplex sequenced reads into their respective treatment groups.

Classification and Quantification of Full-length and Internal-deletion Viral Segments

Demultiplexed amplicon sequences underwent quality control pre-processing prior to deduplication into representative sequences, after which representative sequences were classified into subgroups for DelVGs and full-length, standard viral genomes (SVG).

Quality Control: Our sequencing library preparation strategy began with a 1-cycle each RT-PCR then PCR addition of 12bp-long UMI sequences to the 3’ and 5’ termini of viral genomic RNA, followed by PCR addition of sequencing barcodes to both termini:

5’-barcode—spacer—landing.pad—UMI—uni12—*locus*—uni13—UMI—landing.pad—spacer—barcode-3’

For quality control, we trimmed off barcode and barcode landing pad regions with C*utadapt*, then used *Cutadapt* once more to filter-in only amplicons with a 12bp-long UMI region. Finally, we confirmed the presence of well-formed uni primer regions in the filtered amplicons before advancing to UMI deduplication.

UMI Deduplication:

We used *UMI-Tools* to sequentially group PCR duplicates by UMI, and then collapse them into a single representative read. In the final quality control step, we trimmed the uni primer region off representative reads with *Cutadapt*. By integrating UMI-deduplication into our workflow, we've mitigated the impact of PCR amplification bias on sequencing depths. Consequently, our delVG and SVG count data represent a quantitative measurement of the abundance of RNA molecules (genome segments) from which the amplicons were derived.

DelVG Characterization:

UMI-deduplicated fastq files containing read sequences were processed with the Virus Recombination Mapping (*ViReMa*) software to identify recombination events per genomic read using the following parameters:

--Seed 25 --MicroInDel_Length 20 --Aligner bwa --ErrorDensity 1,25

Additionally, the *-ReadNamesEntry* switch was included in a separate ViReMa run of the same dataset in order to assign read name information to each recombination, which allowed us to collapse deletion events with the same read name into a single delVG observation with in-house Bash and AWK scripts:

--Seed 25 --MicroInDel_Length 20 --Aligner bwa --ErrorDensity 1,25 -ReadNamesEntry

Full-length Viral Genome Characterization:

To characterize SVGs, we began by using the *bwa* alignment tool to determine the properties of reads and their alignment to the reference genome; this information is captured in the bitwise FLAG field (column 2) of the output SAM file. Next we used the *AWK* program to select only reads with proper alignment to the forward and reverse strands of reference genome—bitwise FLAGs 0x0 (0) and 0x10 (16) respectively—and used *AWK* yet again to filter reads that were within ±100bp the length of the reference genomic segment.

Statistics

In general, we relied on linear or linear mixed models to test significance between treatments using base R and the nmle packages, respectively. Owing to the intrinsic heterogeneity of flu infections (Russell, 2018; Wang, 2020), we included bioreplicates as a random factor, unless otherwise indicated.

We tested alpelisib inhibition of PI3K network signaling and its dose dependence, using a linear model and Dunnett's contrasts. We tested influenza activation of PI3K network signaling activity using ANOVA and Tukey's HSD, to test for differences among strains and the mock infection. We tested whether alpelisib affects the production of defective virions, by testing for differences in the proportion of non-clustering units (NCU) according to each alpelisib dose using a linear mixed model. We similarly tested for differences in the total viral particles detected by the cluster-forming assay. Finally, we tested whether alpelisib increases defective viral genome production by examining the proportion of DelVGs in each alpelisib concentration using a linear mixed

model that controlled for viral genome segment identity, as these have documented differences in the production of DelVGs during infection.

Results

1. Alpelisib inhibits PI3K network signaling in MDCK-London cells

We set out to confirm that alpelisib inhibits PI3K network signaling in the MDCK-London cell line, as has been demonstrated in numerous other mammalian cell lines and cell-free assays (Furet, 2013; Fritsch, 2014; Yang, 2019). We leveraged immunocytochemistry and fluorescence microscopy to quantify pAKT activity at the single cell level (Pargett, 2017). We found strong evidence that alpelisib inhibited PI3K network signaling by measuring the activity of the downstream pAKT effector. Increased doses of alpelisib, across a broad 1.25 - 40 µM concentration range, resulted in a clear dose dependent decrease in pAKT activity (Adjusted $R^2 = 0.1672$, $p < 0.00001$, **Figure 2.1A**), with a 4.5342 decrease in AU per µM of alpelisib. In qualitative terms, pAKT activity was clearly downregulated in the alpelisib-treated monolayer (**Figure 2.1B**) relative to the vehicle-treated monolayer (**Figure 2.1C**); whose baseline pAKT activity was dusted across the cytoplasm of some cells and focused in the nuclei of others. Expectedly, the insulin-treated positive control group showed vivid pAKT upregulation, wherein pAKT activity localization went past cytoplasm and nuclei to include the plasma membrane (**Figure 2.1D**, **Supplementary Figure 2.9**).

2.1A

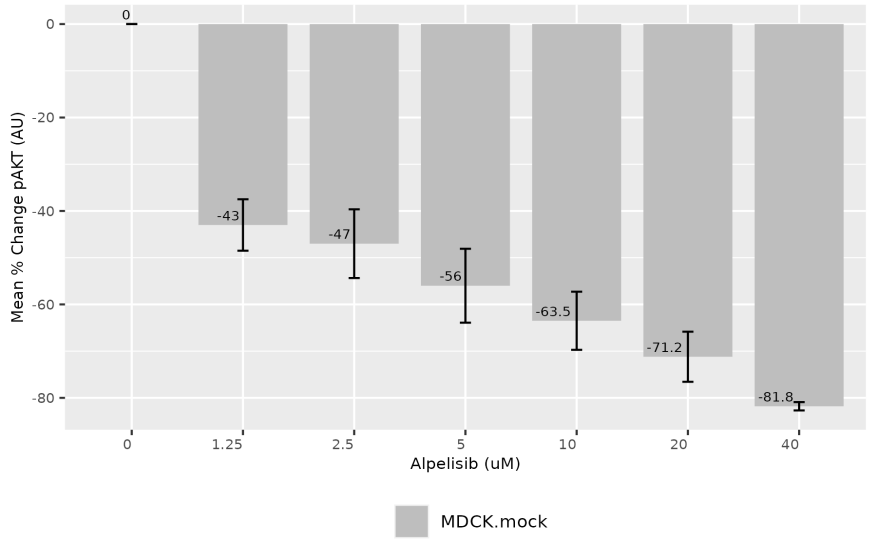
0
-43
-47
-56
-63.5
-71.2
-81.8
0
-20
-40
-60
-80
Mean % Change pAKT (AU)
0
1.25
2.5
5
10
20
40
Alpelisib (uM)
MDCK.mock

2.1B

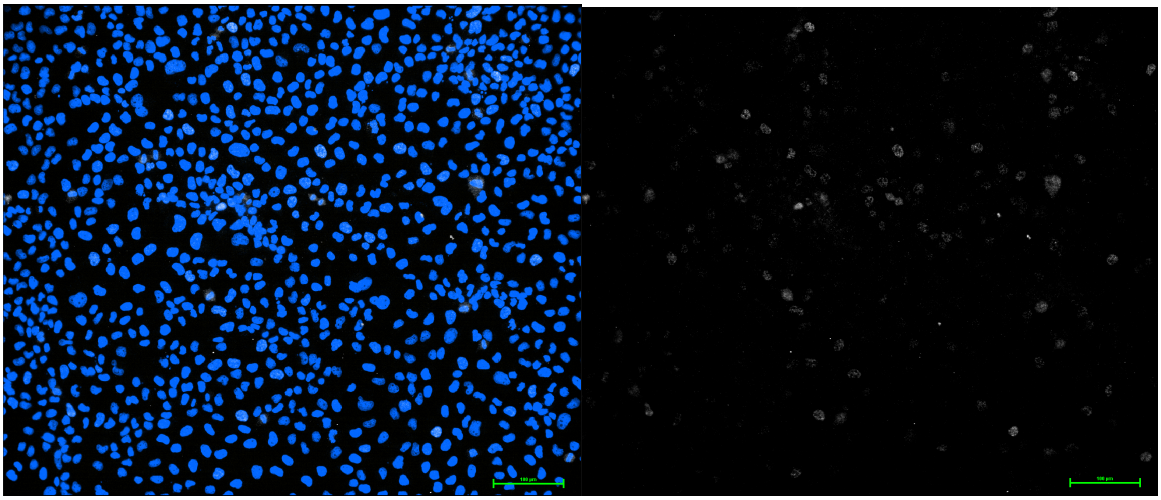

2.1C

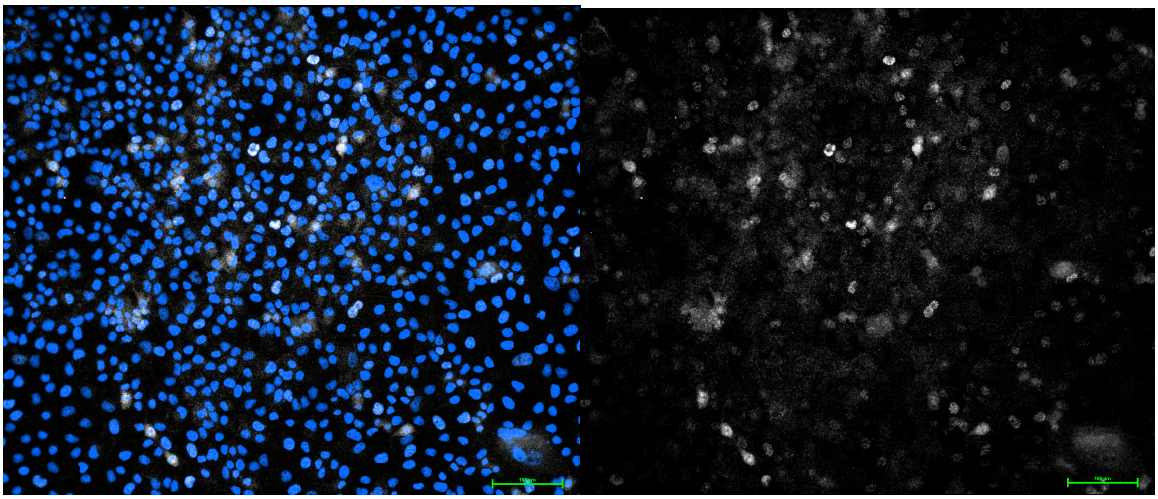

2.1D

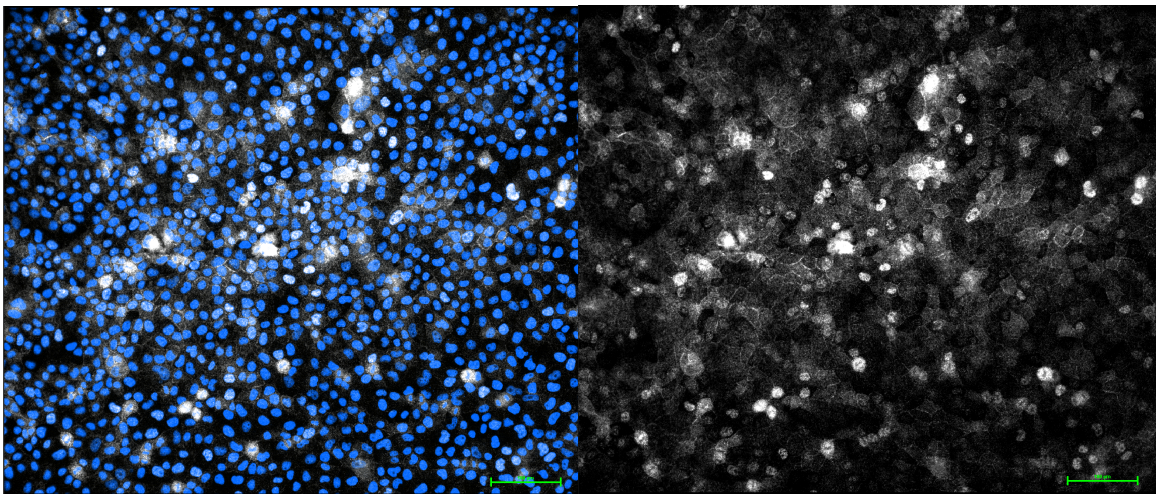

Figure 2.1. **(A) Alpelisib decreases pAKT activity (AU) of MDCK-London in a dose dependent manner**. Mean percent change in pAKT activity (AU) of MDCK-London cells exposed to increasing concentrations of alpelisib; 0 µM alpelisib treatment group received vehicle solvent (DMSO). n = 3 bioreplicates, sem. (**B**) 20 µM alpelisib treated monolayer, (**C**) Vehicle treated monolayer, (**D**) Insulin treated monolayer (positive control). White/Cy5 – pAKT(S473); Blue/ Hoechst – MDCK-London nucleus.

2. Influenza A infection activates PI3K network signaling activity with strain-specificity in MDCK Cells

Class 1a PI3K signaling in host cells can be activated by several Influenza A strains, including A/WSN/1933(H1N1), A/Udorn/72(H3N2), A/Victoria (Hale, 2006; Ayllon, 2012), A/Puerto Rico/8/34(H1N1) (Hale, 2006; Li, 2008; Lopes, 2017), and an unspecified 1918 pandemic H1N1 strain (Cho, 2020). The effector domain of the viral NS1 effector protein is the molecular activator of the PI3K signaling cascade (Hale, 2006; Ayllon, 2012; Cho, 2020), and different influenza strains have been shown to differentially activate PI3K signaling in a tumorigenic cell line (Ayllon, 2012). To avoid confounding our results with the aberrant PI3K signaling typical in cancer cells (Fruman, 2014; Yuan, 2008; Fruman, 2017; Jokinen, 2015), and considering the strain-specific differences in the NS1 effector domain (**Figure 2.2**), we needed to ensure our chosen strains could activate PI3K network signaling in a non-tumorigenic MDCK cell line within the experiment window.

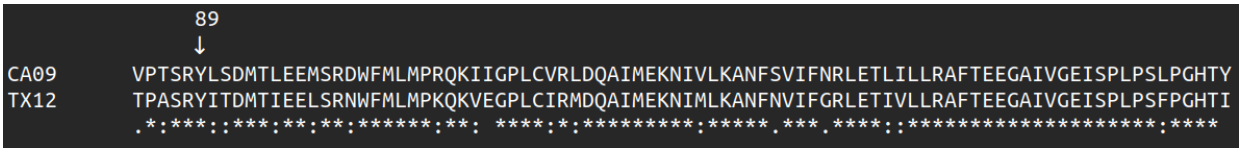

Figure 2.2. **CA09 and TX12 have the highly conserved Y89 residue that is necessary for Class 1a PI3K activation.** Multiple sequence alignment of CA09 and TX12 NS genome segment sequences.

We measured pAKT in CA09 and TX12 infections compared to a mock infection. Both viral infections upregulated pAKT compared to mock infection in a statistically significant way (ANOVA Adjusted $R^2 = 0.2428$, $p < 0.00001$), with CA09 and TX12 increasing the AU by an average of 205.861 and 106.886 respectively (Tukey Contrasts $p < 0.00001$). TX12 upregulation of pAKT was on average -98.976 AU less than CA09 and this effect was statistically significant

(Tukey Contrasts $p < 0.00001$) (**Figure 2.3**). In addition to confirming PI3K activation by CA09, we discovered this trait in TX12 and demonstrated the differential dysregulation of PI3K signaling by both strains in a non-tumorigenic cell line.

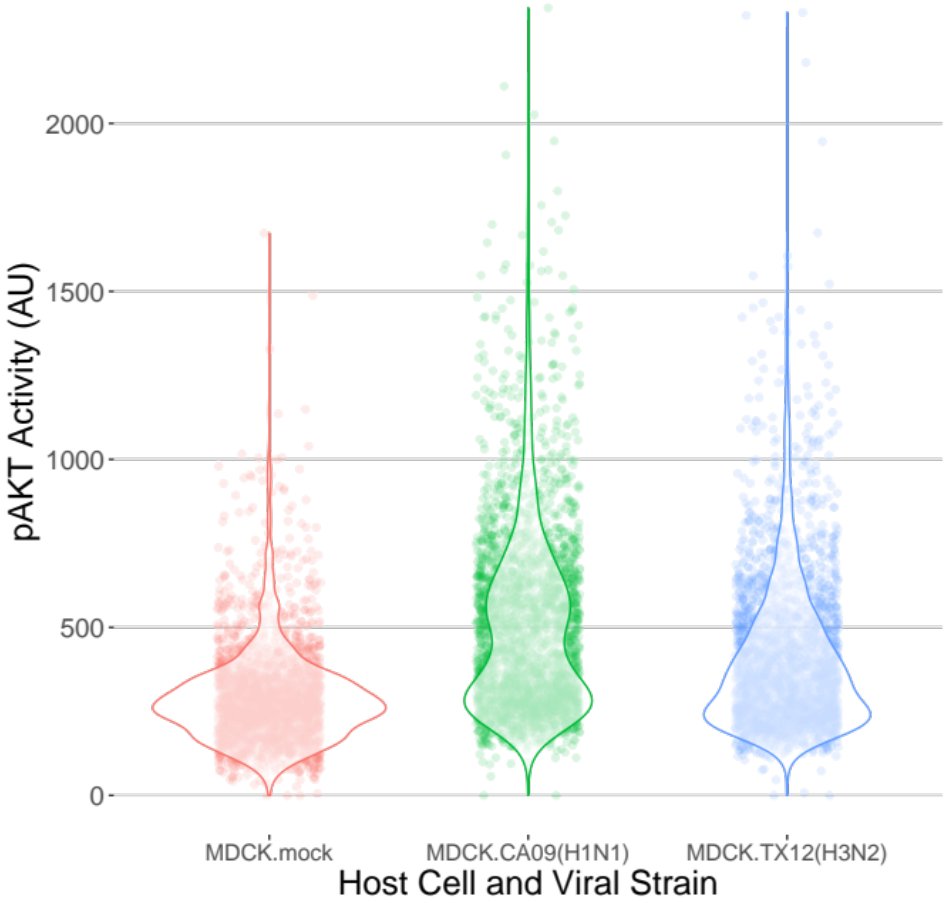

Figure 2.3. **Differential activation of pAKT activity by Influenza A infection**. pAKT activity (AU) of influenza-infected MDCK-London cells. n = 3 bioreplicates, sem.

3. Alpelisib pre-treatment is sufficient to subvert PI3K network signal restoration by Influenza A

To determine PI3K-AKT signaling outcomes under the competing influences of influenza and alpelisib, we measured pAKT activity in cells pre-treated with increasing concentrations of alpelisib and then infected with either CA09 or TX12. We found that alpelisib completely subverted the observed viral PI3K upregulation in a dose-dependent fashion (**Figure 2.4**, **Supplementary Figure 2.9**); in both CA09 (Adjusted $R^2 = 0.3313$, $p < 0.00001$) and TX12 (Adjusted $R^2 = 0.2725$, $p < 0.00001$) strains at alpelisib concentrations from 1.25 – 40 uM. Each 1 µM increase in alpelisib led to a decrease of 6.4280 and 5.9940 AU in CA and TX infections respectively. We note that the qualitative pattern and magnitude of the decrease in AU per µM of alpelisib for cells infected with either strain was strikingly similar in uninfected cells (-4.5342 AU).

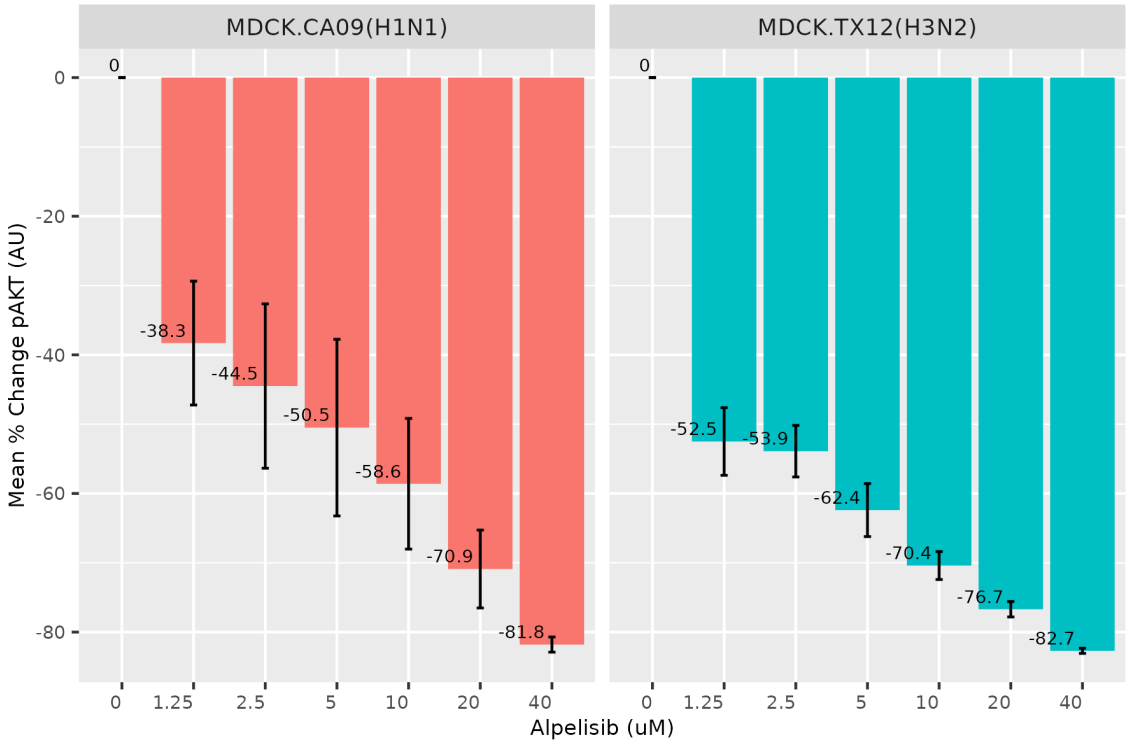

Figure 2.4. **Alpelisib significantly inhibits pAKT activity during Influenza A viral infection**. Mean percent change in pAKT activity (AU) of MDCK-London cells pre-treated with increasing concentrations of alpelisib and then infected with either CA09 or TX12; 0 µM alpelisib treatment group received vehicle solvent (DMSO). n = 3 bioreplicates, sem.

4. The Cluster-Forming Assay can titrate non-infectious/defective Influenza A particles

We developed the cluster-forming assay to simultaneously titrate fully infectious and propagation-incapable particles by combining elements of the conventional plaque assay (Cooper, 1961) and immunofocus assay (Baker, 2013). While the plaque and immunofocus assays respectively use solid or liquid overlay media to sustain inoculated monolayers for the duration of the assay, the cluster-forming assay employs a medium-viscosity overlay that remains semi-solid (Matrosovich, 2006). This medium restricts viral diffusion to neighboring cells much like a plaque assay,

but can be removed for fixation, staining, and imaging of monolayers akin to the immunofocus assay (see Methods). The cluster-forming assay yields immunofluorescence (IF) images where each infection event appears as either a cluster of infected cells (productive clustering unit, PCU) or solitary infected cell foci (non-clustering units, NCU) (**Figure 2.5**, **Supplementary Figures 2.2-2.5**). PCUs represent a productive infection mounted by a single fully infectious virus particle, whereas NCUs represent self-limiting infections mounted by propagation-incapable viral particles.

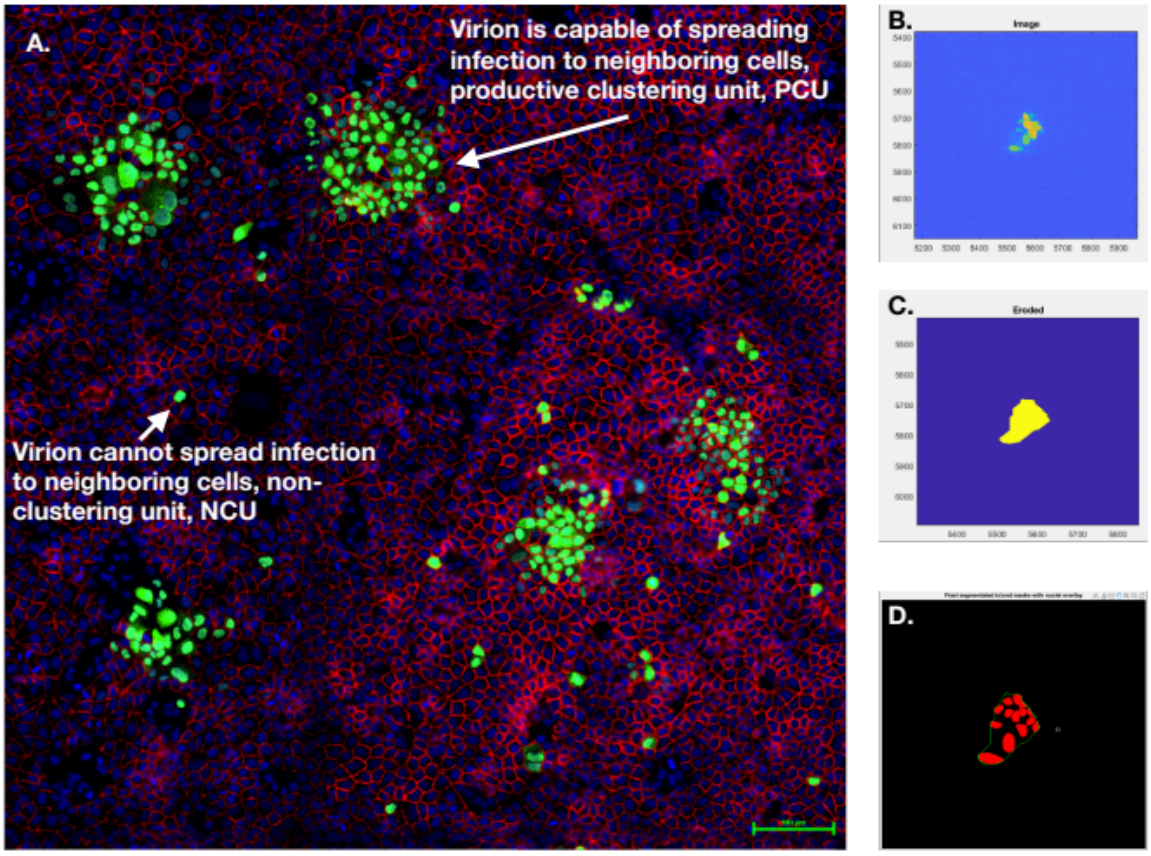

Figure 2.5. **Cluster-forming assay**. **A.** Influenza A Virus infection of MDCK-London cells showing productive and abortive infections. Green/GFP – A/California/07/2009 nucleoprotein; Blue/Hoechst – MDCK-London nucleus; Red/Cy5 – MDCK-London E-cadherin. **B-C**. Stepwise assembly of a mask around the nucleoprotein GFP signal in a productive clustering unit (PCU); starting from the initial cluster-forming assay IF image (**B**) down to final erosion (**C**). **D.** segmentation-mask overlay to size (i.e. number of cells) a PCU.

To count PCUs and NCUs, cluster-forming assay IF images (**Figure 2.5A**) were put through an automated image analysis pipeline we developed using MATLAB's image processing toolbox. Our guiding design principle was to cordon—or mask—nucleoprotein fluorescence signals (GFP) in the IF image as independent infection events, then overlay said mask with the host nuclei segmentation Hoechst signal to reveal the number of cells each infection event had spread to. We began stepwise assembly of masks around the GFP signals (**Figure 2.5B-C**) by binarizing IF images with the *imbinarize* function to make object detection possible, followed by the removal of small, noisy pixels with *bwareaopen*. Masks were sequentially dilated then filled with *imdilate* and *imfill* functions respectively to smoothen them out and ensure they did not contain holes. To finish the mask assembly, masks were eroded with *imerode* to undo the signal expansion done in the dilation step (**Figure 2.5C**). Undesired masks were filtered out by thresholding the min/max mask area and removing masks that did not contain any nuclei, leaving bona fide infection events—or clusters—that are counted and assigned a unique identity number, a *clusterID* (**Figure 2.5D**).

The cluster-forming assay is a highly reproducible (**Figure 2.6**) improvement of the conventional immunofocus and plaque assays that provides increased resolution of viral infectivity. In addition to quantifying FIPs—as was possible with a conventional plaque assay—it is now possible to simultaneously quantify SIPs in the same sample with high-throughput. This is significant because access to two sub-populations of infectious viral particles makes it possible to determine total infectious particles, and thus relative abundances as well as; both of which are indispensable metrics for the quantitation of viral interference within the host.

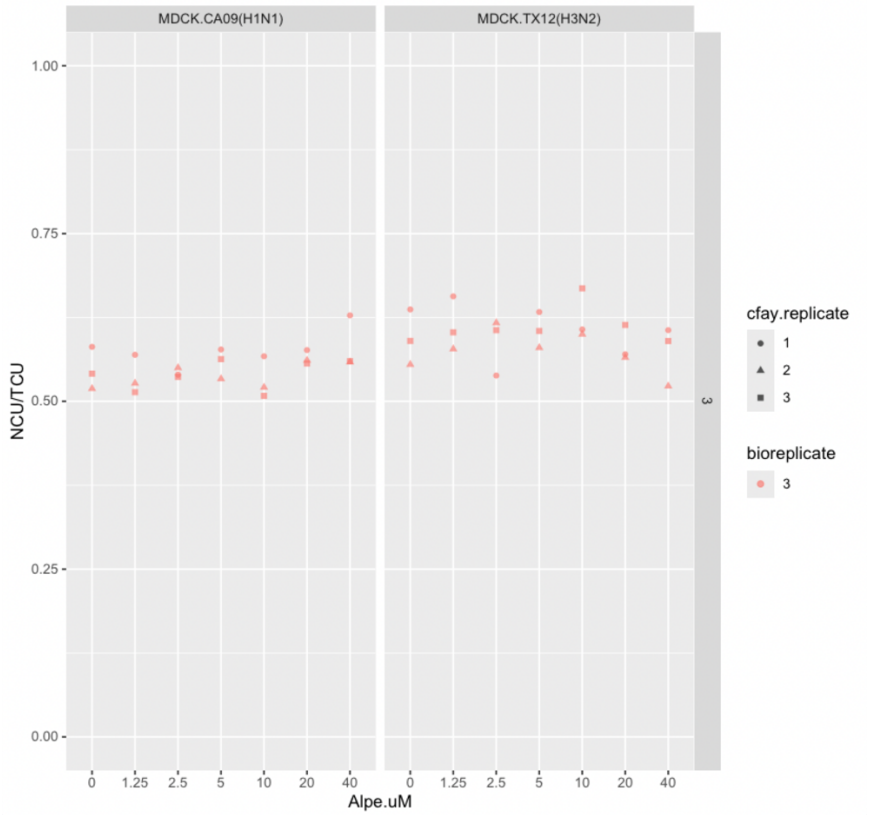

Figure 2.6. **The cluster forming assay is highly reproducible**. The proportion of non-clustering units (over total clustering units, aka total infection events) titrated from supernatants of 18 hr CA09 and TX12 infections of cells pre-treated with different concentrations of alpelisib. Each point is a technical replicate; i.e. a titration of the same infection supernatant. The 0 µM alpelisib treatment group received vehicle solvent (DMSO).

5. Alpelisib affects the production of defective particles early in Influenza A infection

To determine whether alpelisib pre-exposure of cells affected CA09 or TX12 infection, we used the cluster-forming assay to screen a broad dosage range of alpelisib pre-treatment concentrations (**Figure 2.7**). Specifically, we sought to determine if alpelisib pre-treatment (0, 1.25, 2.5, 5, 10, 20, and 40 µM) affected the production of defective/non-infectious particles, reported here as the relative abundance or proportion of NCUs. We conducted Linear mixed-effects modeling

(nmle) to analyze each alpelisib treatment as a factor because a dose-dependent response was not found for either infection. Alpelisib pre-treatment significantly altered the proportion of NCUs in TX12 ($p < 0.0001$), but in CA09, no treatment was significantly different against the control. In TX12, concentrations of 2.5, 5, 10, and 20 μM alpelisib increased the percentage of NCUs by 6.37%, 11.946%, 8.511% and 6.70% respectively, and these effects were statistically significant (all $p < 0.0388$).

We also examined whether alpelisib pre-treatment affected the total viral yield, here measured by total clustering units (TCU/mL), which is analogous to plaque forming units (PFU/mL). In CA09 infections, alpelisib was a statistically significant factor affecting TCUs (Adjusted $R^2 = 0.8247$, $p < 0.00001$); alpelisib concentrations of 2.5, 10, and 40 μM were significantly different from control, changing TCUs by an average of 36.2222, 40.5556, -36.0000 TCU/mL, respectively. In TX12 infections, alpelisib was not a statistically significant factor in explaining TCUs ($p < 0.0632$), and there were no significant differences between alpelisib treatments.

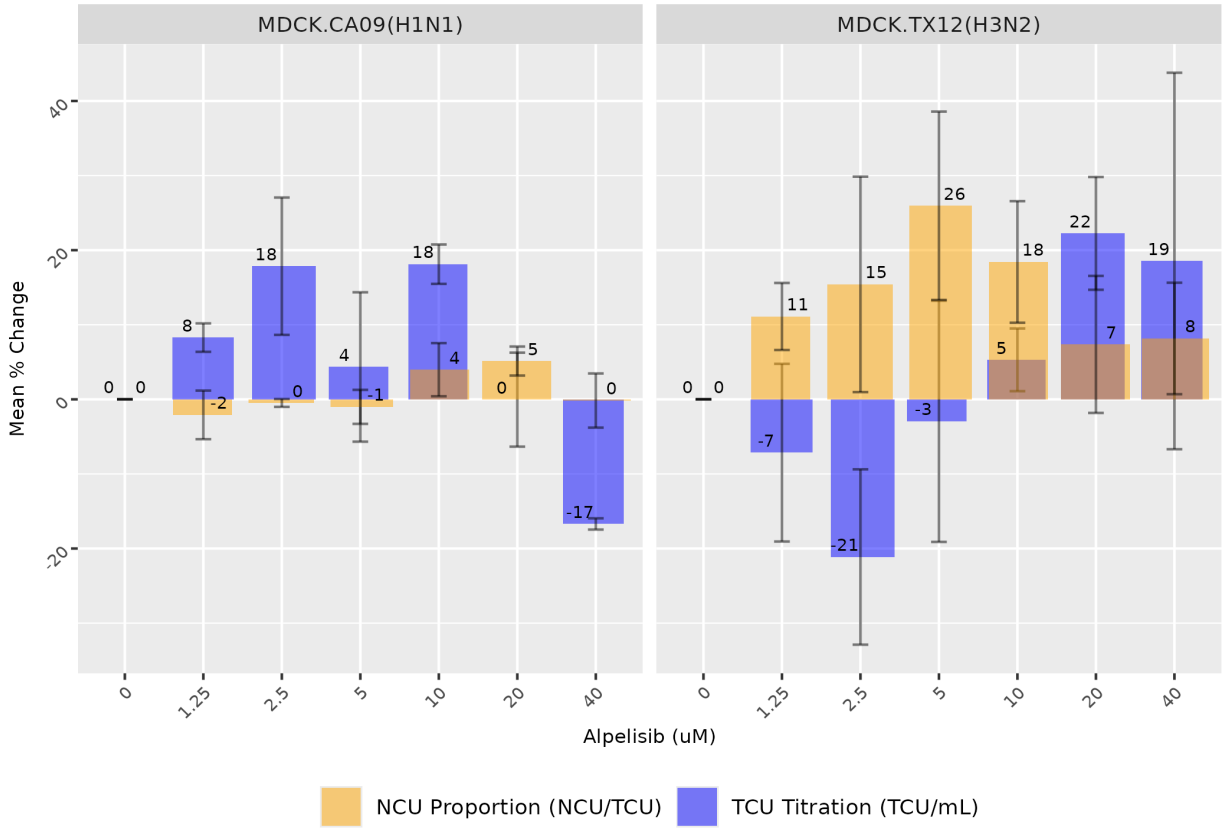

Figure 2.7. Alpelisib can affect the proportion of defective particles, as well as the total particle yield in a strain dependent manner. Alpelisib had the most marked effects on total particles in CA09 (Left) and on the proportion of defective particles in TX12 (Right). Percent changes in TCU (purple) and NCU relative abundance (orange) in CA09 and TX12 at 18 h.p.i. under different concentrations of alpelisib; no trypsin. 0 µM alpelisib treatment group received vehicle solvent (DMSO). n = 3 bioreplicates, sem.

6. Alpelisib increases defective viral genome production early in Influenza A infection

We found alpelisib caused changes in infectiousness at the particle level and thus were interested in whether alpelisib pre-exposure caused an increase in defective viral genomes. We sequenced viral supernatants from the same infections that were used in the cluster-forming assay (Heading 5) using two MinION flow cells, which yielded a total of 27.42 M reads. After quality control for

well-formed amplicons (perfect UMIs, Influenza A-specific terminal uni12/13 regions) and de-deduplicating unique molecular identifiers (UMI) we obtained 120,652.10 ± 70,902.90 reads per infection (CA09: 148,943 ± 78,828; TX12: 92,362 ± 49,104).

We note that these read counts are produced from de-duplicated reads, reflecting an estimate of the RNA genome content whether deletion-containing or not (total viral genomes, TVG) in the supernatants (**Figure 2.8**). We found no significant difference in the total number of viral genomes and there was no dose-dependent effect of alpelisib. This result suggests that the effects of alpelisib pre-treatment were specific to defective viral genomes, as we report below.

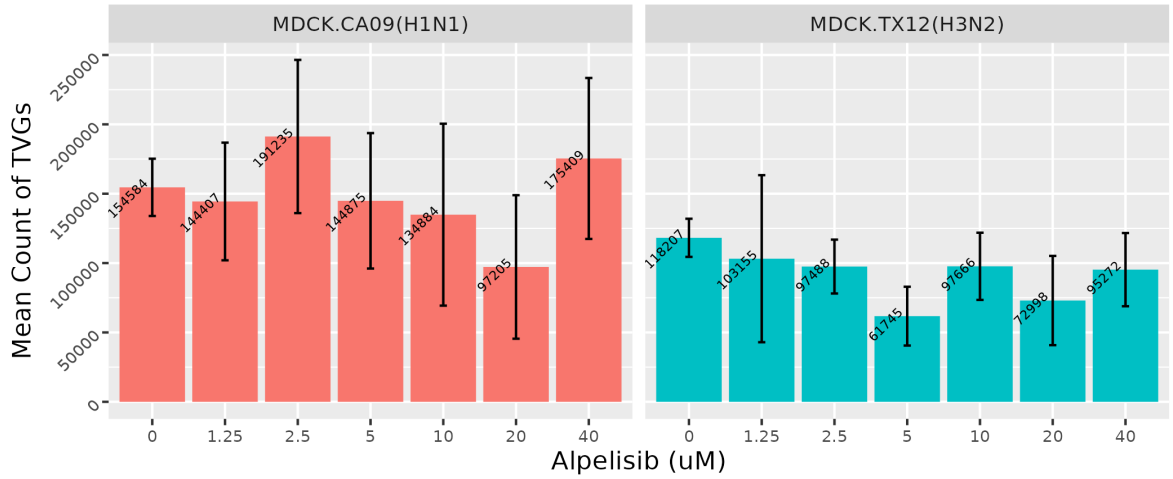

Figure 2.8. No significant differences in total viral genomes as a function of alpelisib pre-treatment concentration. Mean count of total viral genomes (CA09/TX12) recovered at 18 h.p.i. under different concentrations of alpelisib; no trypsin. 0 µM alpelisib treatment group received vehicle solvent (DMSO). n = 3 bioreplicates, sem.

To determine if alpelisib pre-treatment of cells increased the defective viral genome production, we tested for differences in the proportion of defective viral genomes between the mock-infected control and a wide range of alpelisib concentrations. The vehicle-treated control yielded 3903.67 ± 995.55 DelVGs for CA09 and 3601.67 ± 577.42 for TX12 as detected by ViReMa, which respectively represents 2.52% and 3.07% of total viral genomes (154584, 118207). The overall

proportion of defective viral genomes increased as a function of increasing alpelisib concentration in CA09 infections (Adjusted R^2 = 0.400, p = 0.008; **Figure 2.9**, Left). Alpelisib explained 19.96% of the variation in the proportion of defective viral genomes, with each 1 µM increase of alpelisib increasing the total proportion of DVGs by 0.005929%. Infections with TX12 showed this increasing trend, however the model was not statistically significant (Adjusted R^2 = 0.1037, p = 0.1907, **Figure 2.9**, Right).

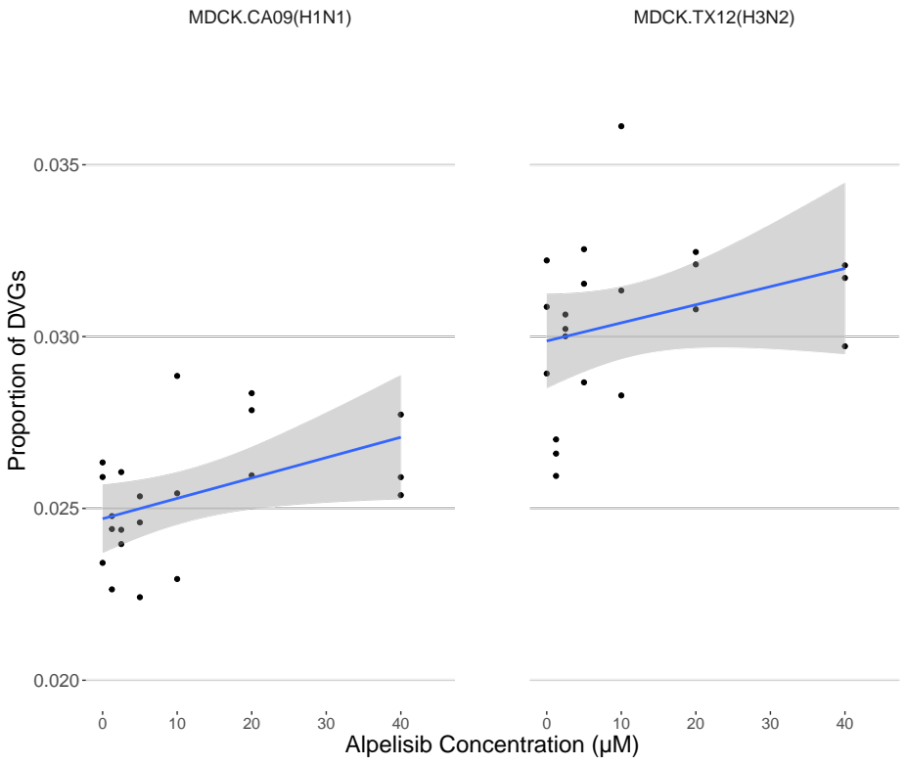

Figure 2.9. **Alpelisib pre-treatment of cells increases the proportion of defective particles**. Overall proportion of DelVGs (i.e. total DelVGs regardless of segment origin) as a function of concentration of alpelisib pre-treatment. The CA09 regression is statistically significant (p = 0.008), while TX12's is not (p = 0.1907). Three independent infections with CA09 and TX12 per concentration at 18 h.p.i. under different concentrations of alpelisib pre-treatment; no trypsin. 0 µM alpelisib treatment group received vehicle solvent (DMSO).

Influenza viral genome segments have known variation in their propensity to generate defective viral genomes. In particular, the polymerase complex genes (PB2, PB1, and PA) are known to

generate most of the DelVGs in a given influenza infections (Saira, 2013; Wu, 2022). Thus, we used a mixed linear model to test whether DelVG proportion changed on a per-segment basis (modeling the interaction of segment and alpelisib concentration). We examined differences in the proportion of DelVGs treating each concentration as a factor, as there was not a dose-dependent effect per-segment (**Figure 2.10**). Alpelisib pre-treatment had a statistically significant effect on per-segment proportion of DelVGs (**Figure 2.10**), in both CA09 (Adjusted $R^2 = 0.4885$, $p < 0.00001$) and TX12 (Adjusted $R^2 = 0.3843$, $p < 0.00001$) infections.

In CA09 infections, statistically significant increases in DelVG proportion were found at the 20 μM pre-treatment for segments PB1, PA and HA, with respective increases of 0.3979, 0.2398, and 0.1260 proportion units relative to the comparison group (NS segment, which had the lowest proportion of DelVGs). The CA09 strain has been documented to have higher DelVG production in the HA segment, compared to other strains (Alnaji, 2019). In TX12 infections, statistically significant increases were found across all polymerase complex segments at the same 20 μM concentration, and also across a broader range of concentrations compared to the CA09 infection. In particular, the PA segment showed statistically significant differences at the 2.5-40 μM concentrations. The PB2 segment showed statistically significant increases in the proportion of DelVGs at the 10 (0.0466) and 20 μM (0.0331) doses, while the PB1 segment showed statistically significant increases at the 20 (0.0700476) and 40 μM (0.0351) doses. Note that all statistically significant changes were increases, and quantified relative to the NS segment as with CA09.

Collectively, these results suggest that alpelisib pre-treatment at 20 µM increases DelVG production in both CA09 and TX12 strains in the polymerase complex segments, which are known to have the highest probability of generating DelVGs. Furthermore, there is a dose-dependent increase in the proportion of DelVGs as alpelisib concentration increased in CA09 infections (**Figure 2.9**). This same trend was evident in TX12 infections, but the linear regression was not statistically significant.

Figure 2.10. **Per segment proportion of total viral genomes (CA09/TX12) that are DVGs at 18 h.p.i. under different concentrations of alpelisib**; no trypsin. The DVG-spawning probability of each segment as a fraction. 0 µM alpelisib treatment group received vehicle solvent (DMSO). n = 3 bioreplicates, sem.

Discussion

To investigate the dependence of influenza progeny infectivity on host cell metabolic signaling, we reprogrammed host PI3K network signaling during flu infection with alpelisib, monitored the intervening metabolic state with cellular-level resolution immunofluorescence microscopy, and determined the change in proportion of non-infectious progeny virus with our newly developed cluster-forming assay. The proportion of non-infectious particles in a flu infection is emerging as a crucial determinant of pathogenic outcomes, and non-infectious particles are being directly used as antiviral treatments (Smith, 2016; Meng, 2017; Wasik, 2018; Zhao, 2018; Bdier, 2019; Yamagata, 2019; Tapia, 2019; Harding, 2019). We established that host cell PI3K network signaling activity can influence the proportion of non-infective particles produced by influenza in two strains. First, we found that alpelisib suppresses PI3K-AKT pathway signaling activity in MDCK-London cells in a dose-dependent manner (**Figure 2.1**). Second, we found that alpelisib treatment keeps PI3K-AKT signaling pathway activity suppressed during Influenza A infection in MDCK-London cells (**Figure 2.4**), counteracting influenza's upregulation of PI3K signaling (**Figure 2.3**; Hale, 2006; Ayllon, 2012). Finally, as predicted by our hypothesis, we found that alpelisib treatment induces a reproducible and statistically significant increase in the proportion of non-infectious progeny during Influenza A infection (**Figure 2.7**). We also found evidence that alpelisib increases the proportion of defective viral genomes produced by polymerase complex segments in both CA09 and TX12 infections (**Figure 2.10**) and that CA09 showed a statistically significant dose-dependent increase in the overall proportion of defective viral genomes (**Figure 2.9**). Collectively, these findings establish the host cell's metabolic signaling profile as a means to directly modulate the infectivity of progeny Influenza A virus, and further validates the

use of metabolic signal modulation as a means to drive influenza infections toward milder clinical outcomes.

To our knowledge, our study is the first to examine the role of host metabolic state in the production of non-infectious influenza progeny particles and defective viral genomes (Dimmock, 2014; Manzoni, 2018; Vignuzi, 2019; Wu, 2022). Specifically, we show differential dysregulation of PI3K signaling activity in a non-tumorigenic cell line during infection by two different Influenza A strains, CA09 and TX12, then override this host-virus interaction using alpelisib, and finally show an increase in DelVGs and defective particle production. The host metabolic state can affect influenza infection in terms of clinical outcomes as shown in studies of obesity, cancer etc. For instance, obesity—a host metabolic state characterized by chronic inflammation and dysregulated immune responses—has been associated with increased titers of infectious progeny (Honce, 2019; Honce, 2020). Similarly, at the cellular level, cross-talk between Influenza A and host metabolic signaling effectors has been shown to affect the production of infectious progeny (Hale, 2006; Li, 2008; Smallwood, 2017; Kuss-Duerkop 2017). However, the production of non-infectious progeny during different metabolic states had not previously been investigated; an extremely relevant line of investigation given that up to 90% of total viral particles are non-infectious (Brooke, 2013; Brooke, 2017; Diefenbacher, 2018), and that these particles have a role in clinical outcomes (Dimmock, 2014; Vasilijevic, 2017). Our findings confirm that interrupting virus-induced upregulation of host growth signaling can increase non-infectious Influenza A particle production, providing novel insight into the crosstalk between Influenza A and host metabolism. The molecular mechanisms that underlie and influence non-infectious particle formation re-

main unclear. Until now, these investigations have focused primarily on the viral side of the equation, identifying viral genome mutations and infection multiplicity as variables influencing the production of non-infectious progeny across different strains (Von Magnus, 1954; Rodriguez, 2013; Vasilijevic, 2017; Perez-Cidoncha, 2014). Our study addresses the need to better understand the still unknown mechanisms that spawn non-infectious progeny by providing a more complete picture of how metabolic state affects Influenza A pathogenesis.

Our study combines single-cell immunofluorescence quantification with a novel assay that quantifies the proportion of non-infectious virus particles, providing a more accurate measurement of the infectious potential of a virus population (Brooke, 2013). Building on previous methods (Brooke, 2013; Amarilla, 2021; Cacciabue, 2019), our cluster-forming assay combined the infection localization of a conventional plaque assay with the immunocytochemical staining and microscopy of the standard immunofocus assay. By pairing this assay with an automated image analysis pipeline, we were able to capture influenza infectivity at a more detailed resolution than is possible with either parent assay alone (See Supplementary Material). By resolving NCUs (non-infectious particles) and PCUs (fully infectious particles) apart from each other, the cluster-forming assay has revealed strain-specific and dose-specific effects of alpelisib on key markers of defective interference at just 18 h.p.i. These novel outcomes represent early onset alterations to the trajectories of standard CA09 and TX12 infections, and each of these altered trajectories is uniquely desirable for different real-world therapeutic and prophylactic applications, provided they persist into later time points. Pharmacologically increasing the *in situ* spawn rate of non-infectious particles is a viable and novel therapeutic possibility, provided the underlying physio-

logical factors become better understood. One aspect that our study does not address is the definition of the non-infectious particle component. Although the cluster-forming assay accurately titrates infectious and non-infectious particles, it was not designed to identify whether those non-infectious particles represent DIPs, particles with lethal or nonsense mutations, or particles that contain segments with defects in transcription (Brooke 2013); an area that requires further study. We additionally expect the cluster-forming assay to facilitate future screens to uncover evermore druggable modulators of *in situ* non-infectious particles and DelVG production during Influenza A infection.

Based on the established cross-talk between effector proteins of both host cell metabolic signaling and Influenza A (Hale, 2006; Li, 2008; Smallwood, 2017; Kuss-Duerkop 2017), we hypothesized that pro-growth metabolic signal inhibition with alpelisib would induce abortive infectivity in progeny flu particles. Our prediction proved out, and uncovering more inducers in this manner will guide future investigations into the molecular mechanism through which DVGs emerge and non-infectious progeny particles accumulate. In turn, knowledge of these mechanisms will facilitate the development of more targeted abortive infectivity induction strategies for broad-spectrum anti-influenza therapeutics. DI is already being weaponized in the form of exogenously administered recombinant Influenza A virions called therapeutic interfering particles (TIPs), which have been engineered to contain one or more DelVGs. TIPs are propagation-incapable, and their administration attenuates Influenza A pathogenesis in a strain-indiscriminate (Smith 2016; Zhao, 2018), dose-dependent manner (Smith, 2016; Meng, 2017; Wasik, 2018; Zhao, 2018; Bdier, 2019; Yamagata, 2019; Tapia, 2019; Harding, 2019). Our study opens the possibility of using

host cell metabolic state as a strategic therapeutic target because of its readily responsive and reversible system-wide reach. Picomolar perturbations of host cell metabolism can drive system-wide reconfiguration of critical processes into countless unique endpoints; too many endpoints for Influenza A to possibly adapt against. Future research should address the composition of non-infectious progeny particles, and which PI3K downstream effector pathways transduce the signal(s) that ultimately impacts *de novo* non-infectious particle emergence. In sum, our research shows the promise of the host cell's vast metabolic signaling network as a quick-response, therapeutically actionable, druggable target with the potential to steer flu pathology away from fatal towards mild outcomes.

Acknowledgements

This project was funded by NIH grants 4R00AI119401-02 and 1R01AI179873-01 to SDM. IA was supported by NIH grant 4R00AI119401-02 and 1R01AI179873-01 to SDM and a Craft Consult Biotechnology Dissertation Fellowship. John Albeck kindly provided training and access to his fluorescence microscopy resources and infrastructure. John Albeck and Enoch Baldwin provided helpful feedback on this manuscript. Ted Ross kindly provided strains from his collection.

References

1. ACKERMANN WW, KLERNSCHMIDT E. Concerning the relation of the Krebs cycle to virus propagation. J Biol Chem. 1951 Mar;189(1):421-8. PMID: 14832255.

2. Alnaji FG, Holmes JR, Rendon G, Vera JC, Fields CJ, Martin BE, Brooke CB. Sequencing Framework for the Sensitive Detection and Precise Mapping of Defective Interfering Particle-Associated Deletions across Influenza A and B Viruses. J Virol. 2019 May 15;93(11):e00354-19. doi: 10.1128/JVI.00354-19. PMID: 30867305; PMCID: PMC6532088.

3. Alnaji FG, Brooke CB. Influenza virus DI particles: Defective interfering or delightfully interesting? PLoS Pathog. 2020 May 21;16(5):e1008436. doi: 10.1371/journal.ppat.1008436. PMID: 32437428; PMCID: PMC7241698.

4. Alnaji FG, Reiser WK, Rivera-Cardona J, Te Velthuis AJW, Brooke CB. Influenza A Virus Defective Viral Genomes Are Inefficiently Packaged into Virions Relative to Wild-Type Genomic RNAs. mBio. 2021 Dec 21;12(6):e0295921. doi: 10.1128/mBio.02959-21. Epub 2021 Nov 23. PMID: 34809454; PMCID: PMC8609359.

5. Al-Saffar NM, Jackson LE, Raynaud FI, Clarke PA, Ramírez de Molina A, Lacal JC, Workman P, Leach MO. The phosphoinositide 3-kinase inhibitor PI-103 downregulates choline kinase alpha leading to phosphocholine and total choline decrease detected by magnetic resonance spectroscopy. Cancer Res. 2010 Jul 1;70(13):5507-17. doi: 10.1158/0008-5472.CAN-09-4476. Epub 2010 Jun 15. PMID: 20551061; PMCID: PMC2896552.

6. Amarilla AA, Modhiran N, Setoh YX, Peng NYG, Sng JDJ, Liang B, McMillan CLD, Freney ME, Cheung STM, Chappell KJ, Khromykh AA, Young PR, Watterson D. An Optimized High-Throughput Immuno-Plaque Assay for SARS-CoV-2. Front Microbiol. 2021 Feb 12;12:625136. doi: 10.3389/fmicb.2021.625136. PMID: 33643253; PMCID: PMC7906992.

7. Ayllon J, Hale BG, García-Sastre A. Strain-specific contribution of NS1-activated phosphoinositide 3-kinase signaling to influenza A virus replication and virulence. J Virol. 2012 May;86(9):5366-70. doi: 10.1128/JVI.06722-11. Epub 2012 Feb 15. PMID: 22345452; PMCID: PMC3347353.

8. Baker SF, Guo H, Albrecht RA, García-Sastre A, Topham DJ, Martínez-Sobrido L. Protection against lethal influenza with a viral mimic. J Virol. 2013 Aug;87(15):8591-605. doi: 10.1128/JVI.01081-13. Epub 2013 May 29. PMID: 23720727; PMCID: PMC3719819.

9. Bdeir N, Arora P, Gärtner S, Hoffmann M, Reichl U, Pöhlmann S, Winkler M. A system for production of defective interfering particles in the absence of infectious influenza A virus. PLoS One. 2019 Mar 1;14(3):e0212757. doi: 10.1371/journal.pone.0212757. PMID: 30822349; PMCID: PMC6396908.

10. Brennan JW, Sun Y. Defective viral genomes: advances in understanding their generation, function, and impact on infection outcomes. mBio. 2024 May 8;15(5):e0069224. doi: 10.1128/mbio.00692-24. Epub 2024 Apr 3. PMID: 38567955; PMCID: PMC11077978.

11. Brooke CB, Ince WL, Wrammert J, Ahmed R, Wilson PC, Bennink JR, Yewdell JW. Most influenza a virions fail to express at least one essential viral protein. J Virol. 2013 Mar;87(6):3155-62. doi: 10.1128/JVI.02284-12. Epub 2013 Jan 2. Erratum in: J Virol. 2013 Jul;87(14):8267. PMID: 23283949; PMCID: PMC3592173.

12. Brooke CB. Biological activities of 'noninfectious' influenza A virus particles. Future Virol. 2014 Jan;9(1):41-51. doi: 10.2217/fvl.13.118. PMID: 25067941; PMCID: PMC4109409.

13. Brooke CB. Population Diversity and Collective Interactions during Influenza Virus Infection. J Virol. 2017 Oct 27;91(22):e01164-17. doi: 10.1128/JVI.01164-17. PMID: 28855247; PMCID: PMC5660503.

14. Cacciabue M, Currá A, Gismondi MI. ViralPlaque: a Fiji macro for automated assessment of viral plaque statistics. PeerJ. 2019 Sep 24;7:e7729. doi: 10.7717/peerj.7729. PMID: 31579606; PMCID: PMC6764358.

15. Cho JH, Zhao B, Shi J, Savage N, Shen Q, Byrnes J, Yang L, Hwang W, Li P. Molecular recognition of a host protein by NS1 of pandemic and seasonal influenza A viruses. Proc Natl Acad Sci U S A. 2020 Mar 24;117(12):6550-6558. doi: 10.1073/pnas.1920582117. Epub 2020 Mar 9. PMID: 32152123; PMCID: PMC7104383.

16. COOPER PD. The plaque assay of animal viruses. Adv Virus Res. 1961;8:319-78. doi: 10.1016/s0065-3527(08)60689-2. PMID: 13881155.

17. Dadonaite B, Gilbertson B, Knight ML, Trifkovic S, Rockman S, Laederach A, Brown LE, Fodor E, Bauer DLV. The structure of the influenza A virus genome. Nat Microbiol. 2019 Nov;4(11):1781-1789. doi: 10.1038/s41564-019-0513-7. Epub 2019 Jul 22. PMID: 31332385; PMCID: PMC7191640.

18. Davis AR, Hiti AL, Nayak DP. Influenza defective interfering viral RNA is formed by internal deletion of genomic RNA. Proc Natl Acad Sci U S A. 1980 Jan;77(1):215-9. doi: 10.1073/pnas.77.1.215. PMID: 6928614; PMCID: PMC348239.

19. Diefenbacher M, Sun J, Brooke CB. The parts are greater than the whole: the role of semi-infectious particles in influenza A virus biology. Curr Opin Virol. 2018 Dec;33:42-46. doi: 10.1016/j.coviro.2018.07.002. Epub 2018 Jul 24. PMID: 30053722; PMCID: PMC6642613.

20. Dimmock NJ, Easton AJ. Defective interfering influenza virus RNAs: time to reevaluate their clinical potential as broad-spectrum antivirals? J Virol. 2014 May;88(10):5217-27. doi: 10.1128/JVI.03193-13. Epub 2014 Feb 26. PMID: 24574404; PMCID: PMC4019098.

21. Engels G, Hierweger AM, Hoffmann J, Thieme R, Thiele S, Bertram S, Dreier C, Resa-Infante P, Jacobsen H, Thiele K, Alawi M, Indenbirken D, Grundhoff A, Siebels S, Fischer N, Stojanovska V, Muzzio D, Jensen F, Karimi K, Mittrücker HW, Arck PC, Gabriel G. Pregnancy-Related Immune Adaptation Promotes the Emergence of Highly Virulent H1N1 Influenza Virus Strains in Allogenically Pregnant Mice. Cell Host Microbe. 2017 Mar 8;21(3):321-333. doi: 10.1016/j.chom.2017.02.020. PMID: 28279344.Farrell A, Phan T, Brooke CB, Koelle K, Ke R. Semi-infectious particles contribute substantially to influenza virus within-host dynamics when infection is dominated by spatial structure. Virus Evol. 2023 Mar 21;9(1):vead020. doi: 10.1093/ve/vead020. PMID: 37538918; PMCID: PMC10395763.

22. Felt SA, Sun Y, Jozwik A, Paras A, Habibi MS, Nickle D, Anderson L, Achouri E, Feemster KA, Cárdenas AM, Turi KN, Chang M, Hartert TV, Sengupta S, Chiu C, López CB. Detection of respiratory syncytial virus defective genomes in nasal secretions is associated with distinct clinical outcomes. Nat Microbiol. 2021 May;6(5):672-681. doi: 10.1038/s41564-021-00882-3. Epub 2021 Apr 1. PMID: 33795879; PMCID: PMC9098209.

23. Fruman DA, Rommel C. PI3K and cancer: lessons, challenges and opportunities. Nat Rev Drug Discov. 2014 Feb;13(2):140-56. doi: 10.1038/nrd4204. PMID: 24481312; PMCID: PMC3994981.

24. Fruman DA, Chiu H, Hopkins BD, Bagrodia S, Cantley LC, Abraham RT. The PI3K Pathway in Human Disease. Cell. 2017 Aug 10;170(4):605-635. doi: 10.1016/j.cell.2017.07.029. PMID: 28802037; PMCID: PMC5726441.

25. Frensing T, Heldt FS, Pflugmacher A, Behrendt I, Jordan I, Flockerzi D, Genzel Y, Reichl U. Continuous influenza virus production in cell culture shows a periodic accumulation of defective interfering particles. PLoS One. 2013 Sep 5;8(9):e72288. doi: 10.1371/journal.pone.0072288. PMID: 24039749; PMCID: PMC3764112.

26. Furet P, Guagnano V, Fairhurst RA, Imbach-Weese P, Bruce I, Knapp M, Fritsch C, Blasco F, Blanz J, Aichholz R, Hamon J, Fabbro D, Caravatti G. Discovery of NVP-BYL719 a potent and selective phosphatidylinositol-3 kinase alpha inhibitor selected for clinical evaluation. Bioorg Med Chem Lett. 2013 Jul 1;23(13):3741-8. doi: 10.1016/j.bmcl.2013.05.007. Epub 2013 May 14. Erratum in: Bioorg Med Chem Lett. 2013 Aug 15;23(16):4723. PMID: 23726034.

27. Fritsch C, Huang A, Chatenay-Rivauday C, Schnell C, Reddy A, Liu M, Kauffmann A, Guthy D, Erdmann D, De Pover A, Furet P, Gao H, Ferretti S, Wang Y, Trappe J, Brachmann SM, Maira SM, Wilson C, Boehm M, Garcia-Echeverria C, Chene P, Wiesmann M, Cozens R, Lehar J, Schlegel R, Caravatti G, Hofmann F, Sellers WR. Characterization of the novel

and specific PI3Kα inhibitor NVP-BYL719 and development of the patient stratification strategy for clinical trials. Mol Cancer Ther. 2014 May;13(5):1117-29. doi: 10.1158/1535-7163.MCT-13-0865. Epub 2014 Mar 7. PMID: 24608574.

28. Gardner EM, Beli E, Clinthorne JF, Duriancik DM. Energy intake and response to infection with influenza. Annu Rev Nutr. 2011 Aug 21;31:353-67. doi: 10.1146/annurev-nutr-081810-160812. PMID: 21548773.

29. Hale BG, Jackson D, Chen YH, Lamb RA, Randall RE. Influenza A virus NS1 protein binds p85beta and activates phosphatidylinositol-3-kinase signaling. Proc Natl Acad Sci U S A. 2006 Sep 19;103(38):14194-9. doi: 10.1073/pnas.0606109103. Epub 2006 Sep 8. PMID: 16963558; PMCID: PMC1599933.

30. Hara K, Nakazono Y, Kashiwagi T, Hamada N, Watanabe H. Co-incorporation of the PB2 and PA polymerase subunits from human H3N2 influenza virus is a critical determinant of the replication of reassortant ribonucleoprotein complexes. J Gen Virol. 2013 Nov;94(Pt 11):2406-2416. doi: 10.1099/vir.0.053959-0. Epub 2013 Aug 12. PMID: 23939981.

31. Harding AT, Haas GD, Chambers BS, Heaton NS. Influenza viruses that require 10 genomic segments as antiviral therapeutics. PLoS Pathog. 2019 Nov 15;15(11):e1008098. doi: 10.1371/journal.ppat.1008098. PMID: 31730644; PMCID: PMC6881065.

32. Honce R, Schultz-Cherry S. Impact of Obesity on Influenza A Virus Pathogenesis, Immune Response, and Evolution. Front Immunol. 2019 May 10;10:1071. doi: 10.3389/fimmu.2019.01071. PMID: 31134099; PMCID: PMC6523028.

33. Honce R, Karlsson EA, Wohlgemuth N, Estrada LD, Meliopoulos VA, Yao J, Schultz-Cherry S. Obesity-Related Microenvironment Promotes Emergence of Virulent Influenza Virus Strains. mBio. 2020 Mar 3;11(2):e03341-19. doi: 10.1128/mBio.03341-19. PMID: 32127459; PMCID: PMC7064783.

34. Hopkins BD, Goncalves MD, Cantley LC. Insulin-PI3K signalling: an evolutionarily insulated metabolic driver of cancer. Nat Rev Endocrinol. 2020 May;16(5):276-283. doi: 10.1038/s41574-020-0329-9. Epub 2020 Mar 3. PMID: 32127696; PMCID: PMC7286536

35. Huang AS, Baltimore D. Defective viral particles and viral disease processes. Nature. 1970 Apr 25;226(5243):325-7. doi: 10.1038/226325a0. PMID: 5439728.

36. Jaworski E, Routh A. Parallel ClickSeq and Nanopore sequencing elucidates the rapid evolution of defective-interfering RNAs in Flock House virus. PLoS Pathog. 2017 May 5;13(5):e1006365. doi: 10.1371/journal.ppat.1006365. PMID: 28475646; PMCID: PMC5435362.

37. Jokinen E, Koivunen JP. MEK and PI3K inhibition in solid tumors: rationale and evidence to date. Ther Adv Med Oncol. 2015 May;7(3):170-80. doi: 10.1177/1758834015571111. PMID: 26673580; PMCID: PMC4406912.

38. Karst SM, Ziels RM, Kirkegaard RH, Sørensen EA, McDonald D, Zhu Q, Knight R, Albertsen M. High-accuracy long-read amplicon sequences using unique molecular identifiers with Nanopore or PacBio sequencing. Nat Methods. 2021 Feb;18(2):165-169. doi: 10.1038/s41592-020-01041-y. Epub 2021 Jan 11. PMID: 33432244.

39. Kuss-Duerkop SK, Wang J, Mena I, White K, Metreveli G, Sakthivel R, Mata MA, Muñoz-Moreno R, Chen X, Krammer F, Diamond MS, Chen ZJ, García-Sastre A, Fontoura BMA. Influenza virus differentially activates mTORC1 and mTORC2 signaling to maximize late stage replication. PLoS Pathog. 2017 Sep 27;13(9):e1006635. doi: 10.1371/journal.ppat.1006635. PMID: 28953980; PMCID: PMC5617226.

40. Lopes AM, Domingues P, Zell R, Hale BG. Structure-Guided Functional Annotation of the Influenza A Virus NS1 Protein Reveals Dynamic Evolution of the p85β-Binding Site during Circulation in Humans. J Virol. 2017 Oct 13;91(21):e01081-17. doi: 10.1128/JVI.01081-17. PMID: 28814525; PMCID: PMC5640874.

41. Li Y, Anderson DH, Liu Q, Zhou Y. Mechanism of influenza A virus NS1 protein interaction with the p85beta, but not the p85alpha, subunit of phosphatidylinositol 3-kinase (PI3K) and up-regulation of PI3K activity. J Biol Chem. 2008 Aug 22;283(34):23397-409. doi: 10.1074/jbc.M802737200. Epub 2008 Jun 5. PMID: 18534979.

42. Luo Y, Xu W, Li G, Cui W. Weighing In on mTOR Complex 2 Signaling: The Expanding Role in Cell Metabolism. Oxid Med Cell Longev. 2018 Oct 30;2018:7838647. doi: 10.1155/2018/7838647. PMID: 30510625; PMCID: PMC6232796.

43. Manzoni TB, López CB. Defective (interfering) viral genomes re-explored: impact on antiviral immunity and virus persistence. Future Virol. 2018 Jul;13(7):493-503. doi: 10.2217/fvl-2018-0021. Epub 2018 Jun 12. PMID: 30245734; PMCID: PMC6136085.

44. Matrosovich M, Matrosovich T, Garten W, Klenk HD. New low-viscosity overlay medium for viral plaque assays. Virol J. 2006 Aug 31;3:63. doi: 10.1186/1743-422X-3-63. PMID: 16945126; PMCID: PMC1564390.

45. Meng B, Bentley K, Marriott AC, Scott PD, Dimmock NJ, Easton AJ. Unexpected complexity in the interference activity of a cloned influenza defective interfering RNA. Virol J. 2017 Jul 24;14(1):138. doi: 10.1186/s12985-017-0805-6. PMID: 28738877; PMCID: PMC5525295.

46. Milne I, Stephen G, Bayer M, Cock PJ, Pritchard L, Cardle L, Shaw PD, Marshall D. Using Tablet for visual exploration of second-generation sequencing data. Brief Bioinform. 2013 Mar;14(2):193-202. doi: 10.1093/bib/bbs012. Epub 2012 Mar 24. PMID: 22445902.

47. Nayak DP, Sivasubramanian N, Davis AR, Cortini R, Sung J. Complete sequence analyses show that two defective interfering influenza viral RNAs contain a single internal deletion of a polymerase gene. Proc Natl Acad Sci U S A. 1982 Apr;79(7):2216-20. doi: 10.1073/pnas.79.7.2216. PMID: 6954536; PMCID: PMC346162.

48. Octaviani CP, Goto H, Kawaoka Y. Reassortment between seasonal H1N1 and pandemic (H1N1) 2009 influenza viruses is restricted by limited compatibility among polymerase subunits. J Virol. 2011 Aug;85(16):8449-52. doi: 10.1128/JVI.05054-11. Epub 2011 Jun 15. PMID: 21680507; PMCID: PMC3147997.

49. Odagiri T, Tashiro M. Segment-specific noncoding sequences of the influenza virus genome RNA are involved in the specific competition between defective interfering RNA and its progenitor RNA segment at the virion assembly step. J Virol. 1997 Mar;71(3):2138-45. doi: 10.1128/JVI.71.3.2138-2145.1997. PMID: 9032347; PMCID: PMC191316.

50. Pargett M, Gillies TE, Teragawa CK, Sparta B, Albeck JG. Single-Cell Imaging of ERK Signaling Using Fluorescent Biosensors. Methods Mol Biol. 2017;1636:35-59. doi: 10.1007/978-1-4939-7154-1_3. PMID: 28730471; PMCID: PMC8005261.

51. Pelz L, Rüdiger D, Dogra T, Alnaji FG, Genzel Y, Brooke CB, Kupke SY, Reichl U. Semi-continuous Propagation of Influenza A Virus and Its Defective Interfering Particles: Analyzing the Dynamic Competition To Select Candidates for Antiviral Therapy. J Virol. 2021 Nov 23;95(24):e0117421. doi: 10.1128/JVI.01174-21. Epub 2021 Sep 22. PMID: 34550771; PMCID: PMC8610589.

52. Perez-Cidoncha M, Killip MJ, Oliveros JC, Asensio VJ, Fernández Y, Bengoechea JA, Randall RE, Ortín J. An unbiased genetic screen reveals the polygenic nature of the influenza virus anti-interferon response. J Virol. 2014 May;88(9):4632-46. doi: 10.1128/JVI.00014-14. Epub 2014 Feb 26. PMID: 24574395; PMCID: PMC3993829.

53. Ranum JN, Ledwith MP, Alnaji FG, Diefenbacher M, Orton R, Sloan E, Güereca M, Feltman EM, Smollett K, da Silva Filipe A, Conley M, Russell AB, Brooke CB, Hutchinson E, Mehle A. Cryptic proteins translated from deletion-containing viral genomes dramatically expand the influenza virus proteome. Nucleic Acids Res. 2024 Apr 12;52(6):3199-3212. doi: 10.1093/nar/gkae133. PMID: 38407436; PMCID: PMC11014358.

54. Rodriguez A, Falcon A, Cuevas MT, Pozo F, Guerra S, García-Barreno B, Martinez-Orellana P, Pérez-Breña P, Montoya M, Melero JA, Pizarro M, Ortin J, Casas I, Nieto A. Characterization in vitro and in vivo of a pandemic H1N1 influenza virus from a fatal case.

PLoS One. 2013;8(1):e53515. doi: 10.1371/journal.pone.0053515. Epub 2013 Jan 10. PMID: 23326447; PMCID: PMC3542358.

55. Rolfes MA, Flannery B, Chung JR, O'Halloran A, Garg S, Belongia EA, Gaglani M, Zimmerman RK, Jackson ML, Monto AS, Alden NB, Anderson E, Bennett NM, Billing L, Eckel S, Kirley PD, Lynfield R, Monroe ML, Spencer M, Spina N, Talbot HK, Thomas A, Torres SM, Yousey-Hindes K, Singleton JA, Patel M, Reed C, Fry AM; US Influenza Vaccine Effectiveness (Flu VE) Network, the Influenza Hospitalization Surveillance Network, and the Assessment Branch, Immunization Services Division, Centers for Disease Control and Prevention. Effects of Influenza Vaccination in the United States During the 2017-2018 Influenza Season. Clin Infect Dis. 2019 Nov 13;69(11):1845-1853. doi: 10.1093/cid/ciz075. PMID: 30715278; PMCID: PMC7188082.

56. Routh A, Johnson JE. Discovery of functional genomic motifs in viruses with ViReMa-a Virus Recombination Mapper-for analysis of next-generation sequencing data. Nucleic Acids Res. 2014 Jan;42(2):e11. doi: 10.1093/nar/gkt916. Epub 2013 Oct 16. PMID: 24137010; PMCID: PMC3902915.

57. Russell AB, Trapnell C, Bloom JD. Extreme heterogeneity of influenza virus infection in single cells. Elife. 2018 Feb 16;7:e32303. doi: 10.7554/eLife.32303. PMID: 29451492; PMCID: PMC5826275.

58. Saha A, Connelly S, Jiang J, Zhuang S, Amador DT, Phan T, Pilz RB, Boss GR. Akt phosphorylation and regulation of transketolase is a nodal point for amino acid control of purine synthesis. Mol Cell. 2014 Jul 17;55(2):264-76. doi: 10.1016/j.molcel.2014.05.028. Epub 2014 Jun 26. PMID: 24981175; PMCID: PMC4104231.

59. Saira K, Lin X, DePasse JV, Halpin R, Twaddle A, Stockwell T, Angus B, Cozzi-Lepri A, Delfino M, Dugan V, Dwyer DE, Freiberg M, Horban A, Losso M, Lynfield R, Wentworth DN, Holmes EC, Davey R, Wentworth DE, Ghedin E; INSIGHT FLU002 Study Group; INSIGHT FLU003 Study Group. Sequence analysis of in vivo defective interfering-like RNA of influenza A H1N1 pandemic virus. J Virol. 2013 Jul;87(14):8064-74. doi: 10.1128/JVI.00240-13. Epub 2013 May 15. PMID: 23678180; PMCID: PMC3700204.

60. Smallwood HS, Duan S, Morfouace M, Rezinciuc S, Shulkin BL, Shelat A, Zink EE, Milasta S, Bajracharya R, Oluwaseum AJ, Roussel MF, Green DR, Pasa-Tolic L, Thomas PG. Targeting Metabolic Reprogramming by Influenza Infection for Therapeutic Intervention. Cell Rep. 2017 May 23;19(8):1640-1653. doi: 10.1016/j.celrep.2017.04.039. PMID: 28538182; PMCID: PMC5599215.

61. Smith CM, Scott PD, O'Callaghan C, Easton AJ, Dimmock NJ. A Defective Interfering Influenza RNA Inhibits Infectious Influenza Virus Replication in Human Respiratory Tract Cells: A Potential New Human Antiviral. Viruses. 2016 Aug 22;8(8):237. doi: 10.3390/v8080237. PMID: 27556481; PMCID: PMC4997599.

62. Sotcheff S, Zhou Y, Yeung J, Sun Y, Johnson JE, Torbett BE, Routh AL. ViReMa: a virus recombination mapper of next-generation sequencing data characterizes diverse recombinant viral nucleic acids. Gigascience. 2023 Mar 20;12:giad009. doi: 10.1093/gigascience/giad009. PMID: 36939008; PMCID: PMC10025937.

63. Tange, O. (2022, May 22). GNU Parallel 20220522 ('NATO'). Zenodo. https://doi.org/10.5281/zenodo.6570228

64. Tapia F, Laske T, Wasik MA, Rammhold M, Genzel Y, Reichl U. Production of Defective Interfering Particles of Influenza A Virus in Parallel Continuous Cultures at Two Residence Times-Insights From qPCR Measurements and Viral Dynamics Modeling. Front Bioeng Biotechnol. 2019 Oct 18;7:275. doi: 10.3389/fbioe.2019.00275. PMID: 31681751; PMCID: PMC681321.

65. Vasilijevic J, Zamarreño N, Oliveros JC, Rodriguez-Frandsen A, Gómez G, Rodriguez G, Pérez-Ruiz M, Rey S, Barba I, Pozo F, Casas I, Nieto A, Falcón A. Reduced accumulation of defective viral genomes contributes to severe outcome in influenza virus infected patients. PLoS Pathog. 2017 Oct 12;13(10):e1006650. doi: 10.1371/journal.ppat.1006650. PMID: 29023600; PMCID: PMC5638565.

66. Vignuzzi M, López CB. Defective viral genomes are key drivers of the virus-host interaction. Nat Microbiol. 2019 Jul;4(7):1075-1087. doi: 10.1038/s41564-019-0465-y. Epub 2019 Jun 3. PMID: 31160826; PMCID: PMC7097797.

67. VON MAGNUS P. Incomplete forms of influenza virus. Adv Virus Res. 1954;2:59-79. doi: 10.1016/s0065-3527(08)60529-1. PMID: 13228257.

68. Wang C, Forst CV, Chou TW, Geber A, Wang M, Hamou W, Smith M, Sebra R, Zhang B, Zhou B, Ghedin E. Cell-to-Cell Variation in Defective Virus Expression and Effects on Host Responses during Influenza Virus Infection. mBio. 2020 Jan 14;11(1):e02880-19. doi: 10.1128/mBio.02880-19. PMID: 31937643; PMCID: PMC6960286.

69. Wang C, Honce R, Salvatore M, Chow D, Randazzo D, Yang J, Twells NM, Mahal LK, Schultz-Cherry S, Ghedin E. Influenza Defective Interfering Virus Promotes Multiciliated Cell Differentiation and Reduces the Inflammatory Response in Mice. J Virol. 2023 Jun 29;97(6):e0049323. doi: 10.1128/jvi.00493-23. Epub 2023 May 31. PMID: 37255439; PMCID: PMC10308934.

70. Wasik MA, Eichwald L, Genzel Y, Reichl U. Cell culture-based production of defective interfering particles for influenza antiviral therapy. Appl Microbiol Biotechnol. 2018 Feb;102(3):1167-1177. doi: 10.1007/s00253-017-8660-3. Epub 2017 Dec 5. PMID: 29204901; PMCID: PMC5778153.

71. Wee P, Wang Z. Epidermal Growth Factor Receptor Cell Proliferation Signaling Pathways. Cancers (Basel). 2017 May 17;9(5):52. doi: 10.3390/cancers9050052. PMID: 28513565; PMCID: PMC5447962.

72. Winter G, Fields S, Ratti G. The structure of two subgenomic RNAs from human influenza virus A/PR/8/34. Nucleic Acids Res. 1981 Dec 21;9(24):6907-15. doi: 10.1093/nar/9.24.6907. PMID: 7335495; PMCID: PMC327650.

73. Wu M, Zhou E, Sheng R, Fu X, Li J, Jiang C, Su W. Defective Interfering Particles of Influenza Virus and Their Characteristics, Impacts, and Use in Vaccines and Antiviral Strategies: A Systematic Review. Viruses. 2022 Dec 12;14(12):2773. doi: 10.3390/v14122773. PMID: 36560777; PMCID: PMC9781619.

74. Yamagata Y, Muramoto Y, Miyamoto S, Shindo K, Nakano M, Noda T. Generation of a purely clonal defective interfering influenza virus. Microbiol Immunol. 2019 May;63(5):164-171. doi: 10.1111/1348-0421.12681. Epub 2019 May 17. PMID: 30997933.

75. Yang J, Nie J, Ma X, Wei Y, Peng Y, Wei X. Targeting PI3K in cancer: mechanisms and advances in clinical trials. Mol Cancer. 2019 Feb 19;18(1):26. doi: 10.1186/s12943-019-0954-x. PMID: 30782187; PMCID: PMC6379961.

76. Yuan TL, Cantley LC. PI3K pathway alterations in cancer: variations on a theme. Oncogene. 2008 Sep 18;27(41):5497-510. doi: 10.1038/onc.2008.245. PMID: 18794884; PMCID: PMC3398461.

77. Zhao H, To KKW, Chu H, Ding Q, Zhao X, Li C, Shuai H, Yuan S, Zhou J, Kok KH, Jiang S, Yuen KY. Dual-functional peptide with defective interfering genes effectively protects mice against avian and seasonal influenza. Nat Commun. 2018 Jun 15;9(1):2358. doi: 10.1038/s41467-018-04792-7. PMID: 29907765; PMCID: PMC6004018.

Supplementary Materials

Cluster-forming Assay

The cluster-forming assay combines the infection localization of a conventional plaque assay with the immunofluorescence (IF) staining and microscopy of a conventional immunofocus assay to capture influenza infectivity at a deeper resolution than possible with either parent assay alone.

Overnight MDCK-London cells—1.04 x 10^5 total cells per well—were seeded into collagen-treated, glass-bottom 96-well tissue culture plates in MEM plus 5% FBS media to achieve 100% confluence in 24 hr. Confluent monolayers were then inoculated with serial dilutions of virus stock and incubated for 1 hr to allow for virus-monolayer adsorption, after which inoculum was aspirated and monolayers washed with MEM plus 2% bovine serum albumin and 1% Anti-Anti (Virus Infection Media; VIM). At this juncture, the conventional plaque assay or immunofocus assay would respectively see a solid or liquid overlay medium applied to the inoculated monolayers. The cluster-forming assay, on the other hand, applies a low to medium-viscosity overlay medium (VIM plus 4% carboxymethyl cellulose and 1 ug/mL TPCK-Trypsin) that remains in a semi-solid state at the end of the assay. This viscous overlay restricts diffusion of progeny virus to directly adjacent cells much like a conventional plaque assay, but has the added benefit of being removable via an aspirator pipette so that monolayers may be fixed, stained with IF antibodies, and imaged. Overlaid monolayers were incubated an additional 11 hours, at which point overlay media was aspirated and monolayers fixed with 4% PFA. Fixed monolayers were stained with fluorophore-conjugated IF antibodies targeting Influenza A nucleoprotein, counterstained

with Hoechst, and imaged via fluorescence microscopy. The output at this juncture is an IF image of an flu-infected monolayer (**Supplementary Figure 2.1**) wherein each cluster of infected cells represents a productive infection mounted by a single propagation-capable virion—a *productive clustering unit* (PCU)—while solitary infection foci represent abortive infections mounted by propagation-incapable virus—*non-clustering units* (NCU).

2.1A

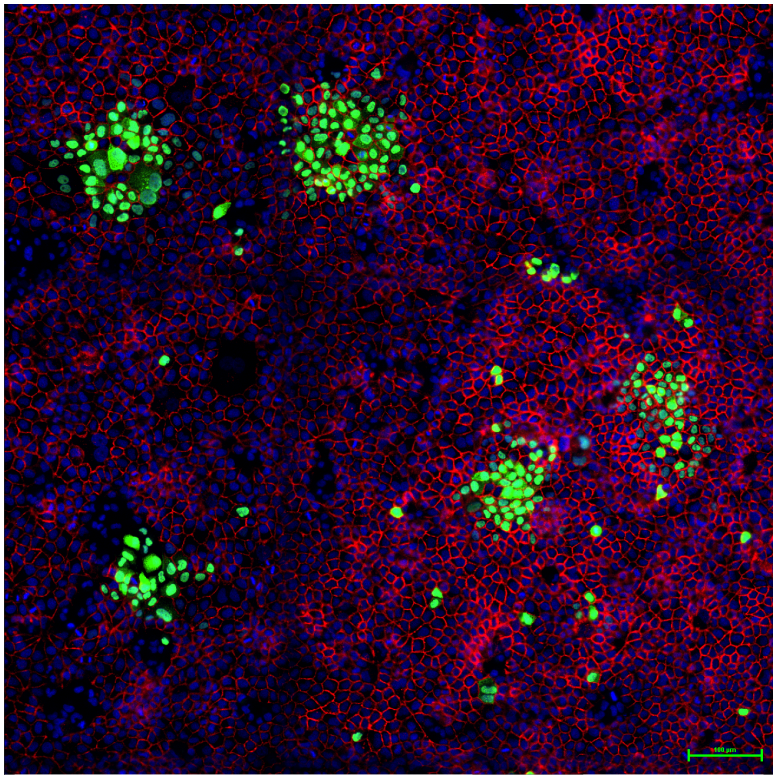

2.1B

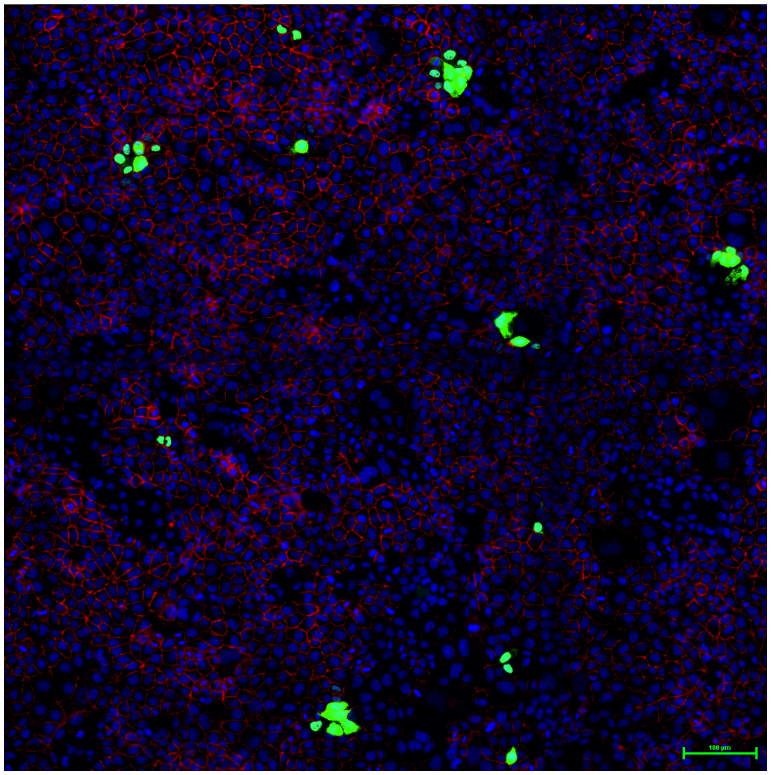

Supplementary Figure 2.1. Cluster-forming assay of Influenza A Virus on MDCK-London cells showing productive and abortive infections. Green/GFP – A/California/07/2009 nucleoprotein (**A**), A/Texas/50/2012 nucleoprotein (**B**); Blue/Hoechst – MDCK-London nucleus; Red/Cy5 – MDCK-London E-cadherin (**A**) or β-catenin (**B**).

Our proof of concept cluster-forming assays worked as designed; propagation-incapable virus mounted abortive infections as evidenced by NCUs, while propagation-capable virus mounted productive infections as evidenced by PCUs. Ordinarily, PCUs and NCUs would be tallied and titrated, but minor optimization of a few parameters was necessary to boost assay precision. Chief among these parameters were *monolayer integrity* and *PCU spillover*.

Monolayer Integrity: Monolayer damage and stripping undermines cluster-forming assay precision because the signal of an infection event is diminished—or lost outright—with each sloughed cell. This is especially relevant for abortive infections, whose assay signal is transmitted by a sin-

gle cell, the sloughing of which results in underreporting and underestimation of NCU titer and NCU proportion. Therefore, it is imperative that monolayer integrity be preserved at all steps. We discovered that not prewarming reagents to room temperature or 37 °C—i.e. rapid reduction in temperature—caused monolayers to peel (**Supplementary Figure 2.2A**). That said, monolayer damage was consistently and primarily observed in monolayer regions of lower cell density (**Supplementary Figure 2.2B**). We found that seeding at higher cell density—upwards of 1.6 x 10^4 to 1.04 x 10^5 cells per well—and seeding more evenly with a wide-bore 2mL serological pipette in place of a multichannel pipette was sufficient to mitigate monolayer damage in future assays (**Supplementary Figure 2.3A**). However, PCU spillover and streaks remained an issue; especially for a fast growing strain like the pandemic A/California/07/2009(H1N1) (**Supplementary Figure 2.3B-C**).

2.2A

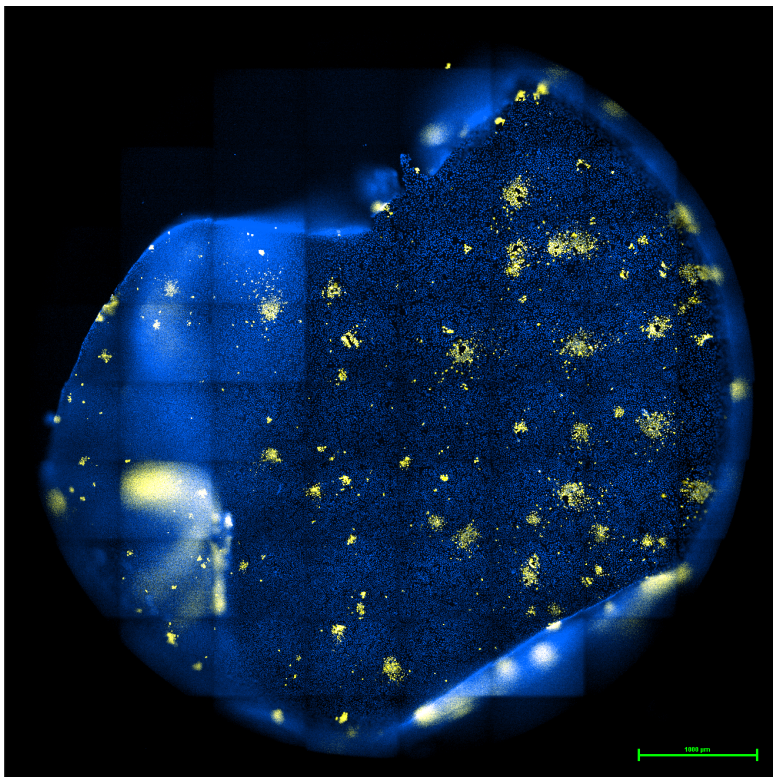

2.2B

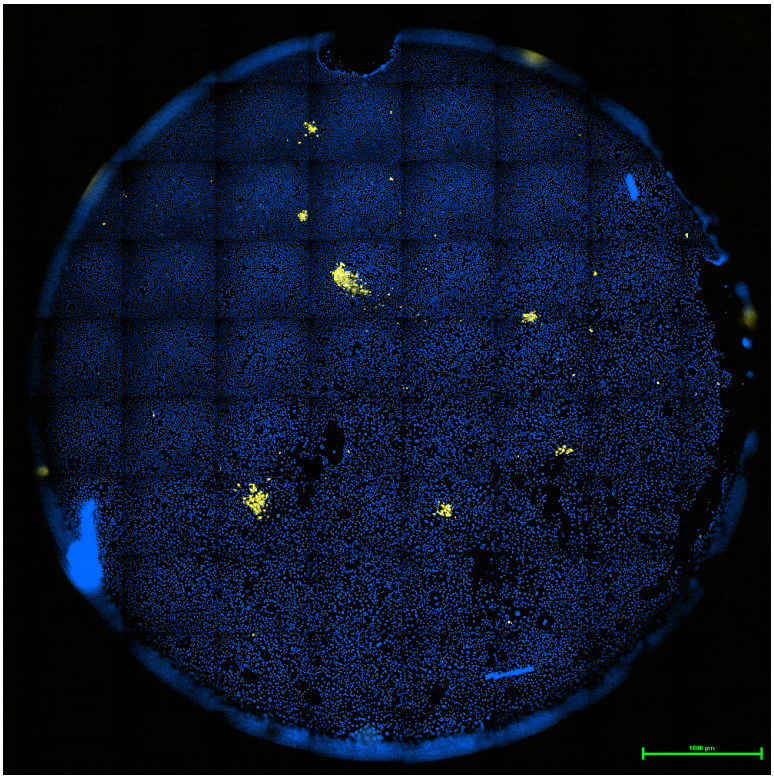

2.2C

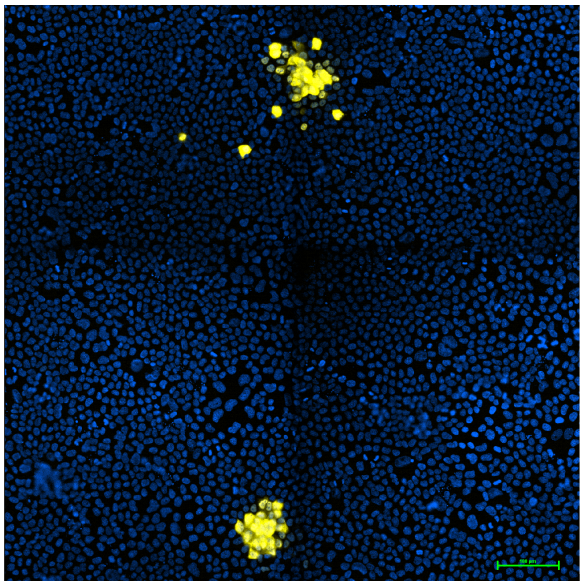

2.2D

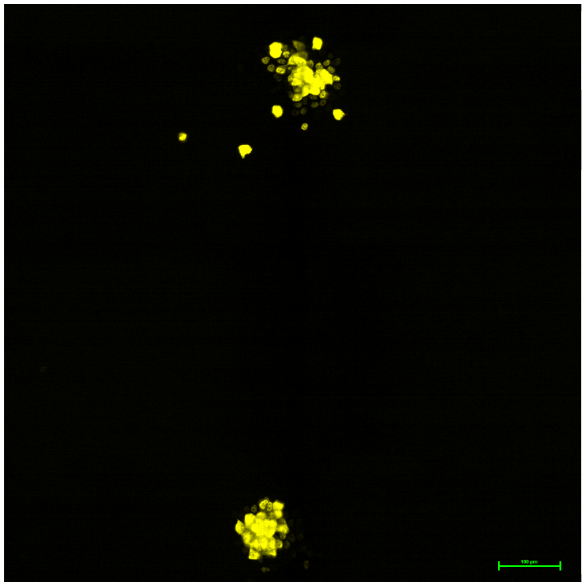

2.2E

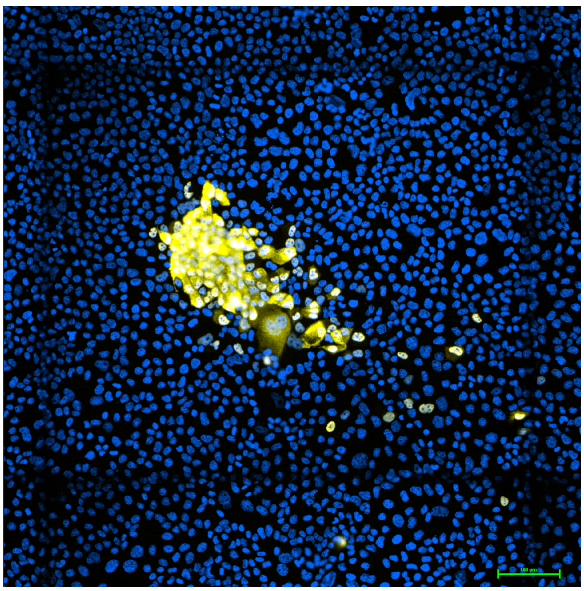

2.2F

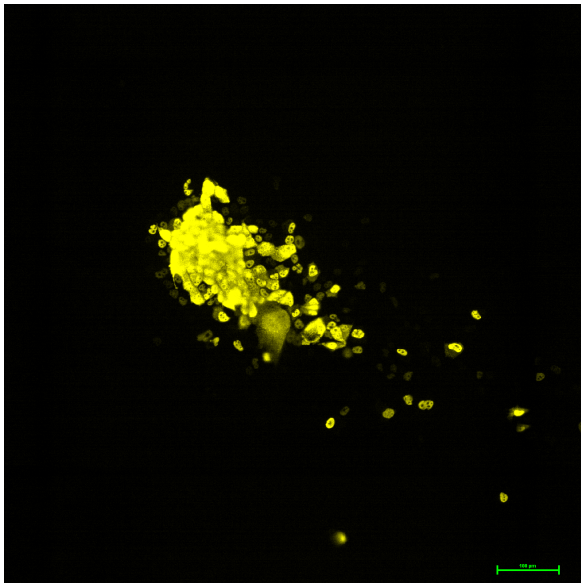

Supplementary Figure 2.2. Early proof of concept cluster-forming assay. (**A**) Monolayer peeling following exposure to cold (4 °C) reagents; always pre-warm reagents to between room temp and 37 °C before use. (**B**) Monolayer damage in low cell density areas; seed monolayers uniformly and at sufficient cell density. (**C, D**) PCU spillover. (**E, F**) PCU streak/comet. Yellow/YFP – A/Texas/50/2012 nucleoprotein ; Blue/Hoechst – MDCK-London nucleus.

PCU spillover: In a cluster-forming assay, *spillover* has occurred if there are satellite single-cell infection event(s) surrounding a PCU (**Supplementary Figure 2.2C-F, 2.3B-C**). Spillover un-

dermines assay accuracy because it is unclear if these solitary infection events are progeny virus spawned by the closeby PCU, or a bona fide NCU from the initial inoculum. To mitigate PCU spillover, we pursued optimizations under certain key considerations. First, longer assay run times allow for farther diffusion of progeny virus from ground zero of a PCU infection. Second, less viscosity in the semi-solid overlay media increases flux of convection currents in the media, which also facilitates diffusion of progeny virus from ground zero of the PCU infection. As spillover was evident under conditions of 2% CMC and 19 hr assay runtime (**Supplementary Figure 2.2C-F, 2.3B-C**), we tested 8 hr, 10 hr, and 12 hr assay runtimes under 2% and 4% CMC. We found spillover to be mitigated under all tested conditions, however 8 hr and 10 hr were insufficient durations for PCUs to fully bloom and be counted as such, especially in slower growing strains like A/Texas/50/2012(H3N2) (**Supplementary Figure 2.4**). We also observed minor but inconsistent monolayer damage in the 2% CMC treatment groups, compared with no such damage in the 4% CMC groups. This damage was not observed during previous 19 hr assays, most likely because monolayer damage at the 12 hr time point had an additional 7 hr of recovery and resealing. Based on these findings, we settled on 4% CMC and 12 hr runtime for future assays involving A/California/07/2009(H1N1) and A/Texas/50/2012(H3N2) (**Supplementary Figure 2.5**).

BIOHACKER ALERT: Do not make CMC stock in microwave. Autoclave at 121°C for 30 min.

2.3A

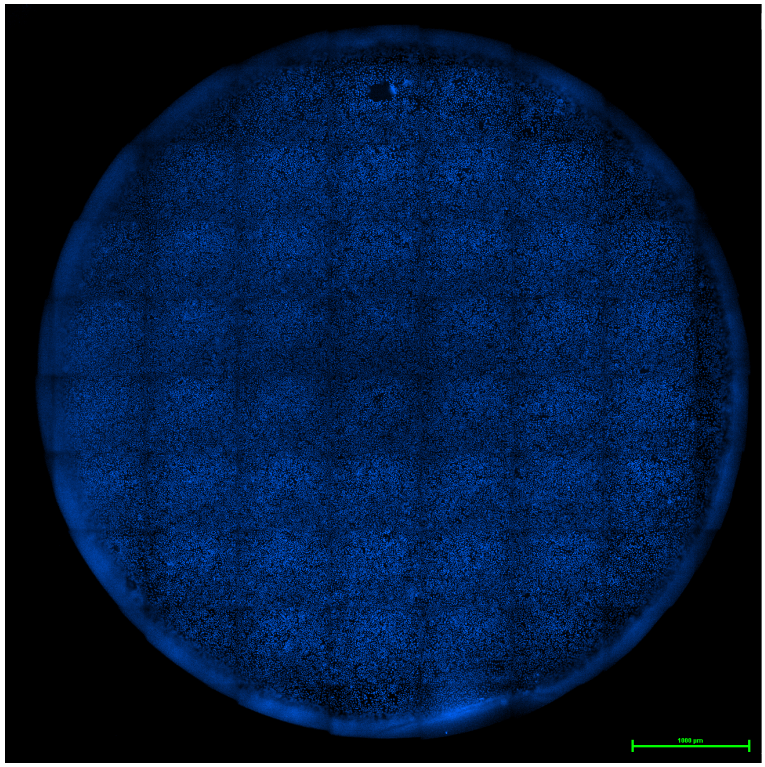

2.3B

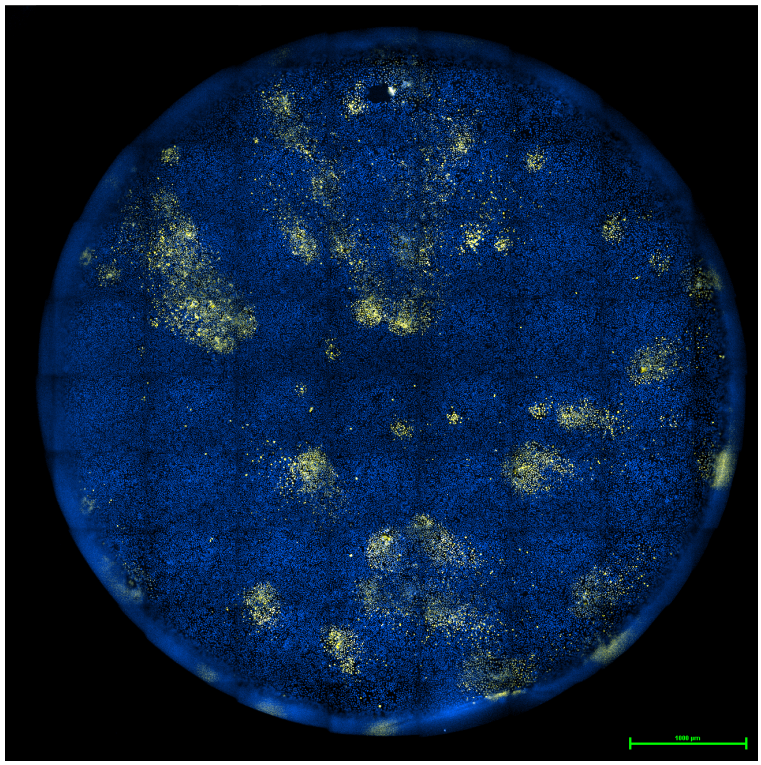

2.3C

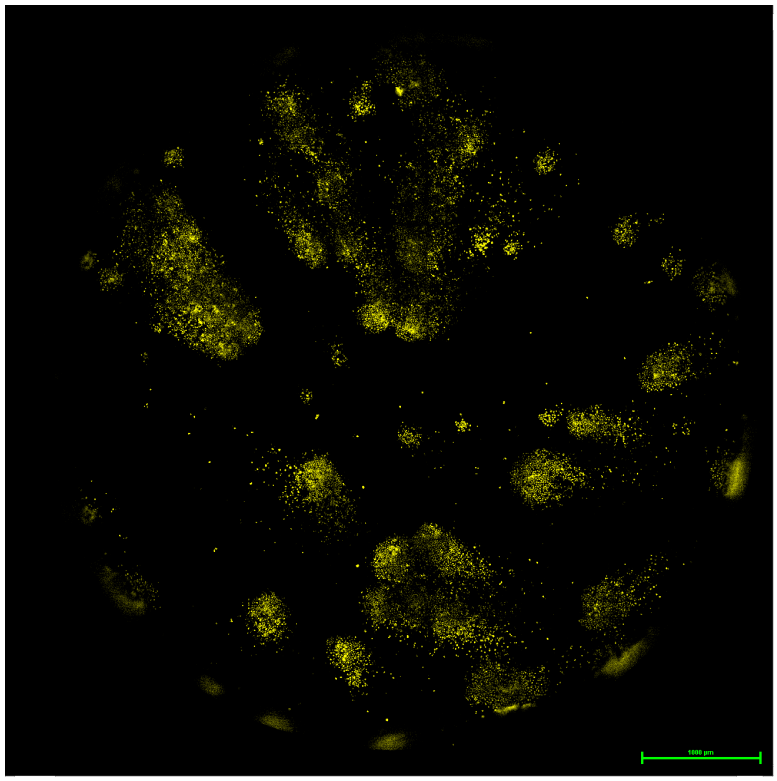

Supplementary Figure 2.3. (**A**) Barring aspirator pipette tip damage, a minimum cell seeding density (1E4 – 1.04E5 cells per well) is required to preserve monolayer integrity. However, PCU spillover and streaks still persist (**B-C**). Yellow/YFP – A/California/07/2009 nucleoprotein ; Blue/Hoechst – MDCK-London nucleus.

2.4A

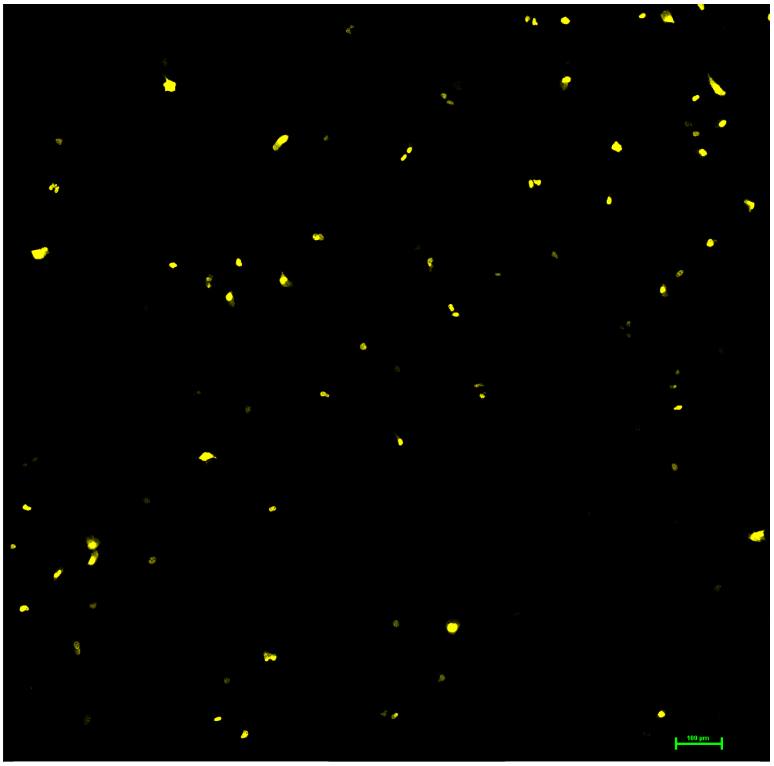

2.4B

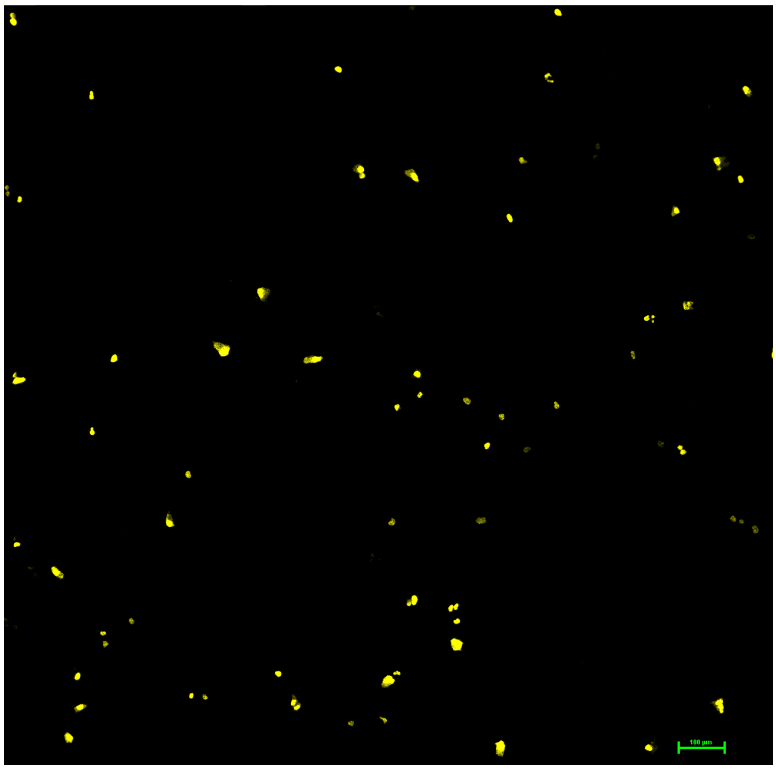

2.4C

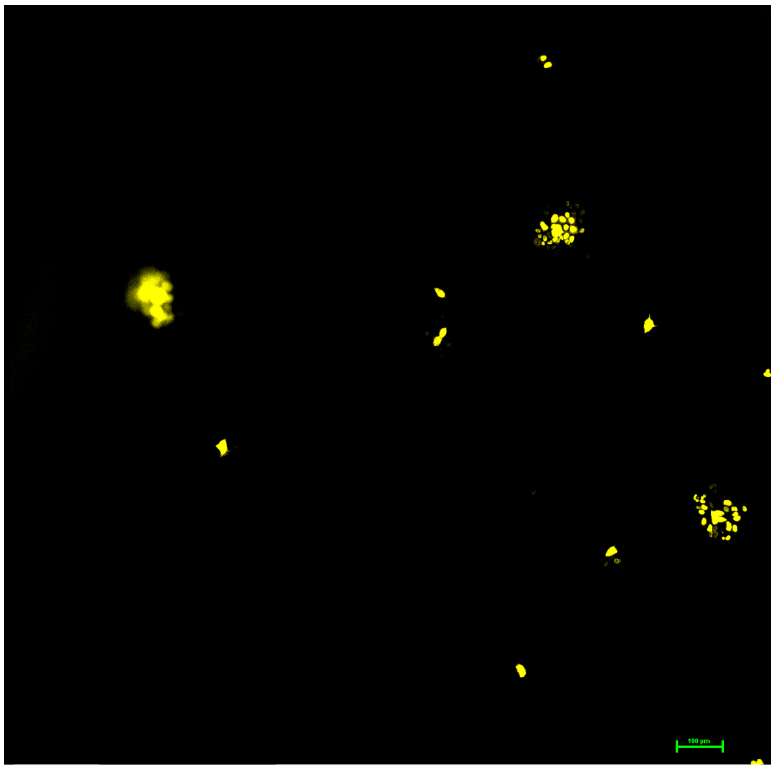

2.4D

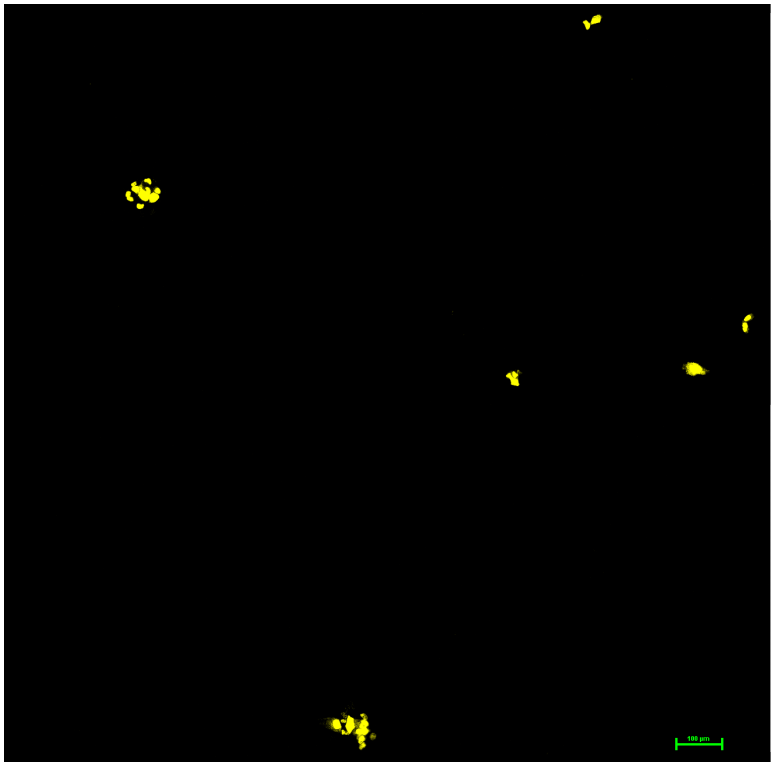

Supplementary Figure 2.4. Cluster-forming assay spillover mitigation; optimization of overlay concentration and assay runtime. (**A**) 8hpi at 2% CMC. (**B**) 8hpi at 4% CMC. (**C**) 12hpi at 2% CMC. (**D**) 12hpi at 4% CMC. Yellow(YFP) – A/California/07/2009 nucleoprotein.

2.5A

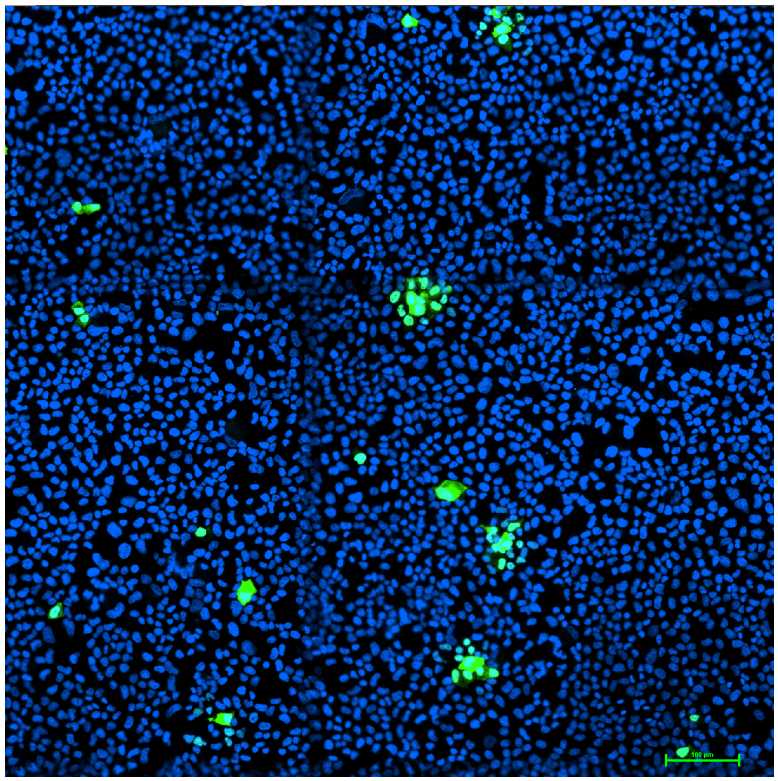

2.5B

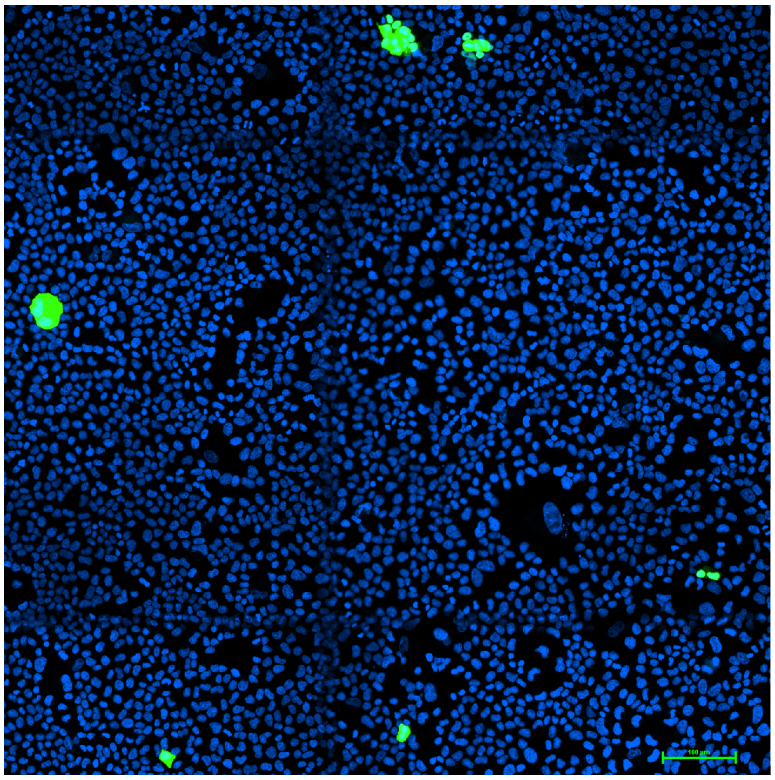

Supplementary Figure 2.5. Optimized cluster-forming assay; with damage-free monolayer and free of PCU spillover or streaks. Green/GFP – A/California/07/2009 nucleoprotein (**A**), A/Texas/50/2012 nucleoprotein (**B**) ; Blue/Hoechst – MDCK-London nucleus.

Cluster-counting Bioinformatics

To count PCUs and NCUs, cluster-forming assay IF images (**Supplementary Figure 2.5**) were put through an automated image analysis pipeline we developed using MATLAB's image processing toolbox. Our guiding design principle was to cordon—or mask—nucleoprotein fluorescence signals (GFP) in the IF image as independent infection events, then overlay said mask with the host nuclei segmentation Hoechst signal to reveal the number of cells each infection event had spread to. We began stepwise assembly of masks around the GFP signals (**Supplementary Figure 2.6**) by binarizing IF images with the *imbinarize* function to make object detection possible, followed by the removal of small, noisy pixels with *bwareaopen*. Masks were sequentially

dilated then filled with *imdilate* and *imfill* functions respectively to smoothen them out and ensure they did not contain holes. To finish the mask assembly, masks were eroded with *imerode* to undo the signal expansion done in the dilation step.

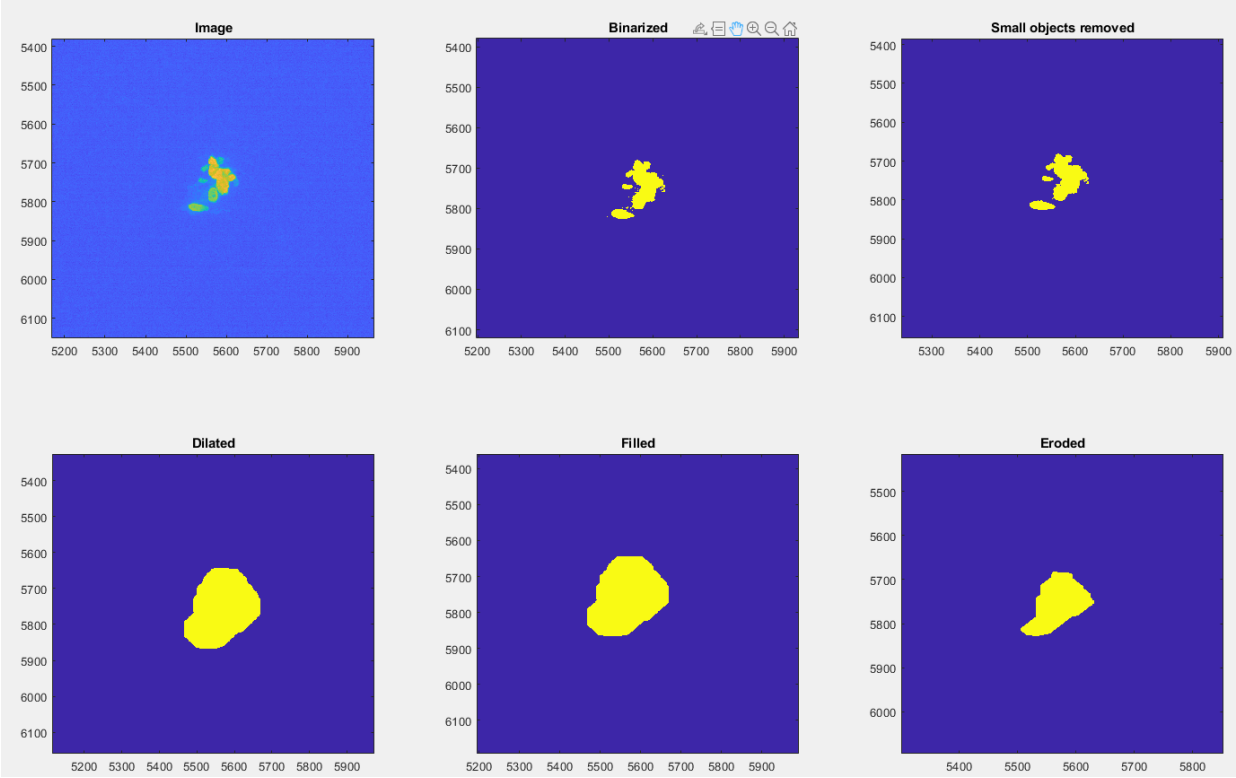

Supplementary Figure 2.6. Stepwise assembly of a mask around the nucleoprotein GFP signal in a productive clustering unit; starting from the initial cluster-forming assay IF image (**top-left**) down to final erosion (**bottom-right**).

At this juncture, the total number of masked objects in the binarized image included desired infection events, as well as undesired background noise from specs and autofluorescence. Undesired masks were filtered out by thresholding the min/max mask area and removing masks that did not contain any nuclei, leaving bona fide infection events—or clusters—that are counted and assigned a unique identity number (clusterID) (**Supplementary Figure 2.7**).

2.7A

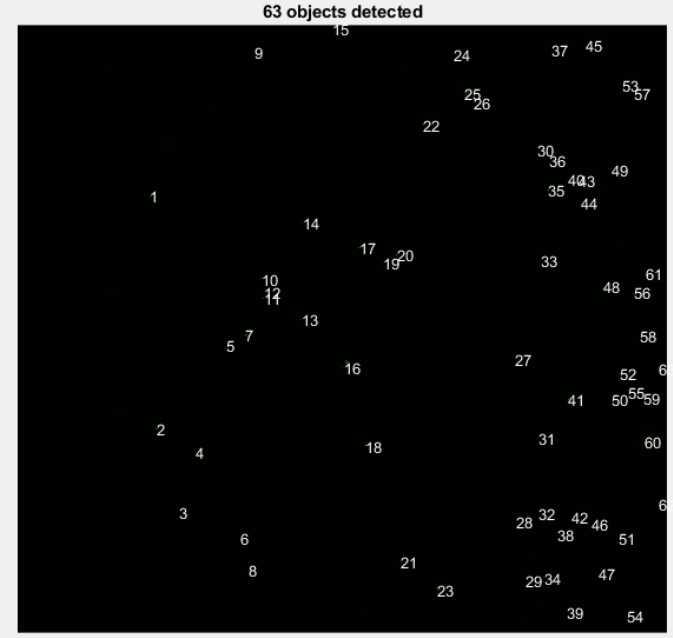

2.7B

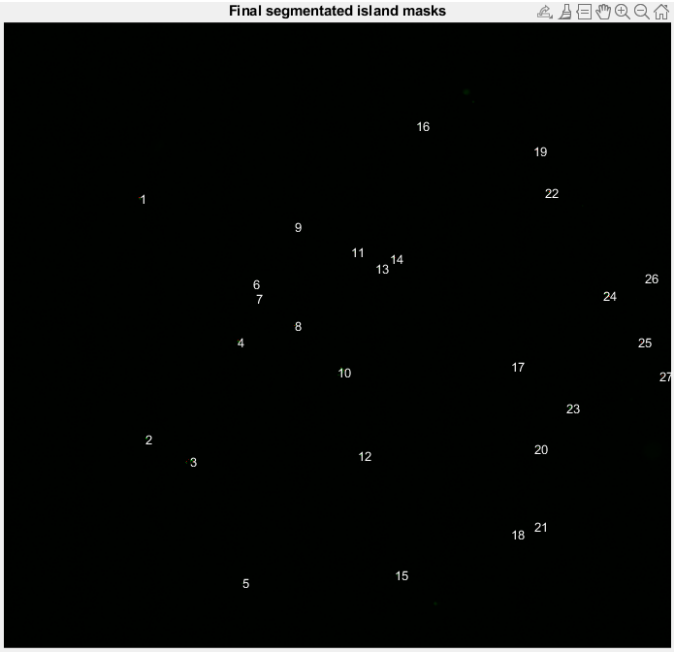

Supplementary Figure 2.7. Masked objects, before (**left**) and after (**right**) removal of background noise from specs and autofluorescence.

Next, segmentation was run on the Hoechst signal in host nuclei and overlaid with the masked clusters to demarcate and count the number of cells each infection had spread to (**Supplementary Figure 2.8**). Cluster data was sequentially exported to a spreadsheet then imported into the R Programming Language, where clusters were classified as PCU (ncell > 1) or NCU (ncell = 1), and after which NCU titer and NCU proportion were successively determined.

2.8A

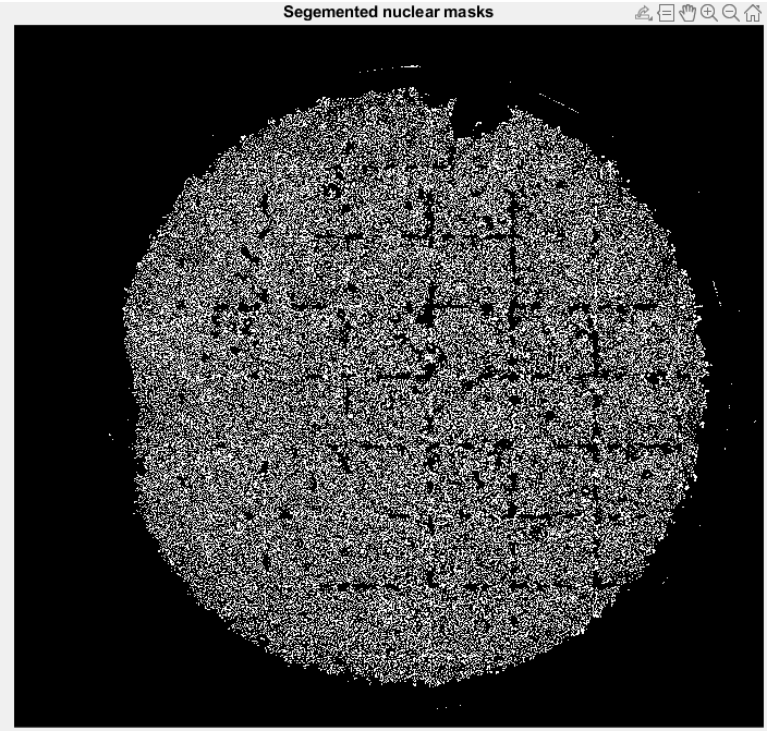

2.8B

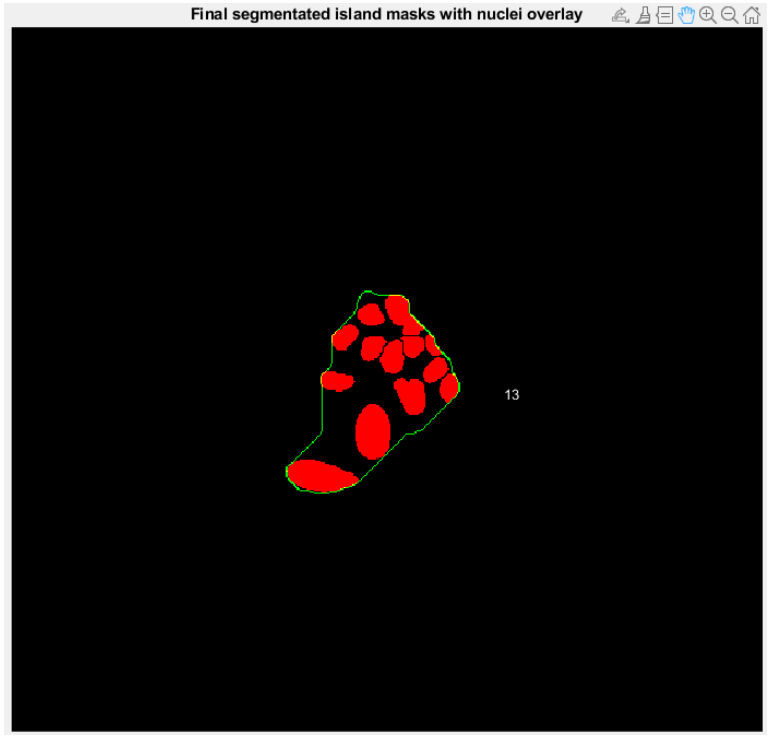

Supplementary Figure 2.8. Nuclear segmentation (**left**) and the segmentation-mask overlay (**right**) to size a clustering unit (PCU).

Insulin activates PI3K network signaling in MDCK-London cells

In addition to exposing uninfected and virus-infected MDCK-London cells to increasing concentrations of alpelisib, a parallel experiment was run in which the same test groups were co-exposed to 10ug/mL of insulin. This experiment confirmed the potentiating effect of insulin on PI3K-AKT signaling activation (positive control for pAKT activation). pAKT activation levels in all parallel insulin exposed experiment groups are higher than their no-insulin counterparts (**Supplementary Figure 2.9**).

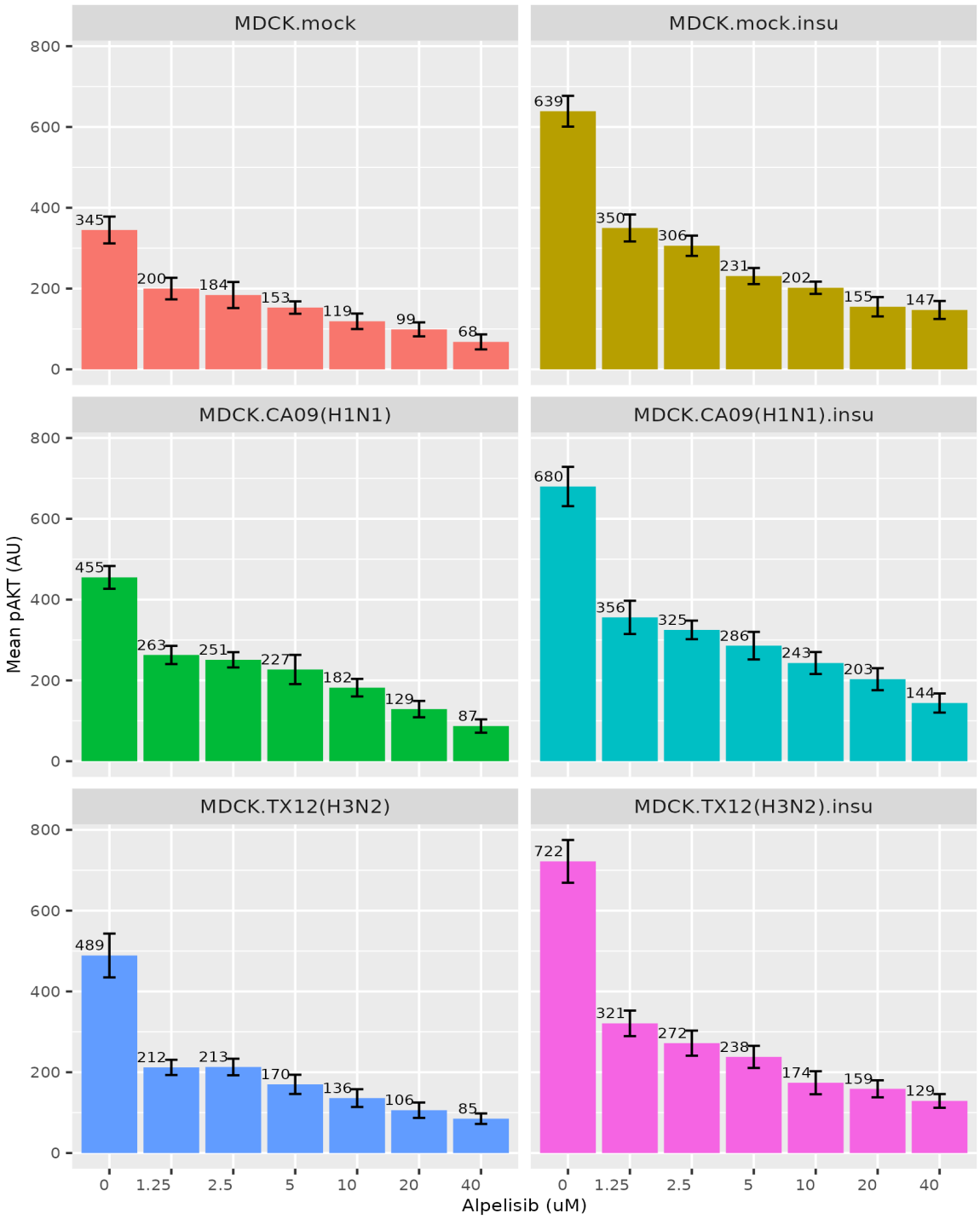

Supplementary Figure 2.9. pAKT activation in mock- and virus-infected MDCK-London cells that were either exposed to different concentrations of alpelisib (left), or co-exposed to 10ug/mL of insulin in addition to alpelisib (right). 0 µM alpelisib treatment group received vehicle solvent (DMSO). n = 3 bioreplicates, sem.

Influenza A defective viral genome production is altered by metabolites, metabolic signaling molecules, and cyanobacteria extracts

Running head: Drug screen defective viral genomes

Ilechukwu Agu[1], Ivy R. José[1], Samuel L. Díaz-Muñoz[1,2*]

[1] Department of Microbiology and Molecular Genetics
University of California, Davis
One Shields Ave
Davis CA 95616

[2] Genome Center
University of California, Davis
One Shields Ave
Davis CA 95616

*Address correspondence to: Samuel L. Díaz Muñoz, samdiazmunoz@ucdavis.edu

Abstract

RNA virus infections are composed of a diverse mix of viral genomes that arise from low fidelity in replication within cells. The interactions between "defective" and full-length viral genomes have been shown to shape pathogenesis, leading to intense research into employing these to develop novel antivirals. In particular, Influenza A defective viral genomes (DVGs) have been associated with milder clinical outcomes. Yet, the full potential of DVGs as broad-spectrum antivirals remains untapped due to the unknown mechanisms of their *de novo* production. Much of the research into the factors affecting defective viral genome production has focused on the virus, while the role of the host has been neglected. We recently showed that altering host cell metabolism away from pro-growth pathways using alpelisib increased the production of Influenza A defective viral genomes. To uncover other drugs that could induce infections to create more DVGs, we subjected active influenza infections of two circulating human subtypes (A/H1N1 & A/H3N2) to a screen of metabolites, metabolic signaling molecules, and

cyanobacteria-derived biologics, after which we quantified the defective viral genomes (specifically deletion-containing viral genomes, DelVGs) and total viral genomes using third generation long-read sequencing. Here we show that metabolites and signaling molecules of host cell central carbon metabolism can significantly alter DelVG production early in Influenza A infection. Adenosine, emerged as a potent inducer of defective viral genomes, significantly amplifying DelVG production across both subtypes. Insulin had similar effects, albeit subtype-specific, predominantly enhancing polymerase segment DVGs in TX12 infections. Tricarboxylic Acid (TCA) cycle inhibitors 4-octyl itaconate and UK5099, along with the purine analog favipiravir, increased total viral genome production across subtypes. Cyanobacterial extracts primarily affected DVG and total viral genome production in TX12, with a specific, almost complete shutdown of influenza antigenic segments. These results underscore the influence of host metabolic pathways on DVG production and suggest new avenues for antiviral intervention, including PI3K-AKT and Ras-MAPK signaling pathways, TCA cycle metabolism, purine-pyrimidine metabolism, polymerase inhibition, and cyanotherapeutic approaches. More broadly, our findings suggest that the social interactions observed between defective and full-length viral genomes, depend not only on the viral actors, but can be altered by the stage provided by the host. Our study advances our fundamental understanding of DVG production mechanisms and highlights the potential of targeting host metabolism to develop broad-spectrum influenza therapeutics.

Introduction

RNA virus infections are not homogenous, instead consisting of a diverse mix of virions with substantial genetic variation. Defective viral particles, named for the defective viral genomes they harbor, are an exceedingly common part of this mix, often outnumbering “standard” virions and genomes. Aside from their abundance, defective viral particles have long been of interest because they require complementation from “standard” viral genomes, yet in many cases they potently interfere with the replication of these very standard genomes. These interactions between virions lead to social dynamics that alter the composition of infections. Recently, defective viral particles have been identified in clinical settings and associated with milder infection outcomes. Intense research efforts have focused on understanding the mechanisms of defective virus emergence and on developing novel, broad-spectrum antivirals.

Influenza A virus remains a substantial public health threat despite yearly vaccination efforts (Rolfes, 2019), which are thwarted by low vaccination rates (Chen, 2022) and high mutability of Influenza A (Pauly, 2017). In the face of antivirals that have not been effective (Hanula, 2024) or that have been rendered ineffective through antiviral resistance (Hurt, 2012; Dong, 2015), defective viral genomes as therapeutics have emerged as a promising alternative. Defective viral genomes in influenza are **Del**etion-containing **V**iral **G**enome (hereafter DelVGs after Alnaji et al. 2019) segments which are packaged into defective interfering particles (Henle, 1943; Von Magnus, 1954; Davis, 1980; Nayak, 1982; Saira, 2013) that hinder productive pathogenesis if they accumulate naturally (Dimmock, 2014; Manzoni, 2018; Vignuzi, 2019; Wu, 2022) or are exogenously introduced (Smith, 2016; Meng, 2017; Wasik, 2018; Zhao, 2018; Bdier, 2019;

Yamagata, 2019; Tapia, 2019; Harding, 2019). However, full weaponization of DelVGs against the flu in a broad-spectrum manner remains unrealized because their *de novo* mechanism of production is unknown, and few factors associated with their production are known (Von Magnus, 1954; Bangham, 1990; Perez-Cidoncha, 2014; Vasilijevic, 2017; Chapter 2). Thus, progress in uncovering novel effectors of DelVG *in situ* production has been slow. There is a critical need to discover novel effectors of DVG production so that the shared characteristics of these inducers may inform the molecular-level events proximal to DVG production.

Research into Influenza A defective interfering particles and their DelVGs has primarily focused on viral factors affecting DelVG production, such as multiplicity of infection, polymerase gene mutations, and each strain's propensity to generate DelVGs (Alnaji, 2019). At a molecular and cellular level, substantial research has focused on polymerase synthesis (Nayak, 1982; Winters, 1981; Alnaji, 2020) and differential packaging (Brooke, 2014; Alnaji, 2021; Meng, 2017; Odagiri, 1997) of defective viral genome segments. Further, there has been considerable effort into the effects that DelVGs have on the host (De, 1980; Tapia, 2013; Frensing, 2014; Vasilijevic, 2017; Wang, 2023). Surprisingly, the potential role of the *host* in influencing DelVG composition has been largely overlooked (Chapter 1; Ginsberg, 1954; Choppin, 1969; Choppin, 1970; De, 1980). Host cell metabolism and metabolic signaling, can affect progeny virus yield and the severity of infection (Ackermann, 1951; Kilbourne, 1959; Blough, 1963; Hale, 2006; Li, 2008; Kuss-Duerkop 2017; Ren, 2021), leading us to investigate the impact of host metabolic signaling on the production of Influenza A defective particles and DelVGs. We recently showed that Alpelisib—a highly selective inhibitor of mammalian phosphoinositide-3 kinase (PI3K) and

its downstream metabolic signaling (Furet, 2013; Fritsch, 2014)—increased DelVG production during Influenza A infection (Chapter 2). On the basis of this association between host metabolism and DelVG production, and the extensively characterized crosstalk between host metabolism and flu pathogenesis (Chapter 1), we hypothesized that other metabolites, metabolic signaling molecules, or other compounds capable of causing metabolic perturbations could increase *de novo* DelVG production in cells.

We set out to test this hypothesis by using third-generation, long-read sequencing to monitor how DelVG production was affected early in infections with A/California/07/2009 (H1N1) and A/Texas/50/2012 (H3N2) strains (CA09 and TX12 hereafter). The metabolic pathways of interest we selected, and their associated drugs, include PI3K-AKT pathway signaling (insulin, alpelisib, MK2206), tricarboxylic acid (TCA) cycle (UK5099, 4-octyl itaconate), and purine-pyrimidine metabolism (adenosine, uridine). We included favipiravir (T-705) in our screen to uncover if its role as a mutagen and elongation terminator of RNA polymerization could impact DVG production; it is a purine base analog that is converted into nucleoside and nucleotide-phosphate forms within cells (Shiraki, 2020). We also included cyanobacteria extracts from *Leptolyngbya*, *Nostoc*, *Oscillatoria*, *Synechococcus*, and *Tolypothrix* to uncover if the known effects of some cyanobacteria extracts on flu pathogenesis (Singh, 2017; Silva, 2018; Mazur-Marzec, 2021) extend to altered DelVG production.

We show that adenosine is a potent amplifier of DelVG production across subtypes, with the largest and most consistent increases of any compound we tested. Meanwhile, the increased

DelVG production associated with insulin was more restricted to the polymerase segments and more pronounced for TX12 than CA09. Additionally, we found that TCA cycle flux inhibitors 4-octyl itaconate (4-OI) and UK5099 are potent amplifiers of total viral genome production across subtypes, and that the purine analog favipiravir also increased total viral genomes across subtypes. Finally, we discovered that cyanobacterial extracts affected defective and total viral genomes primarily in TX12. These results strengthen our previously established association between host metabolism and DelVG production (Chapter 2), further cementing host involvement in the emergence of DelVGs. These results also reveal viral polymerase inhibition and cyanotherapeutic intervention as novel means of altering DelVG production, and steering the trajectory of Influenza A infection. Altogether, our findings mark a step forward in understanding the mechanism of *de novo* DVG production by identifying related environmental effectors. The shared characteristics of these effectors may shed light on the molecular events leading to DVG production and guide highly targeted future research into these mechanisms.

Methods

Cells and Viruses

We obtained MDCK-London cells from the Unites States Centers for Disease Control and Prevention (CDC) Influenza Reagent Resource (IRR). We maintained cells in minimum essential media (MEM) plus 5% fetal bovine serum (FBS). Egg-passaged wildtype A/California/07/2009 (H1N1) and A/Texas/50/2012 (H3N2) were a gift from the lab of Dr. Ted Ross. These initial stocks were double plaque purified in MDCK cells (ATCC/BEI) and propagated thereafter at low infection multiplicity (0.001) in MDCK cells (ATCC/BEI).

Cyanobacteria Culture and Lysis

We cultured *Nostoc punctiforme* (ATCC 29133) in fourfold diluted Allen & Arnon liquid media (AA/4) minus ammonium or other nitrogen source (Allen, 1955); so as to induce heterocyst formation. We cultured *Leptolyngbya boryana* PCC 6306, *Oscillatoria* sp. (ATCC 27930), *Synechococcus elongatus* PCC 7942, and *Tolypothrix* sp. PCC 7601 in BG11 media. All cyanobacteria cultures were incubated at room temperature on shaker platforms (75-100 rpm), and illuminated with three overhead 20-Watt cool-white fluorescent bulbs.

We transferred 6.5 – 7.5 g of each cyanobacteria specimen along with growth media into a sealed centrifuge tube and incubated them for 24 hr at room temperature, in the dark, without shaking. Next, we washed cyanobacteria specimens once in PBS, transferred ~1 g into 1 mL dH_2O, and then froze specimens at -80 °C for 48 hr. After the freezing period, we thawed specimens at room temperature for 24 hr and filter-sterilized the lysate with a 0.22 micron syringe filter. We confirmed lysis and cell death in four of the five specimens; firstly via strain-specific coloration of the lysate (*Leptolyngbya* – cobalt blue, *Nostoc* – purple, *Oscillatoria* – clear/no lysis, *Synechococcus* – pale yellow-green, *Tolypothrix* – indigo), and secondly under the light microscope. Despite the *Oscillatoria* filaments remaining intact, we proceeded with its conditioned freeze-thaw vehicle media (dH_2O).

Drug Screening Assay

We seeded MDCK-London cells overnight in MEM plus 5% FBS media for 21 hr into plastic-bottom 96-well tissue culture plates. We then serum-weaned the fully confluent monolayers for 3

hr in MEM plus 5% bovine serum albumin (BSA). At the start of serum weaning, we spiked a 10 uL pre-treatment of vehicle control (DMSO or dH_2O), cyanobacteria freeze-thaw extract (*Leptolyngbya*, *Nostoc*, *Synechococcus*, *Tolypothrix*), cyanobacteria-conditioned freeze-thaw vehicle medium (*Oscillatoria*), or 21X of small molecule drug (insulin, alpelisib, MK2206, adenosine, uridine, UK5099, 4-octyl itaconate, or favipiravir) directly into 200 uL of the serum weaning supernatant to reach a 1X concentration (1 µM). At the end of serum weaning, we exchanged serum weaning media with MEM plus 2% BSA and 1% Anti-Anti (Virus Infection Media; VIM). We then mock-infected monolayers with VIM, or we virus-infected monolayers at a multiplicity (MOI) of 1; no trypsin was used. As part of the inoculation regimen, we spiked 1.9 uL of vehicle control, cyanobacteria extract, or 21X of signaling molecule into 40 uL of the inoculum supernatant to reach a 1X concentration (1 µM), in order to sustain each treatment's effects for the duration of virus-monolayer adsorption. After the 1 hr adsorption incubation, we aspirated inocula, washed monolayers and topped them with 200 uL VIM, and we spiked 10 uL of vehicle control, cyanobacteria extract, or 21X of signaling molecule directly into VIM supernatant to reach a 1X concentration (1 µM). After 17 hr post infection, we harvested and titrated supernatants to determine the total number of viral genomes, as well as the relative abundances of DVGs versus full-length viral genomes. We ran three biological replicates of the experiment on different days.

Viral Genome Sequencing by Nanopore Long-read Sequencing

We conducted our influenza A viral genome sequencing protocol that sequences and quantifies full-length and deletion-containing viral genome segments, which we have described (Chapter

2). Briefly, we began by isolating viral genomic RNA from 100µL of treatment group supernatants (Zymo Research, Quick-DNA/RNA Viral MagBead kit R2140). Next, we used a 2-cycle RT-PCR reaction (Invitrogen SuperScript™ III One-Step RT-PCR System with Platinum™ Taq DNA Polymerase kit 12574026) to reverse transcribe viral genomic RNA into the first cDNA strand (1st PCR cycle), and then synthesize the second cDNA strand (2nd PCR cycle). The RT reaction to produce the first cDNA strand was primed with a 45bp forward primer (Integrated DNA Technologies) that included a complementary sequence to the uni12 region shared by all flu genomic segments (12bp), flanked with a unique molecular identifier (UMI) sequence (12bp) and a landing pad sequence for downstream barcoding primers (21bp): fwd 5'-TTTCTGTTGGTGCTGATATTGNNNNNNNNNNNNAGCRAAAGCAGG-3'.
The PCR reaction to generate the second cDNA strand was primed with a 47bp reverse primer that included a complementary sequence to the uni13 region shared by all flu genomic segments (13bp), flanked by a UMI sequence (12bp) and the barcoding primer landing pad sequence (22bp): rev 5'-ACTTGCCTGTCGCTCTATCTTCNNNNNNNNNNNNAGTAGAAACAAGG-3'. We used AMPure XP beads (Beckman Coulter, AMPure XP A63881) with manufacturer's instructions to remove excess primers, followed by a 17-cycle amplification PCR (Invitrogen, Platinum SuperFi Master Mix 12358-050) of the umi-tagged reads with barcoding primers (Oxford Nanopore Technologies, PCR Barcoding Expansion 1-96 kit EXP-PBC096). The low number of cycles was designed to minimize PCR duplicates. We then pooled 60 ng of barcoded amplicons from each sample, cleaned and concentrated this pooled sample (Zymo Research, Select-A-Size DNA Clean & Concentrator D4080), and prepared a sequencing library in accordance with manufacturer instructions (Oxford Nanopore Technologies, Ligation-

Sequencing-Kit-V14 SQK-LSK114). We loaded the pooled libraries into an R10 flow cell connected to a MinION MkIB device and ran a 72 hr sequencing protocol from the MinKNOW control software. Upon sequencing run termination, we used the Guppy basecaller software to barcode-demultiplex sequenced reads into their respective treatment groups.

Classification and Quantification of Full-length and Internal-deletion Viral Segments

Demultiplexed amplicon sequences underwent quality control pre-processing prior to deduplication into representative sequences, after which representative sequences were classified into subgroups for DelVGs and full-length, standard viral genomes (SVG).

Quality Control: Our sequencing library preparation strategy began with a 1-cycle each RT-PCR then PCR addition of 12bp-long UMI sequences to the 3’ and 5’ termini of viral genomic RNA, followed by PCR addition of sequencing barcodes to both termini:

5’-barcode—spacer—landing.pad—UMI—uni12—*locus*—uni13—UMI—landing.pad—spacer—barcode-3’

For quality control, we trimmed off barcode and barcode landing pad regions with C*utadapt*, then used *Cutadapt* once more to filter-in only amplicons with a 12bp-long UMI region. Finally, we confirmed the presence of well-formed uni primer regions in the filtered amplicons before advancing to UMI deduplication.

UMI Deduplication*:* We used *UMI-Tools* to sequentially group PCR duplicates by UMI, and then collapse them into a single representative read. In the final quality control step, we trimmed the uni primer region off representative reads with *Cutadapt*. By integrating UMI-deduplication into our workflow, we've mitigated the impact of PCR amplification bias on sequencing depths. Consequently, our DelVG and SVG count data represent a quantitative measurement of the abundance of RNA molecules (genome segments) from which the amplicons were derived.

DelVG Characterization*:* UMI-deduplicated fastq files containing read sequences were processed with the Virus Recombination Mapping (*ViReMa*) software to identify recombination events per genomic read using the following parameters:
--Seed 25 --MicroInDel_Length 20 --Aligner bwa --ErrorDensity 1,25

Additionally, the *-ReadNamesEntry* switch was included in a separate ViReMa run of the same dataset in order to assign read name information to each recombination, which allowed us to collapse deletion events with the same read name into a single DelVG observation using custom Bash and AWK scripts.
--Seed 25 --MicroInDel_Length 20 --Aligner bwa --ErrorDensity 1,25 -ReadNamesEntry

Full-length Viral Genome Characterization*:* To characterize SVGs, we began by using the *bwa* alignment tool to determine the properties of reads and their alignment to the reference genome; this information is captured in the bitwise FLAG field (column 2) of the output SAM file. Next, we used the *AWK* program to select only reads with proper alignment to the forward

and reverse strands of the reference genome—bitwise FLAGs 0x0 (0) and 0x10 (16) respectively —and used *AWK* yet again to filter reads that were within ±100bp the length of the reference genomic segment.

Statistics

In general, we relied on linear or linear mixed models to test significance between treatments using base R and the nmle packages, respectively. Owing to the intrinsic heterogeneity of flu infections (Russell, 2018; Wang, 2020), we included bioreplicates (three independent replicate infections conducted on different days) as a random factor in our models, unless otherwise indicated. We tested two response variables, the proportion of **Del**etion-containing **V**iral **G**enomes (DelVGs, after Alnaji et al. 2019) and the total viral genome count (TVG). In all cases we used per-segment data on DelVGs and TVGs, i.e. each infection had eight TVG and DelVG measurements one, per viral genome segment. We first tested for *any* statistically significant changes in TVG and DelVGs according to drug treatment. To investigate changes in DelVGs and TVGs produced by each genome segment (which have known differences in TVGs and DelVGs), we then proceeded to make models that tested each viral genome segment against the respective vehicle mock infections. When we found that strain was a significant predictor, we ran separate models to estimate coefficients and significance. We only report statistically significant results in the main text, unless otherwise noted.

Results

1. Sequencing and measurement of Influenza A viral genomes is highly consistent

We sequenced supernatants of all infections in a single MinION flow cell, which yielded 12.02M reads. After quality control for well-formed amplicons (perfect UMIs, Influenza A-specific terminal uni12/13 regions) and de-deduplicating unique molecular identifiers (UMI's) we obtained 67,496.81 ± 56,183.60 reads per sample; note that these reads cover the entire genome segment (whether deletion-containing or not) and reflect a quantitative estimate of the vRNA molecules present in the supernatants.

We conducted mock infections using the vehicle for the drugs we screened, namely dH20 and DMSO, to serve as a control and baseline for comparison. Despite high expected variability in individual infections, especially for the production of DelVGs, our control infections with vehicle were highly repeatable in terms of the total viral of genomes (**Figure 3.1**) and the proportion of DVGs.

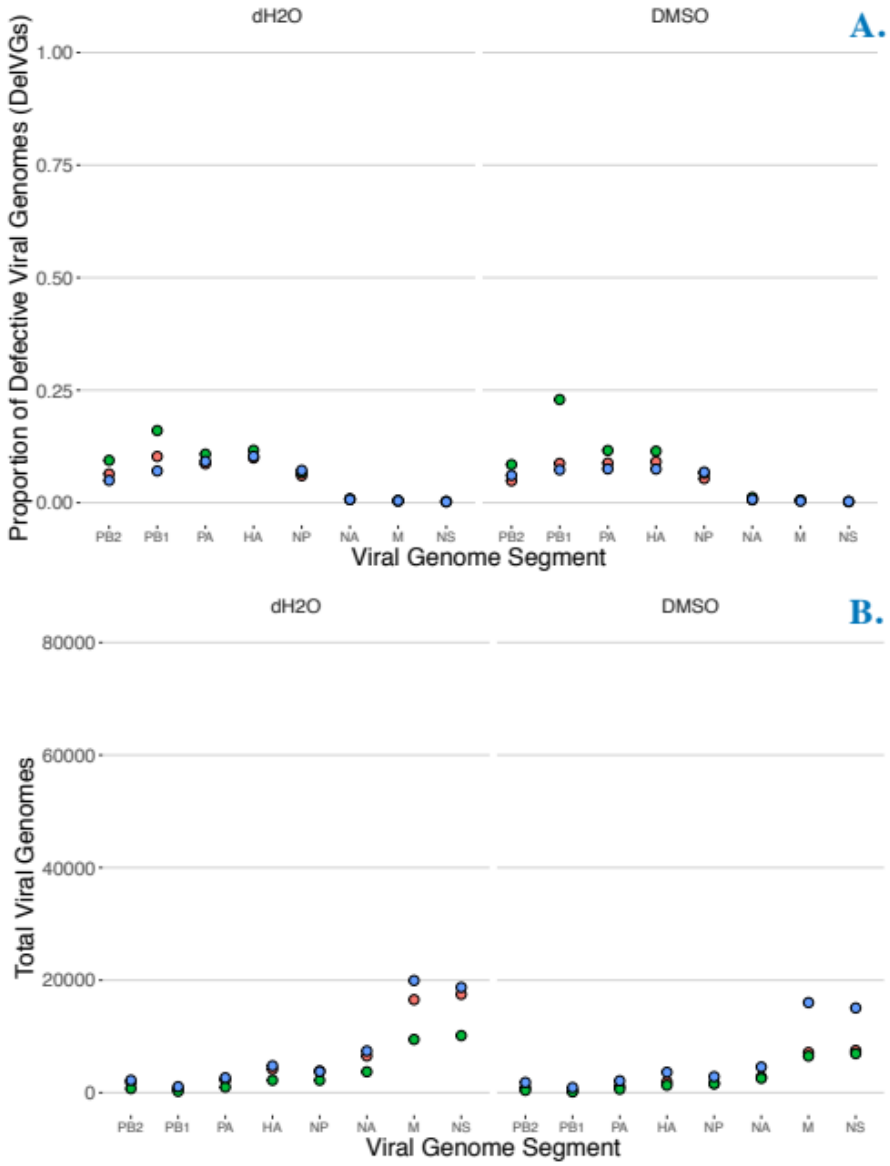

Figure 3.1. **Control infections were highly repeatable**. (**A**)Production of influenza defective viral genomes (here measured as proportion of **Del**etion-containing **V**iral **G**enomes (DelVGs) in strain CA09 (H1N1pdm) after 18 hr of infection (no trypsin) mock-treated with water vehicle (left panel) and DMSO vehicle (right panel). (**B**) Production of influenza **T**otal **V**iral **G**enomes (TVG) in strain CA09 (H1N1pdm) after 18 hr of infection (no trypsin) mock-treated with water vehicle (left panel) and DMSO vehicle (right panel). Point colors represent data from three independent infections conducted on different days (i.e. bioreplicates).

2. Drugs affect Defective Viral Genome Production and Total Viral Genome Production

To determine if any of our treatments affected the proportion of DelVGs produced during an infection, we analyzed differences among treatments using ANOVA, adding bioreplicate and strain as covariates. Drug treatment was a statistically significant predictor ($F = 6.777$, $p < 0.0001$), explaining 13.12% of the variance in the proportion of DelVG among treatments. All statistically significant treatments increased the overall mean percentage of DelVGs from *on average* 7.90% to 25.61% (**Table 3.1**, blue shading), relative to infections with water. The largest increase was caused by adenosine, followed by insulin, MK2206, and uridine (in descending order, **Figure 3.2**; **Table 3.1**). We note that in this model, strain was not a significant predictor of average DelVG proportion across segments ($F = 0.480$, $p < 0.488$) and thus these average increases were significant for both TX12 and CA09 strains.

Treatment	Measurement	Estimate	Standard Error	Pr(>|t|)
Adenosine	**Del**etion-containing **V**iral **G**enomes (proportion)	0.256059	0.035974	2.73e-12
Insulin	**Del**etion-containing **V**iral **G**enomes (proportion)	0.118392	0.035974	0.00105
MK2206	**Del**etion-containing **V**iral **G**enomes (proportion)	0.081722	0.035974	0.02341
Uridine	**Del**etion-containing **V**iral **G**enomes (proportion)	0.082837	0.036573	0.02382
4-OI	**T**otal **V**iral **G**enomes (count)	8438.81	2040.61	3.97e-05
UK5099	**T**otal **V**iral **G**enomes (count)	4355.15	2040.61	0.03317

Table 3.1. **Drugs increase total viral genomes and deletion containing viral genomes**. Statistically significant predictors of the proportion of **Del**etion-containing **V**iral **G**enomes (DelVGs, blue shading) and **T**otal **V**iral **G**enomes (TVG) and their parameter estimates from ANOVA.

We similarly analyzed the number of total viral genomes produced during an infection and found that drug treatment was a statistically significant predictor ($F = 4.439$, $p < 0.0001$), explaining 8.01% of the variance in number of total viral genomes among treatments. The TCA cycle flux inhibitors 4-OI and UK5099 were statistically significant predictors of total viral genomes

(**Table 3.1**, gray shading), increasing TVG count on average by 8,438.81 and 4,355.15 genomes, respectively, relative to infections with water (**Figure 3.2**; **Table 3.1**). Unlike the proportion of DelVGs, strain was a statistically significant predictor of total viral genomes across segments ($F = 6.168$, $p < 0.0132$). TX12 had on average -1,854.71 fewer total viral genomes than CA09.

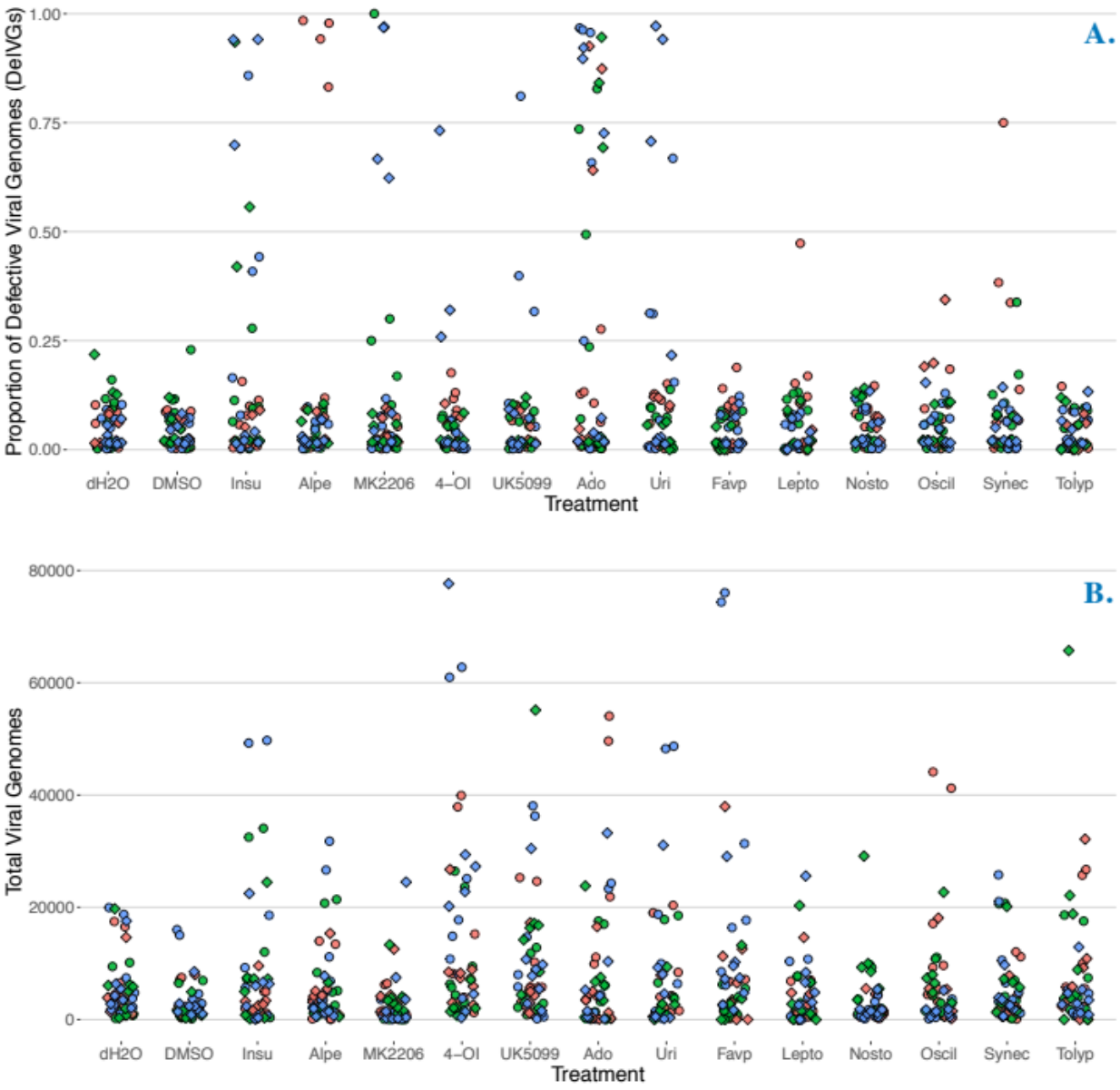

Figure 3.2. **Drug treatment affects defective viral genomes and total viral genomes**. (**A**) Production of influenza defective viral genomes (here measured as proportion of **Del**etion-containing **V**iral **G**enomes (DelVGs) after 18 hr of infection; each point is the proportion of DelVGs in each influenza segment (all segments included in each treatment). (**B**) Production of influenza **T**otal **V**iral **G**enomes (TVG) after 18 hr of infection; each point is the total number of viral genomes of each influenza segment (all segments included in each treatment). The first two treatments (left to right) are vehicle control infections. Point colors represent data from three independent infections conducted on different days (i.e. bioreplicates). The shape of the points represents the strain (circles = CA09(H1N1pdm), diamonds = TX12(H3N2)). The position of points is randomly jittered horizontally for better visibility.

In these two overall models, we did not control for known differences in the proportion of DelVGs in different genome segments (i.e. polymerase complex segments have a higher proportion of DelVGs). To gain insight into the segment-specific effects of each drug, we made linear mixed models for each segment and each vehicle control (DMSO or dH_2O). We report the results for these models below in dedicated sections for each drug and in the supplementary information (see Results and Supplementary Material sections).

3. Adenosine is a potent amplifier of DelVG production across subtypes

Adenosine had the most marked and consistent effect of any of the drugs. Adenosine increased the DelVG proportion in all three polymerase complex segments of the H1N1 and H3N2 strains in a statistically significant way (**Figure 3.3**, **Supplementary Table 3.1**). The magnitude of these increases was substantial, as the average increase in polymerase complex DelVGs ranged from 35.00% to 80.61% compared to the dH_2O vehicle. Adenosine also affected viral genome segments outside the polymerase complex, yielding a statistically significant increase of HA of 33.71% in CA09 infections and a small but statistically significant increase of 0.99% in NP DelVGs in TX12 infections.

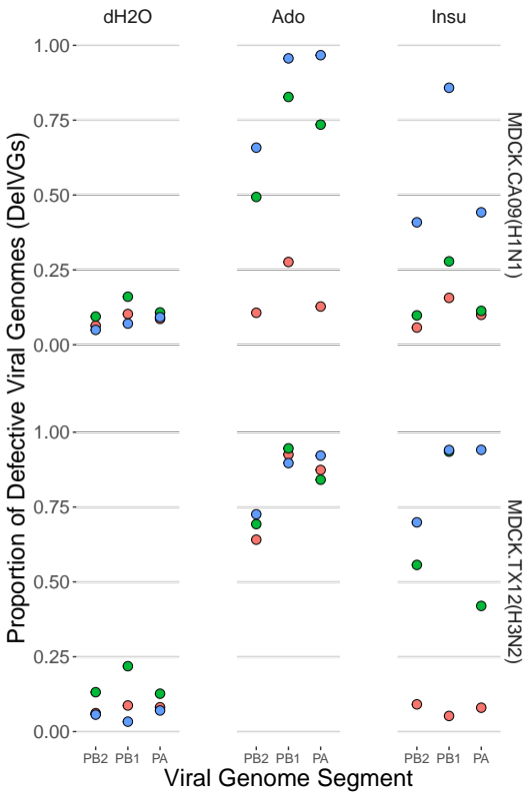

Figure 3.3. **Adenosine and insulin increase polymerase complex defective viral genome segments.** Production of influenza defective viral genomes (here measured as proportion of **Del**etion-containing **V**iral **G**enomes (DelVGs) after 18 hr of infection; each point is the proportion of DelVGs in each influenza segment. Point colors represent data from three independent infections conducted on different days (i.e. bioreplicates).

4. Insulin increases polymerase complex defective viral genomes

Insulin also increased the polymerase complex DelVG percentage, albeit with less consistency among strains than adenosine. For TX12, DelVGs of all three polymerase complex segments increased from 36.56% - 52.96% in a statistically significant manner. In CA09, DelVGs of all three polymerase complex segments also increased (**Figure 3.3**, **Supplementary Table 3.1**), but these increases were not statistically significant.

5. TCA cycle flux inhibitors 4-OI and UK5099 are potent amplifiers of total viral genomes across subtypes

The aerobic glycolysis inducers 4-OI and UK5099 increased overall (i.e. across all segments) TVG production in CA09 infections, as noted above (**Figure 3.4**, **Supplementary Table 3.1**). Moreover, 4-OI increased DelVGs in seven out of eight segments in both strains in a statistically significant manner, with increases of 2,287 up to 11,798 total genomes compared to the DMSO control infections. In the remaining viral genome segment, NS, a statistically significant increase of 33,209 genomes was noted in CA09 infections. UK5099 also yielded statistically significant increases of 5,052 - 20,742 total viral genomes in both strains, but these increases were limited to four segments: HA, NP, NA, and M.

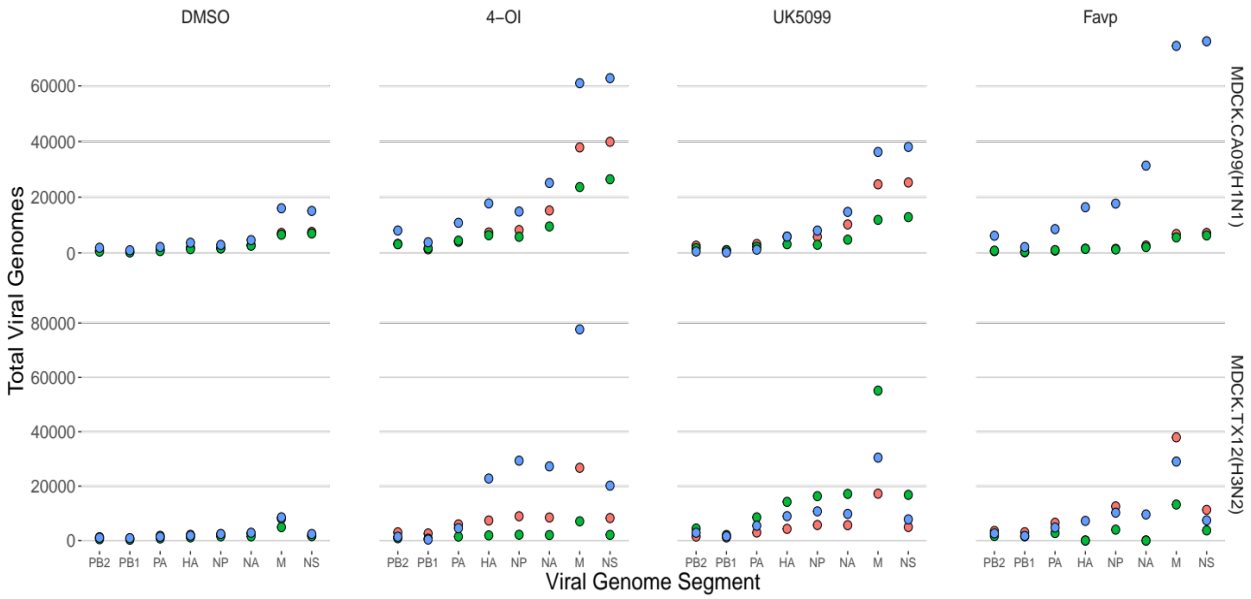

Figure 3.4. **TCA cycle flux inhibitors 4-OI and UK5099 & purine analog favipiravir increase total viral genomes in A/H1N1 and A/H3N2 strains.** Production of influenza **T**otal **V**iral **G**enomes (TVG) after 18hrs of infection; each point is the count of total viral genomes (all segments included in each treatment). Point colors represent data from three independent infections conducted on different days (i.e. bioreplicates).

6. The purine analog favipiravir increased total viral genomes across subtypes

Favipiravir infections showed a statistically significant average increase of 2,768 - 19,298 total viral genomes in segments PA, NP, and M in both CA09 and TX12 strains (**Figure 3.4**, **Supplementary Table 3.1**). Favipiravir also showed a small, but statistically significant, 1.22% decrease in the percentage of DelVGs in TX12 infections (**Supplementary Table 3.1**).

7. Cyanobacterial Extracts affected defective and total viral genomes in TX12 antigenic segments

TX12 infections responded to *Tolypothrix* extracts with a statistically significant increase of an average of 1,410 PB1 total viral genomes, whereas HA and NA registered statistically significant decreases of 3,178-4,163 total viral genomes (**Figure 3.5**, **Supplementary Table 3.1**). Additionally, *Tolypothrix* extracts reduced the NA DelVGs by a statistically significant albeit small 1.15% (**Supplementary Table 3.1**). TX12 infections also had a curious response to *Leptolyngbya* extracts. There were substantial, statistically significant, decreases of 4,135-5,725 total HA and NA viral genome segments. These decreases led to near-zero recovery of HA and NA segments; less than 10-count of each segment in one bioreplicate, and zero in the remaining two bioreplicates (**Figure 3.5** blue box, **Supplementary Table 3.1**). This effect was not an artefact experimentation; it occurred in three separate bioreplicates (run on different days) and supernatants of all treatments were processed individually—from RNA extraction, through successive RT-PCR and barcoding PCR amplification—before being pooled for sequencing library preparation.

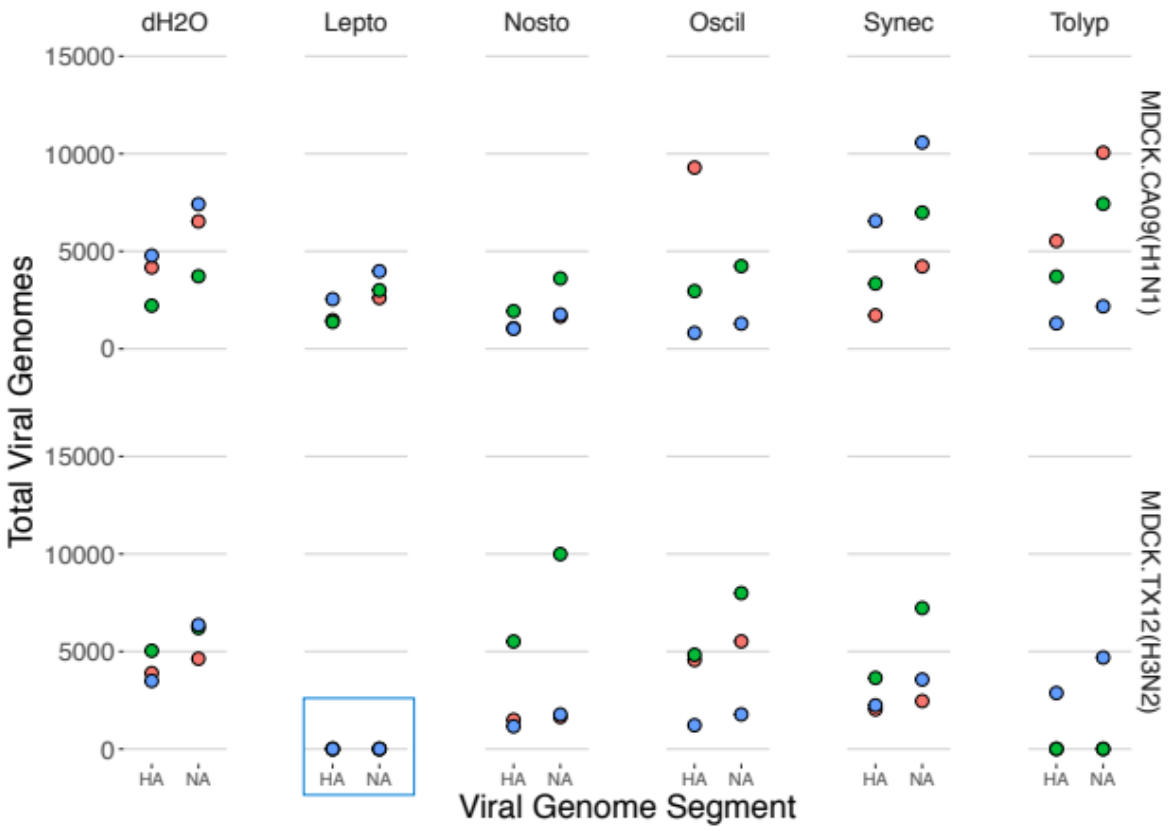

Figure 3.5. **Cyanobacterial extracts suppress total viral genome production in A/H3N2 strain antigenic segments.** Production of influenza **T**otal **V**iral **G**enomes (TVG) after 18 hr of infection; each point is the count of total viral genomes in each influenza segment. Point colors represent data from three independent infections conducted on different days (i.e. bioreplicates).

DISCUSSION

Our study provides significant insights into the role of host metabolism in the production of defective viral genomes (DVGs) during Influenza A virus infection. The identification of adenosine, insulin, TCA cycle inhibitors, favipiravir, and cyanobacterial extracts as modulators of DVG production marks a crucial step toward understanding the de novo mechanisms underlying DVG production and exploring novel antiviral strategies.

Adenosine is a Potent Amplifier of Defective Viral Genome Production

Adenosine emerged as a potent amplifier of DVG production across H1N1 and H3N2 subtypes. The significant increase in polymerase complex DelVGs in both strains suggests that adenosine has a broad-spectrum impact on DVG production. The notable increase in HA DelVGs in CA09 and NP DelVGs in TX12 highlights adenosine's potential to differentially enhance DVG production across various genomic segments. Understanding the adenosine signaling cascade can shed light on the potential pathways of DVG production. For instance, the binding of extracellular adenosine to A_1 G-protein coupled receptors on the MDCK cell plasma membrane triggers a phospholipase C (PLC)-dependent rise in cytosolic concentrations of inositol 1,4,5-triphosphate (IP3) and Ca^{2+}, followed by a three-fold increase in the extracellular efflux of ATP which is dependent on the rapid sequestration of previously cytosolic Ca^{2+} into mitochondria (Migita, 2005; Migita, 2007). While extracellular ATP continues the signaling cascade in an autocrine and paracrine manner, Ca^{2+}-sequestering mitochondria in contact with the endoplasmic reticulum (ER) engage in active trade of ions and membrane lipids (Hirabayashi, 2017). This interaction likely alters the ER lipid makeup and downstream vesicular trafficking to the plasma

membrane, altering membrane rigidity and potentially driving the differential sorting of standard or defective genomes into progeny viral capsids (Blough, 1969; Blough, 1970; Lenard, 1976). Further research into these pathways will systematically reveal the host factors that reliably modulate the adenosine-associated increase in DelVG production.

Insulin has Strain-specific Effects on Polymerase Complex DelVGs

Insulin demonstrated the ability to increase polymerase complex DelVGs, particularly in the TX12 strain. The statistically significant increases observed in TX12, contrasted with the non-significant increases in CA09, suggest a potential subtype-specific mechanism by which insulin signaling modulates DelVG production. Insulin binding to its receptor initiates a signaling cascade through multiple cellular pathways, including phosphoinositide 3-kinase (PI3K)-AKT and Ras-MAPK, which ultimately upregulates glucose uptake and glycolysis to fuel cell-wide anabolism in a HIF-1a and Myc-dependent manner (Hopkins, 2020). Further investigation into the molecular basis of this specificity could uncover critical insights into how host metabolic signals differentially influence viral genome dynamics across influenza subtypes and within segments of a given subtype.

TCA Cycle Inhibitors Enhance Total Viral Genome Production

The TCA cycle inhibitors 4-OI and UK5099 significantly increased TVG production across multiple segments in both strains, highlighting a strong link between TCA cycle flux and viral genome replication. Specifically, the interference of normoxic pyruvate oxidation to CO_2 gas by 4-OI, which inhibits mitochondrial succinate dehydrogenase (Daniels, 2019), and UK5099,

which inhibits mitochondrial pyruvate carriers (Hildyard, 2005), led to significantly increased TVG production. This phenomenon is similar to the Warburg effect observed in tumor cells, where reduced-carbon biomass (pyruvate) is preserved to fuel proliferation (Lunt, 2011; Liu, 2019); in this case, the proliferation of viral genomes. While influenza virus is already known to induce an aerobic glycolysis state during normal pathogenesis (Ren, 2019; Ren, 2021), the addition of 4-OI or UK5099 appears to further enhance this metabolic state. Further research is needed to determine if 4-OI or UK5099 can also affect defective viral genome (DVG) production at different timepoints to fully explore their potential as broad-spectrum DVG-inducing drugs.

Favipiravir Increases Total Viral Genome Production

Favipiravir significantly increased TVGs across subtypes while slightly reducing DelVG proportions in TX12 infections. Considering favipiravir's known role as a mutagen and premature terminator of RNA elongation during influenza replication, the observed increase in total genomes suggests that our chosen dose of favipiravir was insufficient to induce lethal mutagenesis. This hypothesis is supported by two key points: (i) the 1 µM dose of favipiravir used in our study is an order of magnitude lower than its 11 µM EC50 concentration (Vanderlinden, 2016), and (ii) 1 µM favipiravir is easily outcompeted by the 100-200 µM basal intracellular concentration of its nucleotide competitor GTP (Zala, 2017). The observed permissive mutagenesis by favipiravir, coupled with increased TVGs and slightly reduced DVGs, suggests that misincorporation-based mutation may not be a necessary precursor to DelVG production. Further research is needed to better understand the relationship between nucleotide misincorporation and DVG production.

Cyanobacterial Extracts Suppress Production of Antigenic Segments in TX12 (A/H3N2)

The differential response of TX12 segments to cyanobacterial extracts, particularly the substantial decreases in HA and NA segments with *Leptolyngbya* and *Tolypothrix* extracts, highlights the potential of natural products to modulate viral genome dynamics. This underscores the need for further exploration into the active components of these extracts and their mechanisms of action (Singh, 2017; Silva, 2018; Mazur-Marzec, 2021; Tiwari, 2020; Ferrazano, 2020). Notably, the near absence of HA and NA segments in response to *Leptolyngbya* extracts suggests their active exclusion from entry into progeny capsids. This finding points to a non-random, segment-selective force acting on viral segments during replication, cytoskeletal trafficking, and/or progeny capsid assembly, warranting further investigation into the underlying mechanisms.

Implications for Future Research and Therapeutic Development

Overall, our findings reinforce the critical role of host metabolism in influencing DVG production and viral pathogenesis. The identification of metabolic effectors that modulate DVG and TVG production provides a foundation for future research aimed at uncovering the molecular mechanisms driving these effects. Understanding the shared characteristics of these inducers will be pivotal in developing highly targeted antiviral therapies that exploit metabolic vulnerabilities of the influenza virus. Additionally, understanding the role of host metabolism in DelVG production could help to predict how various host states in flu patients (such as diabetes, cancer, pregnancy or other metabolic states) can shape viral evolution and influence disease

severity (Ghedin, 2017). For instance, pregnancy, known to lead to severe flu infections, also leads to the selection of specific mutations that increase pathogencity in H1N1 strains (Engels, 2017). Thus, understanding how metabolic states pre-dispose flu infections to produce more or less DelVGs or TVGs, which can influence disease severity, could be an important clinical tool. In conclusion, this study advances our understanding of the interplay between host metabolism and Influenza A virus genome dynamics. By identifying key metabolic modulators of DVG production, we pave the way for innovative therapeutic strategies that leverage defective interference to combat influenza infections. Future investigations should focus on the detailed molecular pathways involved and the potential for these metabolic effectors to be integrated into broad-spectrum antiviral treatments.

Acknowledgements

This project was funded by NIH grants 4R00AI119401-02 and 1R01AI179873-01 to SDM. IA was support-ed by NIH grant 4R00AI119401-02 and 1R01AI179873-01 to SDM and a Craft Consult Biotechnology Dis-sertation Fellowship. John Albeck and Enoch Baldwin provided helpful feedback on this manuscript. Ted Ross kindly provided Influenza A strains from his collection. John Meeks graciously provided cyanobacteria from his collection.

References

1. ACKERMANN WW, KLERNSCHMIDT E. Concerning the relation of the Krebs cycle to virus propagation. J Biol Chem. 1951 Mar;189(1):421-8. PMID: 14832255.

2. Allen MB, Arnon DI. Studies on Nitrogen-Fixing Blue-Green Algae. I. Growth and Nitrogen Fixation by Anabaena Cylindrica Lemm. Plant Physiol. 1955 Jul;30(4):366-72. doi: 10.1104/pp.30.4.366. PMID: 16654787; PMCID: PMC540664.

3. Alnaji FG, Holmes JR, Rendon G, Vera JC, Fields CJ, Martin BE, Brooke CB. Sequencing Framework for the Sensitive Detection and Precise Mapping of Defective Interfering Particle-Associated Deletions across Influenza A and B Viruses. J Virol. 2019 May 15;93(11):e00354-19. doi: 10.1128/JVI.00354-19. PMID: 30867305; PMCID: PMC6532088.

4. Alnaji FG, Brooke CB. Influenza virus DI particles: Defective interfering or delightfully interesting? PLoS Pathog. 2020 May 21;16(5):e1008436. doi: 10.1371/journal.ppat.1008436. PMID: 32437428; PMCID: PMC7241698.

5. Alnaji FG, Reiser WK, Rivera-Cardona J, Te Velthuis AJW, Brooke CB. Influenza A Virus Defective Viral Genomes Are Inefficiently Packaged into Virions Relative to Wild-Type Genomic RNAs. mBio. 2021 Dec 21;12(6):e0295921. doi: 10.1128/mBio.02959-21. Epub 2021 Nov 23. PMID: 34809454; PMCID: PMC8609359.Chen YH, Chang GK, Kuo SM, Huang SY, Hu IC, Lo YL, Shih SR. Well-tolerated Spirulina extract inhibits influenza virus replication and reduces virus-induced mortality. Sci Rep. 2016 Apr 12;6:24253. doi: 10.1038/srep24253. PMID: 27067133; PMCID: PMC4828654.

6. Bangham CR, Kirkwood TB. Defective interfering particles: effects in modulating virus growth and persistence. Virology. 1990 Dec;179(2):821-6. doi: 10.1016/0042-6822(90)90150-p. PMID: 2238471.

7. Bdeir N, Arora P, Gärtner S, Hoffmann M, Reichl U, Pöhlmann S, Winkler M. A system for production of defective interfering particles in the absence of infectious influenza A virus. PLoS One. 2019 Mar 1;14(3):e0212757. doi: 10.1371/journal.pone.0212757. PMID: 30822349; PMCID: PMC6396908.

8. BLOUGH HA. The effect of vitamin A alcohol on the morphology of myxoviruses. I. The production and comparison of artificially produced filamentous virus. Virology. 1963 Mar;19:349-58. doi: 10.1016/0042-6822(63)90074-6. PMID: 13971826.

9. Blough HA, Merlie JP, Tiffany JM. The fatty acid composition of incomplete influenza virus. Biochem Biophys Res Commun. 1969 Mar 31;34(6):831-4. doi: 10.1016/0006-291x(69)90255-1. PMID: 5779767.

10. Blough HA, Merlie JP. The lipids of incomplete influenza virus. Virology. 1970 Mar;40(3):685-92. doi: 10.1016/0042-6822(70)90213-8. PMID: 5461847.

11. Brooke CB. Biological activities of 'noninfectious' influenza A virus particles. Future Virol. 2014 Jan;9(1):41-51. doi: 10.2217/fvl.13.118. PMID: 25067941; PMCID: PMC4109409.

12. Chen C, Liu X, Yan D, Zhou Y, Ding C, Chen L, Lan L, Huang C, Jiang D, Zhang X, Guan Z, Fu X, Du Y, Lin Y, Zhu C, Wu J, Li L, Yang S. Global influenza vaccination rates and factors associated with influenza vaccination. Int J Infect Dis. 2022 Dec;125:153-163. doi: 10.1016/j.ijid.2022.10.038. Epub 2022 Nov 1. PMID: 36328290.

13. Choppin PW. Replication of influenza virus in a continuous cell line: high yield of infective virus from cells inoculated at high multiplicity. Virology. 1969 Sep;39(1):130-4. doi: 10.1016/0042-6822(69)90354-7. PMID: 4980034.

14. Choppin PW, Pons MW. The RNAs of infective and incomplete influenza virions grown in MDBK and HeLa cells. Virology. 1970 Nov;42(3):603-10. doi: 10.1016/0042-6822(70)90306-5. PMID: 5529979.

15. Daniels BP, Kofman SB, Smith JR, Norris GT, Snyder AG, Kolb JP, Gao X, Locasale JW, Martinez J, Gale M Jr, Loo YM, Oberst A. The Nucleotide Sensor ZBP1 and Kinase RIPK3 Induce the Enzyme IRG1 to Promote an Antiviral Metabolic State in Neurons. Immunity. 2019 Jan 15;50(1):64-76.e4. doi: 10.1016/j.immuni.2018.11.017. Epub 2019 Jan 8. PMID: 30635240; PMCID: PMC6342485.

16. Davis AR, Hiti AL, Nayak DP. Influenza defective interfering viral RNA is formed by internal deletion of genomic RNA. Proc Natl Acad Sci U S A. 1980 Jan;77(1):215-9. doi: 10.1073/pnas.77.1.215. PMID: 6928614; PMCID: PMC348239.

17. De BK, Nayak DP. Defective interfering influenza viruses and host cells: establishment and maintenance of persistent influenza virus infection in MDBK and HeLa cells. J Virol. 1980 Dec;36(3):847-59. doi: 10.1128/JVI.36.3.847-859.1980. PMID: 7463559; PMCID: PMC353712.

18. Dimmock NJ, Easton AJ. Defective interfering influenza virus RNAs: time to reevaluate their clinical potential as broad-spectrum antivirals? J Virol. 2014 May;88(10):5217-27. doi: 10.1128/JVI.03193-13. Epub 2014 Feb 26. PMID: 24574404; PMCID: PMC4019098.

19. Dong G, Peng C, Luo J, Wang C, Han L, Wu B, Ji G, He H. Adamantane-resistant influenza a viruses in the world (1902-2013): frequency and distribution of M2 gene mutations. PLoS One. 2015 Mar 13;10(3):e0119115. doi: 10.1371/journal.pone.0119115. PMID: 25768797; PMCID: PMC4358984.

20. Engels G, Hierweger AM, Hoffmann J, Thieme R, Thiele S, Bertram S, Dreier C, Resa-Infante P, Jacobsen H, Thiele K, Alawi M, Indenbirken D, Grundhoff A, Siebels S, Fischer N, Stojanovska V, Muzzio D, Jensen F, Karimi K, Mittrücker HW, Arck PC, Gabriel G. Pregnancy-Related Immune Adaptation Promotes the Emergence of Highly Virulent H1N1 Influenza Virus Strains in Allogenically Pregnant Mice. Cell Host Microbe. 2017 Mar 8;21(3):321-333. doi: 10.1016/j.chom.2017.02.020. PMID: 28279344.

21. Ferrazzano GF, Papa C, Pollio A, Ingenito A, Sangianantoni G, Cantile T. Cyanobacteria and Microalgae as Sources of Functional Foods to Improve Human General and Oral Health. Molecules. 2020 Nov 6;25(21):5164. doi: 10.3390/molecules25215164. PMID: 33171936; PMCID: PMC7664199.

22. Frensing T, Pflugmacher A, Bachmann M, Peschel B, Reichl U. Impact of defective interfering particles on virus replication and antiviral host response in cell culture-based influenza vaccine production. Appl Microbiol Biotechnol. 2014 Nov;98(21):8999-9008. doi: 10.1007/s00253-014-5933-y. Epub 2014 Aug 19. PMID: 25132064.

23. Furet P, Guagnano V, Fairhurst RA, Imbach-Weese P, Bruce I, Knapp M, Fritsch C, Blasco F, Blanz J, Aichholz R, Hamon J, Fabbro D, Caravatti G. Discovery of NVP-BYL719 a potent and selective phosphatidylinositol-3 kinase alpha inhibitor selected for clinical evaluation. Bioorg Med Chem Lett. 2013 Jul 1;23(13):3741-8. doi: 10.1016/j.bmcl.2013.05.007. Epub 2013 May 14. Erratum in: Bioorg Med Chem Lett. 2013 Aug 15;23(16):4723. PMID: 23726034.

24. Fritsch C, Huang A, Chatenay-Rivauday C, Schnell C, Reddy A, Liu M, Kauffmann A, Guthy D, Erdmann D, De Pover A, Furet P, Gao H, Ferretti S, Wang Y, Trappe J, Brachmann SM, Maira SM, Wilson C, Boehm M, Garcia-Echeverria C, Chene P, Wiesmann M, Cozens R, Lehar J, Schlegel R, Caravatti G, Hofmann F, Sellers WR. Characterization of the novel and specific PI3Kα inhibitor NVP-BYL719 and development of the patient stratification strategy for clinical trials. Mol Cancer Ther. 2014 May;13(5):1117-29. doi: 10.1158/1535-7163.MCT-13-0865. Epub 2014 Mar 7. PMID: 24608574.

25. GINSBERG HS. Formation of non-infectious influenza virus in mouse lungs: its dependence upon extensive pulmonary consolidation initiated by the viral inoculum. J Exp Med. 1954 Dec 1;100(6):581-603. doi: 10.1084/jem.100.6.581. PMID: 13211916; PMCID: PMC2136397.

26. Ghedin E, Schultz-Cherry S. Host response: Pregnancy impairs flu defences. Nat Microbiol. 2017 Apr 28;2:17077. doi: 10.1038/nmicrobiol.2017.77. PMID: 28452981.

27. Hale BG, Jackson D, Chen YH, Lamb RA, Randall RE. Influenza A virus NS1 protein binds p85beta and activates phosphatidylinositol-3-kinase signaling. Proc Natl Acad Sci

U S A. 2006 Sep 19;103(38):14194-9. doi: 10.1073/pnas.0606109103. Epub 2006 Sep 8. PMID: 16963558; PMCID: PMC1599933.

28. Hanula R, Bortolussi-Courval É, Mendel A, Ward BJ, Lee TC, McDonald EG. Evaluation of Oseltamivir Used to Prevent Hospitalization in Outpatients With Influenza: A Systematic Review and Meta-Analysis. JAMA Intern Med. 2024 Jan 1;184(1):18-27. doi: 10.1001/jamainternmed.2023.0699. Erratum in: JAMA Intern Med. 2023 Nov 20;: PMID: 37306992; PMCID: PMC10262060.

29. Harding AT, Haas GD, Chambers BS, Heaton NS. Influenza viruses that require 10 genomic segments as antiviral therapeutics. PLoS Pathog. 2019 Nov 15;15(11):e1008098. doi: 10.1371/journal.ppat.1008098. PMID: 31730644; PMCID: PMC6881065.

30. Henle W, Henle G. INTERFERENCE OF INACTIVE VIRUS WITH THE PROPAGATION OF VIRUS OF INFLUENZA. Science. 1943 Jul 23;98(2534):87-9. doi: 10.1126/science.98.2534.87. PMID: 17749157.

31. Hildyard JC, Ammälä C, Dukes ID, Thomson SA, Halestrap AP. Identification and characterisation of a new class of highly specific and potent inhibitors of the mitochondrial pyruvate carrier. Biochim Biophys Acta. 2005 Apr-May;1707(2-3):221-30. doi: 10.1016/j.bbabio.2004.12.005. Epub 2004 Dec 30. PMID: 15863100.

32. Hirabayashi Y, Kwon SK, Paek H, Pernice WM, Paul MA, Lee J, Erfani P, Raczkowski A, Petrey DS, Pon LA, Polleux F. ER-mitochondria tethering by PDZD8 regulates Ca2+ dynamics in mammalian neurons. Science. 2017 Nov 3;358(6363):623-630. doi: 10.1126/science.aan6009. PMID: 29097544; PMCID: PMC5818999.

33. Hopkins BD, Goncalves MD, Cantley LC. Insulin-PI3K signalling: an evolutionarily insulated metabolic driver of cancer. Nat Rev Endocrinol. 2020 May;16(5):276-283. doi: 10.1038/s41574-020-0329-9. Epub 2020 Mar 3. PMID: 32127696; PMCID: PMC7286536.

34. Hurt AC, Chotpitayasunondh T, Cox NJ, Daniels R, Fry AM, Gubareva LV, Hayden FG, Hui DS, Hungnes O, Lackenby A, Lim W, Meijer A, Penn C, Tashiro M, Uyeki TM, Zambon M; WHO Consultation on Pandemic Influenza A (H1N1) 2009 Virus Resistance to Antivirals. Antiviral resistance during the 2009 influenza A H1N1 pandemic: public health, laboratory, and clinical perspectives. Lancet Infect Dis. 2012 Mar;12(3):240-8. doi: 10.1016/S1473-3099(11)70318-8. Epub 2011 Dec 18. PMID: 22186145.

35. KILBOURNE ED. Inhibition of influenza virus multiplication with a glucose antimetabolite (2-deoxy-D-glucose). Nature. 1959 Jan 24;183(4656):271-2. doi: 10.1038/183271b0. PMID: 13622777.

36. Kuss-Duerkop SK, Wang J, Mena I, White K, Metreveli G, Sakthivel R, Mata MA, Muñoz-Moreno R, Chen X, Krammer F, Diamond MS, Chen ZJ, García-Sastre A, Fontoura BMA. Influenza virus differentially activates mTORC1 and mTORC2 signaling to maximize late stage replication. PLoS Pathog. 2017 Sep 27;13(9):e1006635. doi: 10.1371/journal.ppat.1006635. PMID: 28953980; PMCID: PMC5617226.

37. Lenard J, Tsai DK, Compans RW, Landsberger FR. Observations on the membrane organization of standard and incomplete influenza grown in MDBK cells. Virology. 1976 Jun;71(2):389-94. doi: 10.1016/0042-6822(76)90366-4. PMID: 180658.

38. Li Y, Anderson DH, Liu Q, Zhou Y. Mechanism of influenza A virus NS1 protein interaction with the p85beta, but not the p85alpha, subunit of phosphatidylinositol 3-kinase (PI3K) and up-regulation of PI3K activity. J Biol Chem. 2008 Aug 22;283(34):23397-409. doi: 10.1074/jbc.M802737200. Epub 2008 Jun 5. PMID: 18534979.

39. Li Y, Li X, Kan Q, Zhang M, Li X, Xu R, Wang J, Yu D, Goscinski MA, Wen JG, Nesland JM, Suo Z. Mitochondrial pyruvate carrier function is negatively linked to Warburg phenotype in vitro and malignant features in esophageal squamous cell carcinomas. Oncotarget. 2017 Jan 3;8(1):1058-1073. doi: 10.18632/oncotarget.13717. PMID: 27911865; PMCID: PMC5352034.

40. Liu G, Summer R. Cellular Metabolism in Lung Health and Disease. Annu Rev Physiol. 2019 Feb 10;81:403-428. doi: 10.1146/annurev-physiol-020518-114640. Epub 2018 Nov 28. PMID: 30485759; PMCID: PMC6853603.

41. Lunt SY, Vander Heiden MG. Aerobic glycolysis: meeting the metabolic requirements of cell proliferation. Annu Rev Cell Dev Biol. 2011;27:441-64. doi: 10.1146/annurev-cellbio-092910-154237. PMID: 21985671.

42. Manzoni TB, López CB. Defective (interfering) viral genomes re-explored: impact on antiviral immunity and virus persistence. Future Virol. 2018 Jul;13(7):493-503. doi: 10.2217/fvl-2018-0021. Epub 2018 Jun 12. PMID: 30245734; PMCID: PMC6136085.

43. Mazur-Marzec H, Cegłowska M, Konkel R, Pyrć K. Antiviral Cyanometabolites-A Review. Biomolecules. 2021 Mar 22;11(3):474. doi: 10.3390/biom11030474. PMID: 33810129; PMCID: PMC8004682.

44. Meng B, Bentley K, Marriott AC, Scott PD, Dimmock NJ, Easton AJ. Unexpected complexity in the interference activity of a cloned influenza defective interfering RNA. Virol J. 2017 Jul 24;14(1):138. doi: 10.1186/s12985-017-0805-6. PMID: 28738877; PMCID: PMC5525295.

45. Migita K, Lu L, Zhao Y, Honda K, Iwamoto T, Kita S, Katsuragi T. Adenosine induces ATP release via an inositol 1,4,5-trisphosphate signaling pathway in MDCK cells. Biochem Biophys Res Commun. 2005 Mar 25;328(4):1211-5. doi: 10.1016/j.bbrc.2005.01.083. Erratum in: Biochem Biophys Res Commun. 2005 Jun 3;331(2):684. PMID: 15708005.

46. Migita K, Zhao Y, Katsuragi T. Mitochondria play an important role in adenosine-induced ATP release from Madin-Darby canine kidney cells. Biochem Pharmacol. 2007 May 15;73(10):1676-82. doi: 10.1016/j.bcp.2007.01.021. Epub 2007 Jan 20. PMID: 17328869.

47. Milne I, Stephen G, Bayer M, Cock PJ, Pritchard L, Cardle L, Shaw PD, Marshall D. Using Tablet for visual exploration of second-generation sequencing data. Brief Bioinform. 2013 Mar;14(2):193-202. doi: 10.1093/bib/bbs012. Epub 2012 Mar 24. PMID: 22445902.

48. Nayak DP, Sivasubramanian N, Davis AR, Cortini R, Sung J. Complete sequence analyses show that two defective interfering influenza viral RNAs contain a single internal deletion of a polymerase gene. Proc Natl Acad Sci U S A. 1982 Apr;79(7):2216-20. doi: 10.1073/pnas.79.7.2216. PMID: 6954536; PMCID: PMC346162.

49. Odagiri T, Tashiro M. Segment-specific noncoding sequences of the influenza virus genome RNA are involved in the specific competition between defective interfering RNA and its progenitor RNA segment at the virion assembly step. J Virol. 1997 Mar;71(3):2138-45. doi: 10.1128/JVI.71.3.2138-2145.1997. PMID: 9032347; PMCID: PMC191316.

50. Pauly MD, Procario MC, Lauring AS. A novel twelve class fluctuation test reveals higher than expected mutation rates for influenza A viruses. Elife. 2017 Jun 9;6:e26437. doi: 10.7554/eLife.26437. PMID: 28598328; PMCID: PMC5511008.

51. Perez-Cidoncha M, Killip MJ, Oliveros JC, Asensio VJ, Fernández Y, Bengoechea JA, Randall RE, Ortín J. An unbiased genetic screen reveals the polygenic nature of the influenza virus anti-interferon response. J Virol. 2014 May;88(9):4632-46. doi: 10.1128/JVI.00014-14. Epub 2014 Feb 26. PMID: 24574395; PMCID: PMC3993829.

52. Ren L, Zhang W, Han P, Zhang J, Zhu Y, Meng X, Zhang J, Hu Y, Yi Z, Wang R. Influenza A virus (H1N1) triggers a hypoxic response by stabilizing hypoxia-inducible factor-1α via inhibition of proteasome. Virology. 2019 Apr;530:51-58. doi: 10.1016/j.virol.2019.02.010. Epub 2019 Feb 11. PMID: 30780125.

53. Ren L, Zhang W, Zhang J, Zhang J, Zhang H, Zhu Y, Meng X, Yi Z, Wang R. Influenza A Virus (H1N1) Infection Induces Glycolysis to Facilitate Viral Replication. Virol Sin. 2021 Dec;36(6):1532-1542. doi: 10.1007/s12250-021-00433-4. Epub 2021 Sep 14. PMID: 34519916; PMCID: PMC8692537.

54. Rolfes MA, Flannery B, Chung JR, O'Halloran A, Garg S, Belongia EA, Gaglani M, Zimmerman RK, Jackson ML, Monto AS, Alden NB, Anderson E, Bennett NM, Billing L, Eckel S, Kirley PD, Lynfield R, Monroe ML, Spencer M, Spina N, Talbot HK, Thomas A, Torres SM, Yousey-Hindes K, Singleton JA, Patel M, Reed C, Fry AM; US Influenza Vaccine Effectiveness (Flu VE) Network, the Influenza Hospitalization Surveillance Network, and the Assessment Branch, Immunization Services Division, Centers for Disease Control and Prevention. Effects of Influenza Vaccination in the United States During the 2017-2018 Influenza Season. Clin Infect Dis. 2019 Nov 13;69(11):1845-1853. doi: 10.1093/cid/ciz075. PMID: 30715278; PMCID: PMC7188082.

55. Russell AB, Trapnell C, Bloom JD. Extreme heterogeneity of influenza virus infection in single cells. Elife. 2018 Feb 16;7:e32303. doi: 10.7554/eLife.32303. PMID: 29451492; PMCID: PMC5826275.

56. Saira K, Lin X, DePasse JV, Halpin R, Twaddle A, Stockwell T, Angus B, Cozzi-Lepri A, Delfino M, Dugan V, Dwyer DE, Freiberg M, Horban A, Losso M, Lynfield R, Wentworth DN, Holmes EC, Davey R, Wentworth DE, Ghedin E; INSIGHT FLU002 Study Group; INSIGHT FLU003 Study Group. Sequence analysis of in vivo defective interfering-like RNA of influenza A H1N1 pandemic virus. J Virol. 2013 Jul;87(14):8064-74. doi: 10.1128/JVI.00240-13. Epub 2013 May 15. PMID: 23678180; PMCID: PMC3700204.

57. Smith CM, Scott PD, O'Callaghan C, Easton AJ, Dimmock NJ. A Defective Interfering Influenza RNA Inhibits Infectious Influenza Virus Replication in Human Respiratory Tract Cells: A Potential New Human Antiviral. Viruses. 2016 Aug 22;8(8):237. doi: 10.3390/v8080237. PMID: 27556481; PMCID: PMC4997599.

58. Shiraki K, Daikoku T. Favipiravir, an anti-influenza drug against life-threatening RNA virus infections. Pharmacol Ther. 2020 May;209:107512. doi: 10.1016/j.pharmthera.2020.107512. Epub 2020 Feb 22. PMID: 32097670; PMCID: PMC7102570.

59. Silva T, S Salomon P, Hamerski L, Walter J, B Menezes R, Siqueira JE, Santos A, Santos JAM, Ferme N, Guimarães T, O Fistarol G, I Hargreaves P, Thompson C, Thompson F, Souza TM, Siqueira M, Miranda M. Inhibitory effect of microalgae and cyanobacteria extracts on influenza virus replication and neuraminidase activity. PeerJ. 2018 Oct 26;6:e5716. doi: 10.7717/peerj.5716. PMID: 30386690; PMCID: PMC6204821.

60. Singh RS, Walia AK, Khattar JS, Singh DP, Kennedy JF. Cyanobacterial lectins characteristics and their role as antiviral agents. Int J Biol Macromol. 2017 Sep;102:475-496. doi: 10.1016/j.ijbiomac.2017.04.041. Epub 2017 Apr 24. PMID: 28437766.

61. Tange, O. (2022, May 22). GNU Parallel 20220522 ('NATO'). Zenodo. https://doi.org/10.5281/zenodo.6570228

62. Tapia K, Kim WK, Sun Y, Mercado-López X, Dunay E, Wise M, Adu M, López CB. Defective viral genomes arising in vivo provide critical danger signals for the triggering of lung antiviral immunity. PLoS Pathog. 2013 Oct;9(10):e1003703. doi: 10.1371/journal.ppat.1003703. Epub 2013 Oct 31. PMID: 24204261; PMCID: PMC3814336.

63. Tapia F, Laske T, Wasik MA, Rammhold M, Genzel Y, Reichl U. Production of Defective Interfering Particles of Influenza A Virus in Parallel Continuous Cultures at Two Residence Times-Insights From qPCR Measurements and Viral Dynamics Modeling. Front Bioeng Biotechnol. 2019 Oct 18;7:275. doi: 10.3389/fbioe.2019.00275. PMID: 31681751; PMCID: PMC681321.

64. Tiwari AK, Tiwari BS. Cyanotherapeutics: an emerging field for future drug discovery. Applied Phycology. 2020; 1:1, 44-57, DOI:10.1080/26388081.2020.1744480.
65. Vanderlinden E, Vrancken B, Van Houdt J, Rajwanshi VK, Gillemot S, Andrei G, Lemey P, Naesens L. Distinct Effects of T-705 (Favipiravir) and Ribavirin on Influenza Virus Replication and Viral RNA Synthesis. Antimicrob Agents Chemother. 2016 Oct 21;60(11):6679-6691. doi: 10.1128/AAC.01156-16. PMID: 27572398; PMCID: PMC5075073.
66. Vasilijevic J, Zamarreño N, Oliveros JC, Rodriguez-Frandsen A, Gómez G, Rodriguez G, Pérez-Ruiz M, Rey S, Barba I, Pozo F, Casas I, Nieto A, Falcón A. Reduced accumulation of defective viral genomes contributes to severe outcome in influenza virus infected patients. PLoS Pathog. 2017 Oct 12;13(10):e1006650. doi: 10.1371/journal.ppat.1006650. PMID: 29023600; PMCID: PMC5638565.
67. Vignuzzi M, López CB. Defective viral genomes are key drivers of the virus-host interaction. Nat Microbiol. 2019 Jul;4(7):1075-1087. doi: 10.1038/s41564-019-0465-y. Epub 2019 Jun 3. PMID: 31160826; PMCID: PMC7097797.
68. VON MAGNUS P. Incomplete forms of influenza virus. Adv Virus Res. 1954;2:59-79. doi: 10.1016/s0065-3527(08)60529-1. PMID: 13228257.
69. Wang C, Forst CV, Chou TW, Geber A, Wang M, Hamou W, Smith M, Sebra R, Zhang B, Zhou B, Ghedin E. Cell-to-Cell Variation in Defective Virus Expression and Effects on Host Responses during Influenza Virus Infection. mBio. 2020 Jan 14;11(1):e02880-19. doi: 10.1128/mBio.02880-19. PMID: 31937643; PMCID: PMC6960286.

70. Wang C, Honce R, Salvatore M, Chow D, Randazzo D, Yang J, Twells NM, Mahal LK, Schultz-Cherry S, Ghedin E. Influenza Defective Interfering Virus Promotes Multiciliated Cell Differentiation and Reduces the Inflammatory Response in Mice. J Virol. 2023 Jun 29;97(6):e0049323. doi: 10.1128/jvi.00493-23. Epub 2023 May 31. PMID: 37255439; PMCID: PMC10308934.

71. Wasik MA, Eichwald L, Genzel Y, Reichl U. Cell culture-based production of defective interfering particles for influenza antiviral therapy. Appl Microbiol Biotechnol. 2018 Feb;102(3):1167-1177. doi: 10.1007/s00253-017-8660-3. Epub 2017 Dec 5. PMID: 29204901; PMCID: PMC5778153.
72. Winter G, Fields S, Ratti G. The structure of two subgenomic RNAs from human influenza virus A/PR/8/34. Nucleic Acids Res. 1981 Dec 21;9(24):6907-15. doi: 10.1093/nar/9.24.6907. PMID: 7335495; PMCID: PMC327650.
73. Wu M, Zhou E, Sheng R, Fu X, Li J, Jiang C, Su W. Defective Interfering Particles of Influenza Virus and Their Characteristics, Impacts, and Use in Vaccines and Antiviral Strategies: A Systematic Review. Viruses. 2022 Dec 12;14(12):2773. doi: 10.3390/v14122773. PMID: 36560777; PMCID: PMC9781619.
74. Yamagata Y, Muramoto Y, Miyamoto S, Shindo K, Nakano M, Noda T. Generation of a purely clonal defective interfering influenza virus. Microbiol Immunol. 2019 May;63(5):164-171. doi: 10.1111/1348-0421.12681. Epub 2019 May 17. PMID: 30997933.
75. Zala D, Schlattner U, Desvignes T, Bobe J, Roux A, Chavrier P, Boissan M. The advantage of channeling nucleotides for very processive functions. F1000Res. 2017 May 18;6:724. doi: 10.12688/f1000research.11561.2. PMID: 28663786; PMCID: PMC5473427.
76. Zhao H, To KKW, Chu H, Ding Q, Zhao X, Li C, Shuai H, Yuan S, Zhou J, Kok KH, Jiang S, Yuen KY. Dual-functional peptide with defective interfering genes effectively protects mice against avian and seasonal influenza. Nat Commun. 2018 Jun 15;9(1):2358. doi: 10.1038/s41467-018-04792-7. PMID: 29907765; PMCID: PMC6004018.
77. Zhong Y, Li X, Yu D, Li X, Li Y, Long Y, Yuan Y, Ji Z, Zhang M, Wen JG, Nesland JM, Suo Z. Application of mitochondrial pyruvate carrier blocker UK5099 creates metabolic reprogram and greater stem-like properties in LnCap prostate cancer cells in vitro. Oncotarget. 2015 Nov 10;6(35):37758-69. doi: 10.18632/oncotarget.5386. PMID: 26413751; PMCID: PMC4741963.

Supplementary Material

Drugs affect DVG proportion and TVG Production at the segment level for CA09 and TX12

Continued from Result Heading 2, we report the segment-specific effects of drug treatments on DelVG proportion and total genomes that were significant relative to their vehicle control (DMSO, dH_2O). As stated, we analyzed differences among treatments using ANOVA, adding bioreplicate, strain, and segment as covariates.

Strain	Vehicle	Measure	Segment	Treatment	Estimate	Std. Error	t value	Pr(>|t|)	
CA09	H2O	PropDVG	PB1	TxAdo	0.575611	0.204348	2.817	1.24E-02	*
CA09	H2O	PropDVG	PB2	TxAdo	0.350356	0.10737	3.263	0.00488	**
CA09	H2O	PropDVG	PA	TxAdo	0.514519	0.140622	3.659	0.00212	**
TX12	H2O	PropDVG	PB1	TxAdo	0.80981	0.20321	3.985	1.06E-03	*
TX12	H2O	PropDVG	PB2	TxAdo	0.603432	0.122571	4.923	0.000153	**
TX12	H2O	PropDVG	PA	TxAdo	0.78621	0.178854	4.396	0.000451	***
TX12	H2O	PropDVG	NP	TxAdo	0.009966	0.0036557	2.726	0.014943	*
CA09	H2O	PropDVG	HA	TxAdo	0.337257	0.1237154	2.726	0.015	*
TX12	H2O	PropDVG	PB1	TxInsu	0.52964	0.20321	2.606	0.01909	*
TX12	H2O	PropDVG	PA	TxInsu	0.387404	0.178854	2.166	0.045756	*
TX12	H2O	PropDVG	PB2	TxInsu	0.365633	0.122571	2.983	0.008785	**
TX12	H2O	PropDVG	NP	TxInsu	0.007798	0.0036557	2.133	0.048746	*
TX12	DMSO	PropDVG	NA	TxFavp	-0.01216	0.0047605	-2.556	0.0286	*
TX12	H2O	PropDVG	NA	TxLepto	-0.01946	0.004713	-4.13	0.001021	**
TX12	DMSO	PropDVG	NA	TxMK2206	0.014262	0.0047605	2.996	0.0134	*
TX12	H2O	PropDVG	NA	TxTolyp	-0.01150	0.004713	-2.441	0.028536	*
BOTH	DMSO	TVG	PB2	Tx4-OI	2287.3	905.6	2.526	0.0177	*
BOTH	DMSO	TVG	PB1	Tx4-OI	1177.67	462.2	2.548	0.0168	*
BOTH	DMSO	TVG	PA	Tx4-OI	3886.3	1285.5	3.023	0.00543	**
BOTH	DMSO	TVG	HA	Tx4-OI	8590	2447.24	3.51	0.00159	**
BOTH	DMSO	TVG	NP	Tx4-OI	9482.83	2792.07	3.396	0.00213	**
BOTH	DMSO	TVG	NA	Tx4-OI	11798.3	3463.2	3.407	0.00207	**
BOTH	DMSO	TVG	M	Tx4-OI	30476	8857	3.441	0.0019	**

CA09	DMSO	TVG	NS	Tx4-OI	33209	12276	2.705	0.0221	*
BOTH	DMSO	TVG	HA	TxUK5099	5051.67	2447.24	2.064	0.04873	*
BOTH	DMSO	TVG	NP	TxUK5099	6189.17	2792.07	2.217	0.03526	*
BOTH	DMSO	TVG	NA	TxUK5099	7577.3	3463.2	2.188	0.0375	*
BOTH	DMSO	TVG	M	TxUK5099	20742	8857	2.342	0.0268	*
BOTH	DMSO	TVG	PA	TxFavp	2767.7	1285.5	2.153	0.04041	*
BOTH	DMSO	TVG	NP	TxFavp	5809.5	2792.07	2.081	0.04708	*
BOTH	DMSO	TVG	M	TxFavp	19298	8857	2.179	0.0382	*
TX12	H2O	TVG	HA	TxLepto	-4135.67	1052.26	-3.93	0.001336	**
TX12	H2O	TVG	NA	TxLepto	-5725.33	1824.47	-3.138	0.00726	**
TX12	H2O	TVG	PB1	TxTolyp	1410	532.93	2.646	0.0176	*
TX12	H2O	TVG	HA	TxTolyp	-3178	1052.26	-3.02	0.008611	*
TX12	H2O	TVG	NA	TxTolyp	-4163.67	1824.47	-2.282	0.03864	*

Supplemental Table 3.1. **Drugs significantly alter total viral genomes and proportion of deletion containing viral genomes at the segment level**. Segment-specific statistically significant predictors of the proportion of **Del**etion-containing **V**iral **G**enomes (DelVGs) and **T**otal **V**iral **G**enomes (TVG) and their parameter estimates from ANOVA.

3.3A


CA09
DMSO
dH2O
PB2
PB1
PA
HA
NP
NA
M
NS
Mean DVG Proportion per Segment
Treatment
DMSO
Alpe
MK2206
4-OI
UK5099
Favp
dH2O
Insu
Ado
Uri
Lepto
Nosto
Oscil
Synec
Tolyp

3.3B


TX12
DMSO
dH2O
PB2
PB1
PA
HA
NP
NA
M
NS
Mean DVG Proportion per Segment
0.00
0.25
0.50
0.75
0.064 0.085 0.274 0.15 0.086 0.07
0.083 0.449 0.687 0.295 0.078 0.108 0.151 0.096 0.103
0.039 0.061 0.376 0.282 0.089 0.066
0.113 0.673 0.372 0.059 0.085 0.166 0.068 0.055
0.093 0.083 0.38 0.15 0.092 0.094
0.093 0.48 0.379 0.097 0.09 0.125 0.071 0.086
0.017 0.017 0.224 0.02 0.019 0.006
0.018 0.028 0.05 0.108 0 0.022 0.019 0.02 0.008
0.019 0.014 0.039 0.015 0.015 0.014
0.015 0.023 0.025 0.02 0.011 0.017 0.017 0.014 0.012
0.017 0.02 0.032 0.019 0.021 0.005
0.019 0.021 0.027 0.026 0 0.021 0.021 0.02 0.008
0.016 0.016 0.019 0.016 0.015 0.015
0.014 0.017 0.017 0.017 0.018 0.017 0.017 0.015 0.015
0.019 0.02 0.018 0.015 0.015 0.013
0.014 0.016 0.017 0.014 0.018 0.019 0.018 0.019 0.016
DMSO
Alpe
MK2206
4-OI
UK5099
Favp
dH2O
Insu
Ado
Uri
Lepto
Nosto
Oscil
Synec
Tolyp
Treatment

Supplementary Figure 3.3. Mean proportion of total viral genomes per segment that are DVGs at 18 h.p.i. under different treatment conditions; no trypsin. (**A**) CA09. (**B**) TX12. Vehicle treatment groups received either DMSO or dH_2O treatment. n = 3 bioreplicates, sem.

3.4A

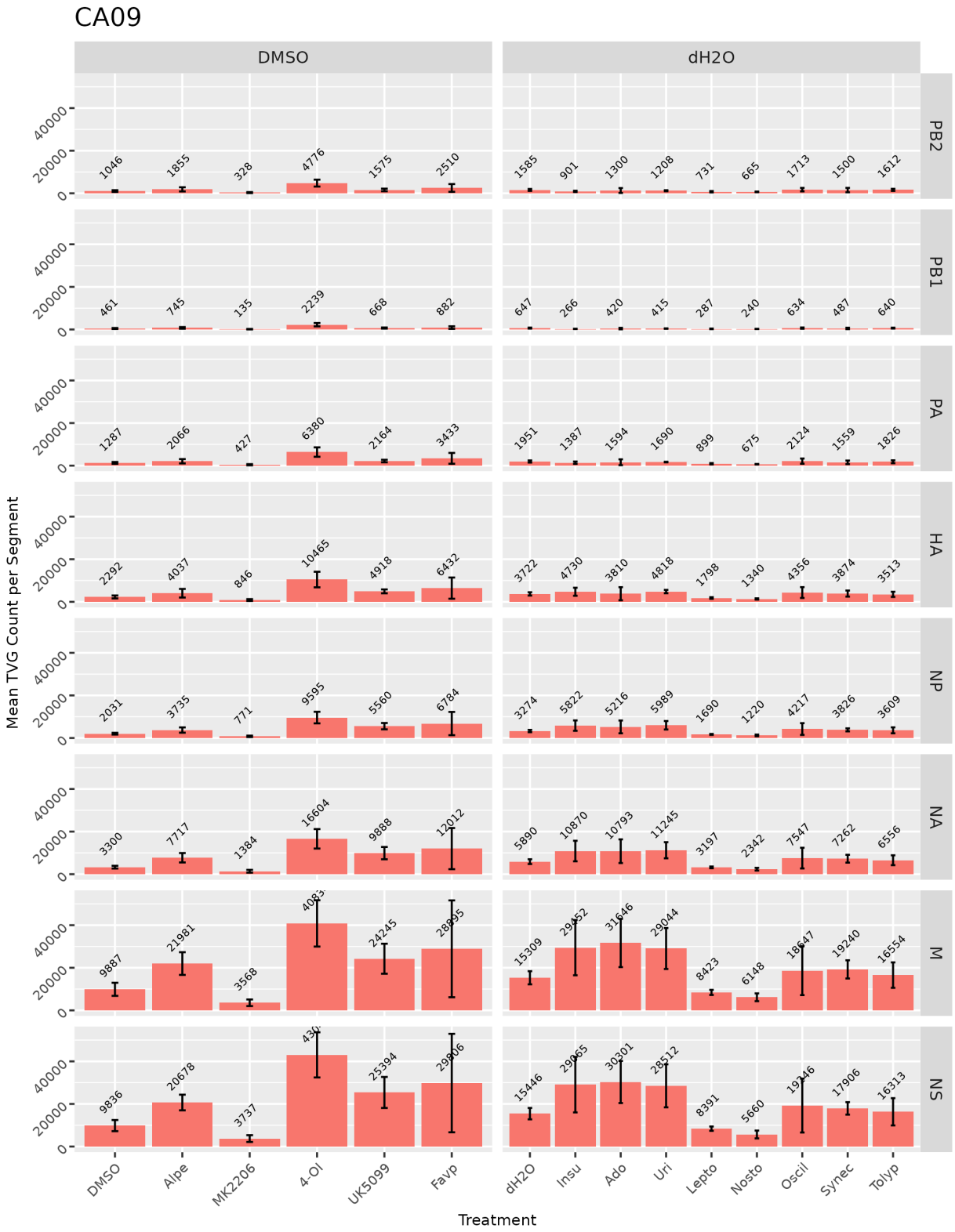
CA09
DMSO
dH2O
PB2
PB1
PA
HA
NP
NA
M
NS
Mean TVG Count per Segment
Treatment
DMSO
Alpe
MK2206
4-OI
UK5099
Favp
dH2O
Insu
Ado
Uri
Lepto
Nosto
Oscil
Synec
Tolyp

3.4B

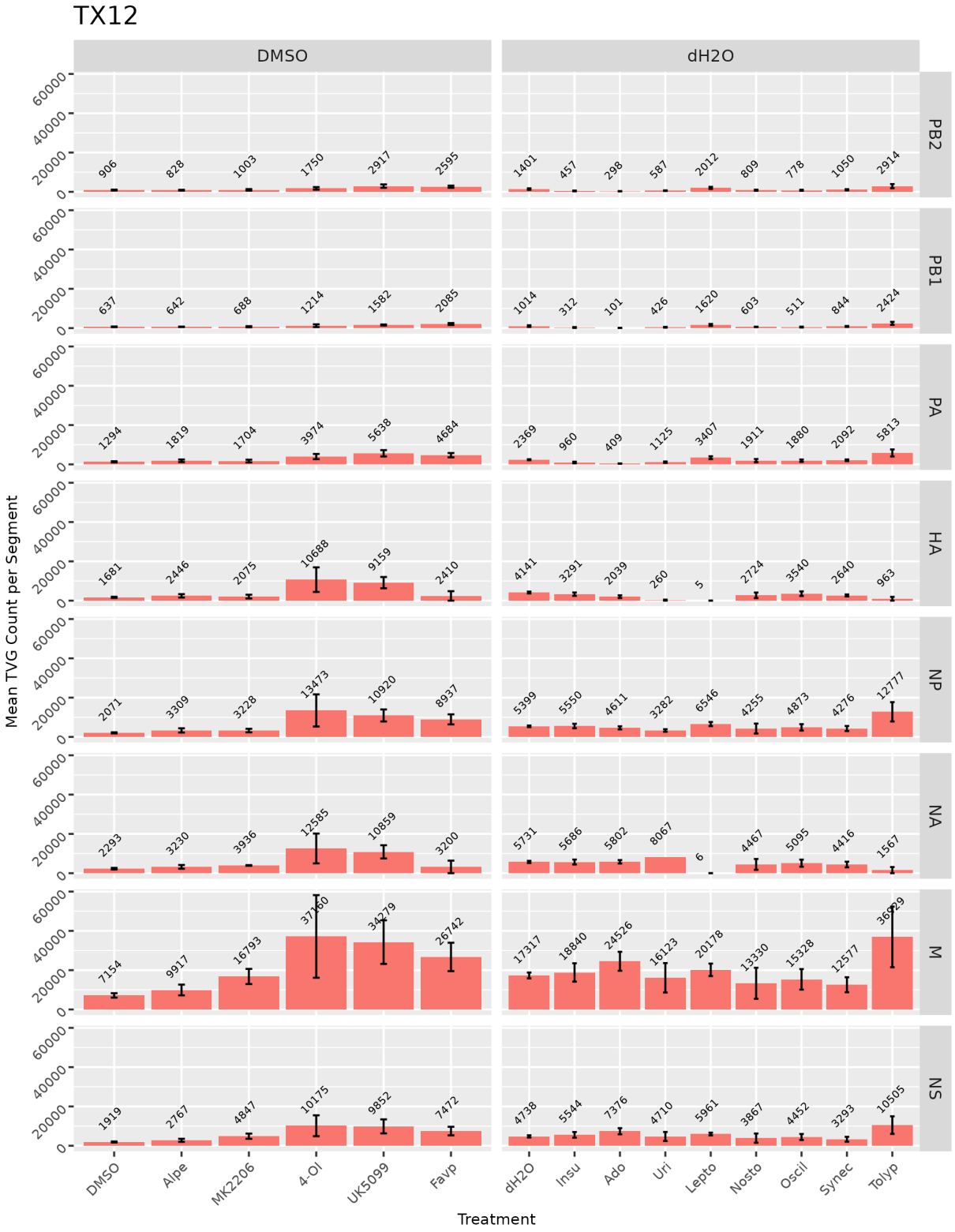
TX12
DMSO
dH2O
PB2
PB1
PA
HA
NP
NA
M
NS
Mean TVG Count per Segment
0
20000
40000
60000
906 828 1003 1750 2917 2595
1401 457 298 587 2012 809 778 1050 2914
637 642 688 1214 1582 2085
1014 312 101 426 1620 603 511 844 2424
1294 1819 1704 3974 5638 4684
2369 960 409 1125 3407 1911 1880 2092 5813
1681 2446 2075 10688 9159 2410
4141 3291 2039 260 5 2724 3540 2640 963
2071 3309 3228 13473 10920 8937
5399 5550 4611 3282 6546 4255 4873 4276 12777
2293 3230 3936 12585 10859 3200
5731 5686 5802 8067 6 4467 5095 4416 1567
7154 9917 16793 37160 34279 26742
17317 18840 24526 16123 20178 13330 15328 12577 36929
1919 2767 4847 10175 9852 7472
4738 5544 7376 4710 5961 3867 4452 3293 10505
DMSO
Alpe
MK2206
4-OI
UK5099
Favp
dH2O
Insu
Ado
Uri
Lepto
Nosto
Oscil
Synec
Tolyp
Treatment

Supplementary Figure 3.4. Mean count of total viral genomes per segment produced after 18 h.p.i. under different treatment conditions; no trypsin. (**A**) CA09. (**B**) TX12. Vehicle treatment groups received either DMSO or dH_2O treatment. n = 3 bioreplicates, sem.

Drugs affect DVG proportion and TVG Production at the genome level for CA09 and TX12

Below are visualizations of DVG relative abundance (**Supplementary Figure 3.1**) and total viral genomes (**Supplementary Figure 3.2**) for CA09 and TX12 *at the genome level*, averaged across three bioreplicates.

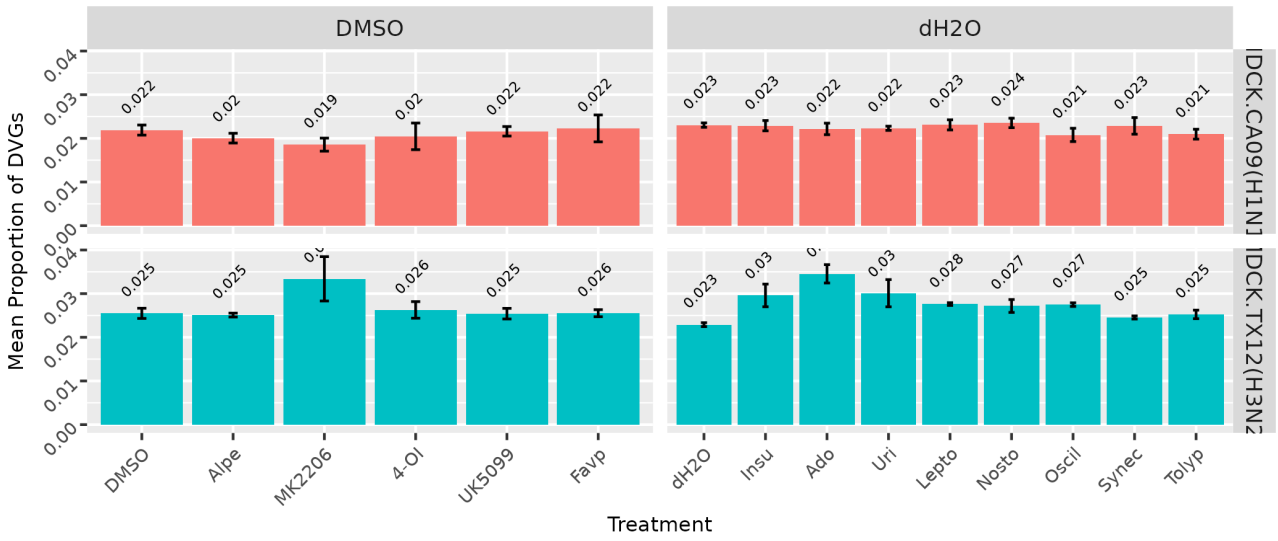

Supplemental Figure 3.1. Mean proportion of total viral genomes (CA09/TX12) that are DVGs after 18 h.p.i. under different treatment conditions; no trypsin. Vehicle treatment groups received either DMSO or dH_2O treatment. n = 3 bioreplicates, sem.

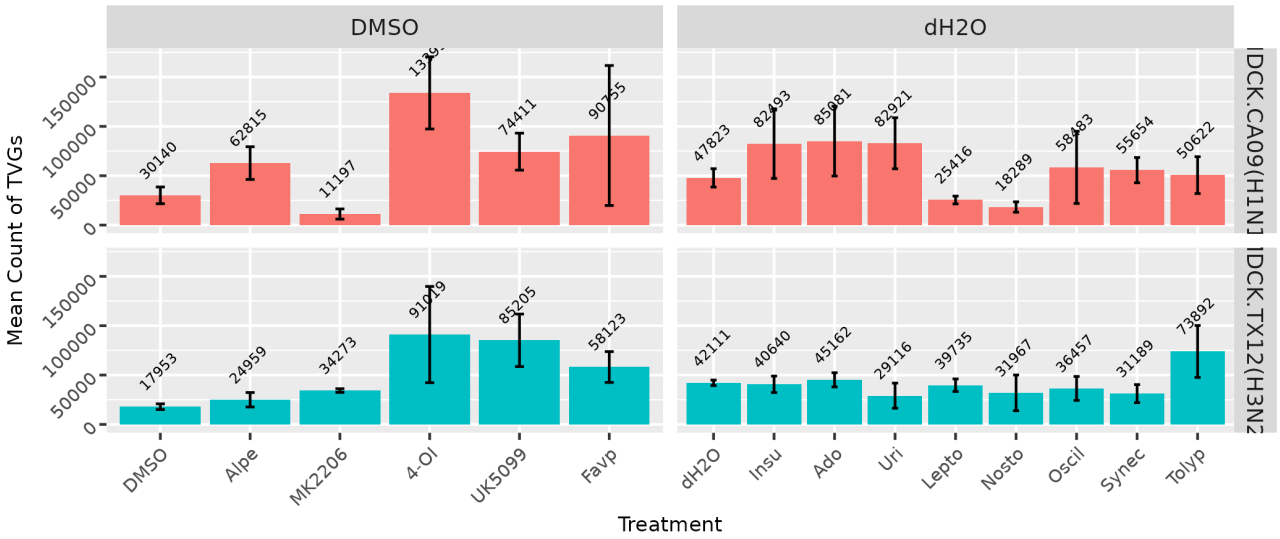

Supplemental Figure 3.2. Mean count of total viral genomes (CA09/TX12) recovered at 18 h.p.i. under different treatment conditions; no trypsin. Vehicle treatment groups received either DMSO or dH_2O treatment. n = 3 bioreplicates, sem.